nature

https://doi.org/10.1038/s41586-023-06651-y

Accelerated Article Preview

Distinguishing features of Long COVID identified through immune profiling

Received: 8 August 2022

Accepted: 18 September 2023

Accelerated Article Preview

Cite this article as: Klein, J. et al. Distinguishing features of Long COVID identified through immune profiling. *Nature* https://doi.org/10.1038/s41586-023-06651-y (2023)

Jon Klein, Jamie Wood, Jillian Jaycox, Rahul M. Dhodapkar, Peiwen Lu, Jeff R. Gehlhausen, Alexandra Tabachnikova, Kerrie Greene, Laura Tabacof, Amyn A. Malik, Valter Silva Monteiro, Julio Silva, Kathy Kamath, Minlu Zhang, Abhilash Dhal, Isabel M. Ott, Gabrielee Valle, Mario Peña-Hernandez, Tianyang Mao, Bornali Bhattacharjee, Takehiro Takahashi, Carolina Lucas, Eric Song, Dayna Mccarthy, Erica Breyman, Jenna Tosto-Mancuso, Yile Dai, Emily Perotti, Koray Akduman, Tiffany J. Tzeng, Lan Xu, Anna C. Geraghty, Michelle Monje, Inci Yildirim, John Shon, Ruslan Medzhitov, Denyse Lutchmansingh, Jennifer D. Possick, Naftali Kaminski, Saad B. Omer, Harlan M. Krumholz, Leying Guan, Charles S. Dela Cruz, David van Dijk, Aaron M. Ring, David Putrino & Akiko Iwasaki

Distinguishing features of Long COVID identified through immune profiling

Jon Klein[1*], Jamie Wood[2*], Jillian Jaycox[1*], Rahul M. Dhodapkar[1,3*], Peiwen Lu[1*], Jeff R. Gehlhausen [1,4*], Alexandra Tabachnikova[1*], Kerrie Greene[1], Laura Tabacof[2], Amyn A. Malik[5], Valter Silva Monteiro[1], Julio Silva[1], Kathy Kamath[6], Minlu Zhang[6], Abhilash Dhal[6], Isabel M. Ott[1], Gabrielee Valle[7], Mario Peña-Hernandez[1,8], Tianyang Mao[1], Bornali Bhattacharjee[1], Takehiro Takahashi[1], Carolina Lucas[1,11], Eric Song[1], Dayna Mccarthy[2], Erica Breyman[2], Jenna Tosto-Mancuso[2], Yile Dai[1], Emily Perotti[1], Koray Akduman[1], Tiffany J. Tzeng[1], Lan Xu[1], Anna C. Geraghty[9], Michelle Monje[9,10], Inci Yildirim[5,11,12,13], John Shon[6], Ruslan Medzhitov[1,10,11], , Denyse Lutchmansingh[7], Jennifer D. Possick[7], Naftali Kaminski[7], Saad B. Omer[5,11,13,14], Harlan M. Krumholz[11,15,16,17], Leying Guan[11,18], Charles S. Dela Cruz[7, 11], David van Dijk[11,19,20†], Aaron M. Ring[1,11†], David Putrino[2,21†], Akiko Iwasaki[1,10,11†]

Affiliations:
1: Department of Immunobiology, Yale School of Medicine, New Haven, CT.
2: Abilities Research Center, Icahn School of Medicine at Mount Sinai, New York City, NY.
3: Department of Ophthalmology, USC Keck School of Medicine, Los Angeles, CA.
4: Department of Dermatology, Yale School of Medicine, New Haven, CT.
5: Yale Institute for Global Health, Yale School of Public Health, New Haven, CT.
6: SerImmune Inc., Goleta, CA.
7: Department of Internal Medicine (Pulmonary, Critical Care, and Sleep Medicine), Yale School of Medicine, New Haven, CT.
8: Department of Microbiology, Yale School of Medicine, New Haven, CT.
9: Department of Neurology and Neurological Sciences, Stanford University, Palo Alto, CA.
10: Howard Hughes Medical Institute, Chevy Chase, MD.
11: Center for Infection and Immunity, Yale School of Medicine, New Haven, CT.
12: Department of Pediatrics (Infectious Diseases), Yale New Haven Hospital, New Haven, CT.
13: Department of Epidemiology of Microbial Diseases, Yale School of Public Health, New Haven, CT.
14: Department of Internal Medicine (Infectious Diseases), Yale School of Medicine, New Haven, CT.
15: Center for Outcomes Research and Evaluation, Yale New Haven Hospital, New Haven, CT.
16: Section of Cardiovascular Medicine, Department of Internal Medicine, Yale School of Medicine, New Haven, CT.
17: Department of Health Policy and Management, Yale School of Public Health, New Haven, CT.
18: Department of Biostatistics, Yale School of Public Health, New Haven, CT.
19: Department of Computer Science, Yale University, New Haven, CT.
20: Department of Internal Medicine (Cardiology), Yale School of Medicine, New Haven, CT.
21: Department of Rehabilitation and Human Performance, Icahn School of Medicine at Mount Sinai, New York City, NY.

*: Indicates equal contribution
†: Co-corresponding authors

Correspondence can be addressed to: akiko.iwasaki@yale.edu, david.putrino@mountsinai.org, aaron.ring@yale.edu, or david.vandijk@yale.edu.

Summary

Post-acute infection syndromes (PAIS) may develop after acute viral disease[1]. Infection with SARS-CoV-2 can result in the development of a PAIS known as "Long COVID" (LC). Individuals with LC frequently report unremitting fatigue, post-exertional malaise, and a variety of cognitive and autonomic dysfunctions[2–4]; however, the biological processes associated with the development and persistence of these symptoms are unclear. Here, 273 individuals with or without LC were enrolled in a cross-sectional study that included multi-dimensional immune phenotyping and unbiased machine learning methods to identify biological features associated with LC. Marked differences were noted in circulating myeloid and lymphocyte populations relative to matched controls, as well as evidence of exaggerated humoral responses directed against SARS-CoV-2 among participants with LC. Further, higher antibody responses directed against non-SARS-CoV-2 viral pathogens were observed among individuals with LC, particularly Epstein-Barr virus. Levels of soluble immune mediators and hormones varied among groups, with cortisol levels being lower among participants with LC. Integration of immune phenotyping data into unbiased machine learning models identified key features most strongly associated with LC status. Collectively, these findings may help guide future studies into the pathobiology of LC and aid in developing relevant biomarkers.

Introduction

Recovery from acute viral infections is heterogeneous and chronic symptoms may linger for months to years in some individuals. Additionally, persistent sequelae may develop after acute infection by a number of viruses from a diverse range of viral families[5–9]. Post-acute infection syndromes (PAIS) microbial infections have also been described for over a century[10,11]. Yet despite their ubiquity, the basic biology underlying PAIS development, even for extensively studied PAIS like myalgic encephalomyelitis/chronic fatigue syndrome (ME/CFS), remains unclear[1,12].

SARS-CoV-2 is a betacoronavirus responsible for at least seven million deaths worldwide[13]. Infection causes COVID-19, which can manifest as a severe respiratory disease marked by extensive immunological and multi-organ system dysfunction[14–19]. Recovery from COVID-19 is often complete; however, individuals (even those with initially mild disease courses) may have significantly increased risks for adverse clinical events and abnormal clinical findings[20–25].

In addition to developing isolated dysfunctions, some convalescent COVID-19 patients may develop a group of new onset or aggravated sequelae known as Long COVID (LC). Clinically, LC presents as a constellation of debilitating symptoms (e.g., unremitting fatigue, post-exertional malaise, cognitive impairment, and autonomic dysfunctions), alongside other less common manifestations[2–4]. These persistent sequelae dramatically impair physical and cognitive function and reduce quality of life[26]. Estimates of LC prevalence vary substantially[27], but prospective studies suggest about one in eight individuals with COVID-19 experience persistent somatic symptoms attributable to past SARS-CoV-2 infection[28]. While the underlying pathogenesis of LC remains unclear, current hypotheses include the persistence of virus or viral remnants in tissue reservoirs; development or aggravation of autoimmunity; microbial dysbiosis; reactivation of non-SARS-CoV-2 latent viral infections; and tissue damage caused by chronic inflammation.

To interrogate the biological underpinnings of LC, a cross-sectional study was designed (Mount Sinai-Yale Long COVID, MY-LC) involving 273 participants comprising five study groups: (1) healthcare workers infected with SARS-CoV-2 before vaccination (HCW); (2) healthy, uninfected, vaccinated controls (healthy controls, HC); (3) previously infected, vaccinated controls without persistent symptoms (convalescent controls, CC); (4) individuals with persistent symptoms after acute infection (Long

COVID, LC); and (5) a second group of individuals with persistent symptoms following acute infection from an independent study (External Long COVID, Ext. LC). Among the CC and LC groups, enrolled participants had primarily mild (non-hospitalised) acute COVID-19 and samples for this study were acquired, on average, more than a year after their acute infection. The HC, CC, and LC groups underwent systematic, multi-dimensional immunophenotyping and unbiased machine learning of aggregated data to identify potential LC biomarkers.

Results

Overview of MY-LC cohort

The MY-LC study enrolled 183 participants (101 LC, 42 CC, and 42 HC) at one study site (Mount Sinai Hospital, New York City, New York) and 90 participants at another (Yale New Haven Hospital, New Haven, CT) for a total of 275 participants. After initial enrollment and preliminary review of electronic medical records, two participants were excluded from the LC group (2.0%, for pharmacologic immunosuppression secondary to primary immune deficiency and solid organ transplant); two from HC (4.8%, for pregnancy and misclassification at enrollment); and three from CC (7.1%, for pregnancy, monogenic disorder, and misclassification at enrollment) resulting in a final study size of 268 individuals (**Fig. 1A**). The proportion of participants excluded from the LC group did not significantly differ from those excluded from the other groups (**Extended Data Table 1**).

Initial comparison of demographic factors showed the LC and CC groups differed in mean age (46 years, LC; 38 years, CC; Kruskal-Wallis post-hoc, $p = 0.0040$). But these groups did not significantly differ in sex; hospitalisation for acute COVID-19 (**Fig. 1B**); or median elapsed time between initial infection and acute disease (**Fig. 1C**). Most acute infections within the LC group (76%) occurred between epidemiological weeks 7–17 of 2020, when parental SARS-CoV-2 strains (WA-1) drove most new cases. Importantly, the aggregated medical history of individuals with LC did not significantly differ from that of CC individuals in baseline prevalence of anxiety or depression. Complete demographic features and medical histories are reported in **Extended Data Table 1**.

Across all surveyed dimensions, participants with LC had significantly higher intensities of reported symptoms and dramatically worsened quality of life (**Extended Data Table 2**, **Extended Data Fig. 1A**). To address whether LC associated with any pattern of survey responses, responses were aggregated into a single classification metric (Long COVID Propensity Score, LCPS) using a parsimonious logistic regression model (LC vs. Other), which demonstrated significant diagnostic potential (0.94 AUC, bootstrap CI: 0.89–0.97) (**Fig. 1D, Extended Data Fig. 1B, Extended Data Table 3**).

Among the self-reported symptoms from the LC group, fatigue (87%), brain fog (78%), memory difficulty (62%), and confusion (55%) were most common (**Fig. 1E**). Postural Orthostatic Tachycardia Syndrome (POTS) was also prevalent; 38% of individuals with LC had formal diagnostic testing and clinical evaluation (**Extended Data Fig. 1C**). Negative impacts on employment status were also reported by half the participants with LC (**Extended Data Fig. 1D**).

To find groups of participants with LC with similar sets of self-reported symptoms, an agglomerative hierarchical clustering of binary symptoms was performed (**Extended Data Fig. 1E**). Three LC clusters were identified (bootstrapped mean cluster-wise Jaccard similarity: cluster 1, 0.75 [95% CI: 0.54–1.00]; cluster 2, 0.60 [0.47–0.94]; and cluster 3, 0.75 [0.56–1.00]). LC clusters were clearly bifurcated by LCPS: cluster 3 had intermediate propensity scores; clusters 1 and 2, more extreme ones (**Extended Data Fig. 1F**).

Circulating immune cell differences

Analysis of peripheral blood mononuclear cell (PBMC) populations revealed a significant difference in circulating immune cell populations among MY-LC cohorts. The median level of non-conventional monocytes ($CD14^{lo}CD16^{hi}$) in the LC group was significantly higher than those in other groups (**Extended Data Fig. 2A, left)**. To determine whether LC significantly associated with levels of non-conventional monocytes after accounting for demographic differences across groups, linear models were developed incorporating age, sex, LC status (binary), and body mass index (BMI). By this approach, LC significantly associated with levels of total non-conventional monocytes (**Extended Data Fig. 3J**) and those expressing MHC Class II (HLA-DR) (**Extended Data Fig. 2A, right**). Parallel investigation of absolute cell counts also revealed increased numbers of circulating non-conventional monocytes (**Extended Data Fig. 4A**).

Systematic analysis of other immune effector populations revealed significantly lower circulating populations of cDC1s among participants with LC (**Extended Data Fig. 2B, left; Extended Data Fig. 4B**). Linear models again found LC status and age significantly associated with circulating cDC1 levels (**Extended Data Fig. 2B, right**). Levels of other circulating granulocyte populations (neutrophils, eosinophils, conventional and intermediate monocytes, plasmacytoid dendritic, and cDC2 populations) did not significantly differ among groups, with substantial heterogeneities noted in LC (**Extended Data Fig. 3A,B**).

The median relative percentage of B lymphocytes was significantly higher in both activated populations ($CD86^{hi}$HLA-DR^{hi}: 17%, LC; 11%, CC; 12%, HC) and double-negative subsets ($IgD^{-}/CD27^{-}/CD24^{-}/CD38^{-}$: 5%; 2%; 2%) (**Extended Data Fig. 2C)**. The absolute count of double-negative B cells also significantly increased in individuals with LC **(Extended Data Fig. 4C)**. LC status was again significantly associated with these effector populations in linear modeling (**Extended Data Fig. 3J**). Circulating levels of various B-cell subsets, including naïve B cells, did not significantly differ among groups (**Extended Data Fig. 3C**).

Circulating T lymphocyte populations were not strikingly different in effector memory subsets ($CD45RA^{-}/CD127^{-}/CCR7^{-}$) (**Extended Data Fig. 2D)**, although absolute counts of $CD4^{+}$ populations significantly increased (**Extended Data Fig. 4D)**. The median relative percentage of circulating $CD4^{+}$ central memory cells ($CD45RA^{-}/CD127^{+}/CCR7^{-}$) was significantly lower in the LC group (27%, LC; 33%, CC; 32%, HC), although groups did not differ by absolute count (**Extended Data Fig. 4D)**. Median percentages of exhausted ($PD\text{-}1^{+}/Tim\text{-}3^{+}$) $CD4^{+}$ subsets ($CD4_{Ex}$) and exhausted $CD8^{+}$ subsets ($CD8_{Ex}$) did not significantly differ (**Extended Data Fig. 2D**), but absolute $CD4_{Ex}$ counts were significantly elevated (**Extended Data Fig. 4D**). Importantly, neither naïve CD4 nor CD8 T cells significantly differed (**Extended Data Fig. 3D**).

After being stimulated with phorbol myristate acetate and ionomycin, $CD4^{+}$ cells from individuals with LC produced significantly higher median levels of intracellular IL-2 (17%, LC; 14%, CC; 13%, HC); IL-4 (11%; 7%; 8%); and IL-6 (1.7%; 1.4%; 1.5%) (**Extended Data Fig. 2E, Extended Data Fig. 4E; top row**), as did $CD8^{+}$ T cells (**Extended Data Fig. 2E, Extended Data Fig. 4E, bottom row**). Both age and LC status were significantly associated with intracellular IL-4 and IL-6 production (**Extended Data Fig. 2K, Extended Data Table 4**). Notably, individuals with LC also had uniquely elevated median levels of IL-4/IL-6 double-positive $CD4^{+}$ T cells (0.3%, LC; 0.2%, CC; 0.2%, HC) and double-positive $CD8^{+}$ T cells (0.5%; 0.2%; 0.2%) (**Extended Data Fig. 2F, Extended Data Fig. 4F**). Levels of IFN-γ and IL-17 (in $CD4^{+}$) and TNF-α and GMZB (in $CD8^{+}$) did not significantly differ across groups (**Extended Data Fig. 3E–I**). To account for heterogeneous levels of circulating immune cell populations, permutational analysis of variance (PERMANOVA) was performed using effector populations with significant differences between groups at baseline. This multivariate analysis showed that LC status and age significantly predicted levels of circulating immune cell populations (**Extended Data Fig. 2G**).

SARS-CoV-2 specific antibody responses

Initial analysis of anti-SARS-CoV-2 antibody responses was performed only for MY-LC participants who received two doses of vaccine. Anti-S1 IgG levels in the LC group were significantly higher than those in the CC group, and levels of total anti-S and anti–receptor-binding domain (RBD) IgG were elevated in the LC group but did not significantly differ from CC-group levels (**Fig. 2A**). Unvaccinated participants with LC had significantly higher anti-N IgG levels than did historical, unvaccinated controls previously exposed to SARS-CoV-2 (**Extended Data Fig. 5A)**.

Linear models were constructed to more fully account for baseline differences (demographics, vaccines at blood draw [VAD]) across cohorts (**Fig. 2B, Extended Data Fig. 5B**), which revealed that LC state was a significant, positive predictor of anti-Spike humoral response after accounting for such differences (**Extended Data Table 5**). To gauge whether the elevated responses were to distinct regions of Spike, anti-SARS-CoV-2 IgG responses against linear peptides were profiled among vaccinated participants. LC participant responses were significantly higher than CC responses against a peptide that confers increased neutralization[29,30], corresponding to amino acid residues 556–572 (1.3×; Outlier Sum, $p = 0.031$). Responses were also higher (1.4×–1.6×) for peptides corresponding to residues 572–586, 625–638, and 682–690 (the furin cleavage site). CC participant responses were higher than LC ones against two S2 peptides (residues 1149–1161, 1.5×; 1256–1266, 2.1×) (**Fig. 2C**). Multiple differentially expressed Spike-binding motifs were mapped onto available trimeric-structure models of Spike (PDB: 6VXX). These mapped to highly surface exposed sites in the protein's natural conformational state, near the S1 RBD (RDPQTLE and KFLPQQ) and the S1/S2 cleavage site (RSVAS, YECDIPIGAGICA, and YMSLG) (**Fig. 2D**), consistent with participants with LC having higher anti-Spike immune responses. By analysing peptide enrichment for Spike motifs corresponding to Protein-based Immunome Wide Association Study (PIWAS)–identified peaks, significantly greater humoral responses against KFLPFQQ (Kruskal-Wallis, $p = 0.023$) (**Fig. 2E**), RDPQTLE ($p = 0.00058$), and LDK[WY]F ($p = 0.0034$) were found (**Extended Data Fig. 5C**). Prevalences of antibody reactivities against KFLPFQQ (Fisher's exact, $p = 0.0060$), RDPQTLE ($p = 0.00015$), LDK[WY]F ($p = 0.00066$), and DISGI ($p = 0.0086$) were also significantly higher among participants with LC than among grouped controls (**Extended Data Fig. 5D**). Statistical modeling accounting for baseline differences (demographics, VAD) revealed LC significantly associated with reactivity against KFLPFQQ, RDPQTLE, and DISGI motifs (**Extended Data Fig. 5E**), but not with reactivity against LDK[WY]F (**Extended Data Fig. 5E**), which was elevated in both CC and LC groups (**Extended Data Fig. 5C**).

Cortisol and soluble immune mediators

Parallel multiplex analysis of circulating hormones and immune mediators in plasma samples revealed groups in the MY-LC cohort significantly differed in median levels of cortisol (Kruskal-Wallis, $p < 0.0001$); complement C4b ($p = 0.0001$); CCL19 ($p = 0.00058$); galectin-1 ($p = 0.0015$); CCL20 ($p = 0.0032$); CCL4 ($p = 0.0092$); APRIL ($p = 0.013$); LH ($p = 0.022$); and IL-5 ($p = 0.024$). Post-hoc comparisons showed the LC group had significantly increased complement C4b, CCL19, CCL20, galectin-1, CCL4, APRIL, and LH; and marginally but significantly decreased IL-5 (**Extended Data Fig. 6A–H**). Additional analysis revealed significant correlations with LCPS scores, particularly for cortisol (**Extended Data Fig. 6I**). In the Ext. LC cohort ($n = 53$, excluding an outlier whose level was >8 standard deviations above median), cortisol levels in the LC group were lower than those in the HC and CC groups (**Fig. 2F)**. Paired levels of adrenocorticotropic hormone (ACTH) were evaluated only in the MY-LC cohort; these did not significantly differ across groups (**Fig. 2G**). Median sample collection times significantly differed only between CC and LC groups, and this difference was modest (65 minutes; Dunn's test, $p = 0.027$) (**Fig. 2H**). Subsequent statistical modeling revealed that LC status significantly associated with lower cortisol levels after accounting for individual differences in age, sex, BMI, sample-collection time, and cohort (MY-LC vs. Ext. LC) (**Fig. 2I, Extended Data Table 6**).

Autoantibodies to exoproteome

Next, antibody reactivity against extracellular proteins was assessed in 98 LC and 38 control participants using rapid extracellular antigen profiling (REAP), a method to measure antibody reactivity against >6,000 extracellular and secreted human proteins[16]. Although participants with LC had a variety of private reactivities against diverse autoantigens (**Fig. 3A**), the number of autoantibody reactivities per participant did not differ across groups (**Fig. 3B**), nor did the number of reactivities significantly correlate with LC clusters (as assessed by LCPS scores) (**Fig. 3C**). Additionally, the number of autoantibody reactivities correlated with neither double-negative B-cell populations nor days from acute symptom onset (**Extended Data Fig. 7A,B**).

Given REAP studies showing functional autoantibodies are elevated in severe acute COVID-19[16], autoantibody reactivities were aggregated into clusters using a manually curated Gene Ontology process list relevant to LC. The magnitudes of reactivity for LC and control groups did not significantly differ in any category (**Extended Data Fig. 5C**). Several reports implicated stereotypical G protein-coupled receptor (GPCR) autoantibodies in LC pathogenesis[31,32] (e.g., targeting beta adrenergic receptors or the angiotensin II receptor). While several GPCR-directed autoantibodies were detected in this study (**Extended Data Fig. 7D**), the number of GPCR reactivities for participants with LC did not differ from that for controls (**Fig. 3D**). Importantly, individual autoantibody reactivities were not significantly more frequent in either participants with LC or in controls (**Fig. 3E**).

Antibody responses to herpesviruses

Given emerging evidence for the role of latent virus reactivation in LC, three complementary approaches were used to examine anti-viral reactivity patterns in the MY-LC cohorts: REAP, serum epitope repertoire analysis (SERA), and ELISA. Global anti-viral responses were first assessed by REAP, which measures antibody reactivity to 225 viral surface proteins (**Supplementary Table 2)**. Reactivities against 38 viral conformational epitopes were detected among 98 LC and 38 control participants (**Extended Data Fig. 8A**). For SARS-CoV2 reactivities, only participants who received two doses of vaccine were analysed**.** Reactivities against non–Omicron variant RBDs in the LC cohort were higher than those in the CC controls **(Fig. 4A)**; however, as with ELISA, this trend was not significant.

Differences in viral reactivities against non-SARS-CoV-2 antigens were striking (**Fig. 4B**). Participants with LC had elevated REAP scores for several herpesvirus antigens, including the Epstein-Barr virus (EBV) minor viral capsid antigen gp23 ($p = 4.62E-3$); the EBV fusion-receptor component gp42 ($p = 3.2E-2$); and the VZV glycoprotein E ($p = 1.51E-2$) (**Extended Data Fig. 8B**). Conversely, participants with LC had lower REAP scores for HSV-1 glycoprotein gL ($p = 4.61E-6$) and gD1, although the difference in gD1 reactivity was not significant.

Next, the SERA platform (a commercially available random bacterial display library with unlimited multiplex capability) was used to orthogonally analyse non-SARS-CoV-2 antigens. SERA includes epitope panels representing 45 pathogens and disease markers, validated using a database of thousands of controls[33]. Importantly, SERA revealed that cohorts significantly differed neither in estimated EBV seroprevalence (**Fig. 4C**) nor for any other tested viral pathogen (**Extended Data Fig. 8C**).

First was assessed whether individuals with LC had higher EBV reactivities because of acute EBV infection. Anti-EBV IgM was not elevated in this group (as measured by SERA) (**Extended Data Fig. 8D**) nor was there evidence of EBV viremia (**Extended Data Fig. 8E,F**), suggesting that the higher reactivity to EBV lytic antigens was more likely caused by recent EBV reactivation than by acute infection. Additionally, these results do not rule out EBV shedding at a local site, such as in saliva[34].

Next was assessed whether differences in baseline seropositivity affected EBV-antigen reactivity. EBV reactivity was analysed only in EBV-seropositive individuals as identified by SERA and by Identifying Motifs Using Next-generation sequencing Experiments (IMUNE). By REAP, seropositive participants with LC had significantly higher reactivity to EBV p23 (Kruskal-Wallis, $p = 0.00095$, **Fig. 4D**) and gp42 (0.0039, **Fig. 4E**) than did seropositive controls. REAP measurements significantly correlated with ELISA measurements ($R = 0.73$, $p \leq 2.2E\text{-}16$), orthogonally validating this finding **(Extended Data Fig. 8G**). In an orthogonal screen of linear peptides with SERA, the LC cohort had greater reactivity against the gp42 linear peptide (PVXF[ND]K) (Kruskal-Wallis, $p = 0.0031$) (**Fig. 4F**). Mapping of this motif onto available structures of gp42 complexed with EBV gH/gL (PDB: 5T1D) showed these residues are exposed on the surface of EBV virions (**Fig. 4G,** *pink residues*).

To investigate lower REAP reactivity to HSV-1 antigens observed in participants with LC, a similar analysis was performed using only HSV-1 seropositive individuals, as identified by SERA. In these individuals, REAP scores for HSV-1 glycoprotein gD1 no longer differed among groups (**Extended Data Fig. 8H**). Post-hoc comparisons for HSV-1 gL also showed the groups did not significantly differ (**Extended Data Fig. 8I**). These data suggested that the lower IgG reactivity to gL in REAP (**Fig. 4B**) is probably caused by lower HSV-1 seroprevalence in the LC group. In aggregated initial REAP and SERA results, individuals with LC had elevated IgG reactivity to EBV and VZV surface antigens without evidence of EBV primary infection or acute viremia.

Additional analysis revealed LCPS significantly correlated with humoral reactivity against neither gp42 PVXF[ND]K nor EBV p23 antigens in EBV-seropositive individuals (**Extended Data Fig. 8J,K**). In contrast**,** reactivity to gp42 PVXF[ND]K correlated with IL-4/IL-6 producing $CD4^+$ T cells in EBV-seropositive individuals with LC ($R = 0.26$, $p = 0.013$) (**Fig. 4H**). This correlation was not observed in control groups. Furthermore, EBV p23 REAP reactivity significantly correlated with terminally differentiated effector memory (T_{EMRA}) $CD4^+$ T cells ($R = 0.26$, $p = 0.018$) (**Fig. 4I**), a subset of cells implicated in protection from CMV[35]. In contrast, anti-SARS-CoV-2 antibody levels did not correlate with IL-4/IL-6 double-positive $CD4^+$ T cells (**Extended Data Fig. 8L-O**).

Unique biological markers of Long COVID

To further account for demographic differences among groups that might affect immunophenotypes, each LC participant was explicitly matched to a control participant by using a Gale-Shapley procedure based on participant age, sex, days from acute COVID-19 symptom onset, and vaccination status. Participants with LC did not differ significantly from controls in these criteria (**Extended Data Fig. 9A**), nor in severity of acute COVID-19 disease (whether hospitalisation was required) (**Extended Data Fig. 9B**). Principal component analysis embedding of matched participants with all collected immunological features clearly distinguished individuals with LC from controls (**Fig. 5A**). Consistent with this, k-nearest neighbours classification on the normalised features efficiently discriminated between groups, with an AUC of 0.94 (95% CI: 0.84–1.00) (**Fig. 5B**). Principal components regression of collated immunological data showed that flow cytometry (pseudo-$R^2 = 59\%$) and plasma proteomics and hormones (pseudo-$R^2 = 74\%$) were most informative for separating groups. A final parsimonious LASSO model similarly achieved good fit (pseudo-$R^2 = 82\%$) (**Fig. 5C)**. Of the features selected for the final model, several associated positively with LC status (serum galectin-1 concentration, IgG against various EBV epitopes); while others associated negatively (serum cortisol; PD-1^+ / $CD4^+$ T_{cm}; cDC1 cells) (**Fig. 5D**). Preliminary external validation in the Ext. LC cohort of selected LASSO-model features revealed similar decreases in cortisol, but galectin-1 and EBV gp42 predicted LC status specifically in the MY-LC cohort **(Extended Data Fig. 9C,D)**, potentially caused by clinical phenotype differences between the MY-LC and Ext. LC cohorts **(Extended Data Fig. 9E).**

Serum cortisol was the most significant predictor of LC status in the model, and cortisol alone achieved an AUC of 0.96 (95% CI: 0.93–0.99) (**Extended Data Fig. 9F, top**). Notably, serum cortisol in the MY-LC cohort was similar in the HC and CC controls, and lower in participants with LC (**Extended Data Fig. 9F, bottom**). When used alone, each of the other selected model features predicted status reasonably well (**Extended Data Fig 9G,H)**. Last, classification accuracies of LCPS models substantially agreed with machine learning ones (Cohen's Kappa, 0.79; 95% CI: 0.65–0.93), suggesting that both participant-reported outcomes and immunological features efficiently predict LC status (**Extended Data Table 7**).

Discussion

Studies of individuals with LC reported diverse changes in immune and inflammatory factors[36,37]. In this study, exploratory analyses identified significant immunological differences between the LC population and demographically matched control populations more than a year from their acute infections. Circulating immune cell populations significantly changed. Populations of non-conventional monocytes, double-negative B cells, and IL-4/IL-6 secreting CD4 T cells increased; and those of conventional DC1 and central memory CD4 T cells decreased. In addition, individuals with LC had higher levels of antibodies to SARS-CoV-2, EBV, and VZV antigens. In contrast, levels of individual autoantibodies to human exoproteome did not significantly differ. Marked differences in levels of circulating cytokines and hormones, particularly cortisol, were noted in participants with LC from both MY-LC and Ext. LC cohorts. Unbiased machine learning revealed several core predictive features of LC status within the MY-LC study, identifying potential targets for additional validation and future biomarker development.

Multiple hypotheses have been proposed for LC pathogenesis, including persistent virus or viral remnants[38], autoimmunity, dysbiosis, latent viral reactivation, and unrepaired tissue damage. The data in this study suggest persistent SARS-CoV-2 viral antigens, reactivation of latent herpesviruses, and chronic inflammation may all contribute to LC. Overall, our data are less consistent with an autoantibody-dominated disease process in LCs. Whether autoreactive T cells play a role in LC pathogenesis was not addressed and requires future investigation.

Immune phenotyping of PBMC populations revealed participants with LC had notably higher levels of circulating non-conventional monocytes associated with various chronic inflammatory and autoimmune conditions[39]. These participants also had significantly lower levels of circulating cDC1 populations, which are responsible for antigen presentation and cytotoxic T cell priming[40]. In addition, the number of $CD4^+$ T_{cm} cells was significantly reduced and the absolute number of exhausted $CD4^+$ T cells was increased. Cerebral spinal fluid from individuals with LC also have elevated levels of $TIGIT^+$ $CD8^+$ T cells, consistent with possible immune exhaustion[41]. After stimulation, T cells from individuals with LC produced significantly more intracellular IL-2 (CD4, CD8), IL-4 (CD4), and IL-6 (CD8). Notably, subsets of participants with LC also had polyfunctional IL-4/IL-6 co-expressing $CD4^+$ T cells, which correlated with reactivity against EBV lytic antigens, but not against SARS-CoV-2 antigens. In aggregate, these findings may be consistent with T_H2-skewed CD4 T cell activation in response to EBV among participants with LC, as suggested for ME/CFS[42]. Levels of IgG against SARS-CoV-2 Spike and S1 in participants with LC were higher than those in vaccination-matched controls, consistent with persistent viral antigens[43–45].

Participants with LC from two sites had significantly decreased systemic cortisol levels; this remained significant after accounting for variations in demographics and sample-collection times. Interestingly, the decreased cortisol did not associate with a compensatory increase in ACTH levels, suggesting the hypothalamic-pituitary axis response to regulate cortisol may be inappropriately blunted. Importantly, ACTH has an extremely short half-life in plasma, which may impair accurately detecting changes. Dedicated studies must confirm these preliminary findings. Intriguingly, an earlier study of 61 survivors of SARS-CoV infection showed similar evidence of hypocortisolemia and blunted ACTH responses three months after acute disease[46]. Furthermore, decreased cortisol levels during the early phases of COVID-19

were associated with development of respiratory LC symptoms[47]. As cortisol is central for a variety of homeostatic and stress responses[48], the current finding of *persistently* lower cortisol levels in those with LC more than a year after acute infection warrants further investigations.

This study also revealed individuals with LC have elevated antibody responses against non-SARS-CoV-2 viral antigens, particularly EBV antigens. EBV viremia occurs during acute COVID-19 in hospitalised patients and predicts development of persistent symptoms in the post-acute period[47]. Other studies implicated recent EBV reactivation with LC development[49,50]. The observation here of elevated IgG against EBV lytic antigens suggests that recent reactivation of latent herpesviruses (EBV, VZV) may be a common feature of LC.

Finally, machine learning models designed to accurately classify LC and control populations (after matching individuals to account for potentially confounding features, like sex, age, days from symptom onset, and vaccination status) identified multiple features that significantly predict LC status. Classifications using only immunological data strongly agreed with classifications using survey scores (LCPS; Cohen's Kappa, 0.764), showing the immunological analyses and patient-reported outcomes used here were highly concordant in diagnosing LC.

This study has several limitations. Primary among these is that few participants were identified by convenience sampling and that recruitment strategies for cases differed from those for controls. Though broadly covering diverse biological features, this study used far fewer independent observations than traditional machine learning studies use (several thousands) to robustly train and optimise classification models. This study was also restricted to analysing peripheral (circulating) immune factors from participants. As LC often presents with organ system–specific dysfunctions, greater analyses of local immune features would crucially extend these findings. Further, analysis of autoantibodies was restricted to the exoproteome. Whether autoantibodies to intracellular antigens or non-protein antigens participate in LC pathogenesis was not tested.

In summary, significant biological differences were identified between participants with LC and demographically and medically matched CC and HC participants, validating extensive reports of persistent symptoms by various individuals with LC and patient advocacy groups. This study provides a basis for future investigations into the immunological underpinnings driving the genesis of LC.

References

1. Choutka, J., Jansari, V., Hornig, M. & Iwasaki, A. Unexplained post-acute infection syndromes. *Nat. Med.* **28**, 911–923 (2022).
2. Thaweethai, T. *et al.* Development of a Definition of Postacute Sequelae of SARS-CoV-2 Infection. *JAMA* (2023) doi:10.1001/jama.2023.8823.
3. Nalbandian, A. *et al.* Post-acute COVID-19 syndrome. *Nat. Med.* **27**, 601–615 (2021).
4. Michelen, M. *et al.* Characterising long COVID: a living systematic review. *BMJ Glob. Health* **6**, e005427 (2021).
5. Wiedemann, A. *et al.* Long-lasting severe immune dysfunction in Ebola virus disease survivors. *Nat. Commun.* **11**, 3730 (2020).
6. Hickie, I. *et al.* Post-infective and chronic fatigue syndromes precipitated by viral and non-viral pathogens: prospective cohort study. *BMJ* **333**, 575 (2006).
7. Paixão, E. S. *et al.* Chikungunya chronic disease: a systematic review and meta-analysis. *Trans. R. Soc. Trop. Med. Hyg.* **112**, 301–316 (2018).
8. Patel, H., Sander, B. & Nelder, M. P. Long-term sequelae of West Nile virus-related illness: a systematic review. *Lancet Infect. Dis.* **15**, 951–959 (2015).
9. Trojan, D. A. & Cashman, N. R. Post-poliomyelitis syndrome. *Muscle Nerve* **31**, 6–19 (2005).
10. Gowers, W. R. A Post-Graduate Lecture on the Nervous Sequelae of Influenza. *The Lancet* **142**, 73–76 (1893).

11. Althus, J. *Influenza : its pathology, symptoms, complications, and sequels its origin and mode of spreading and its diagnosis, prognosis, and treatment.* (Longmans, 1892).
12. Davis, H. E., McCorkell, L., Vogel, J. M. & Topol, E. J. Long COVID: major findings, mechanisms and recommendations. *Nat. Rev. Microbiol.* **21**, 133–146 (2023).
13. Dong, E., Du, H. & Gardner, L. An interactive web-based dashboard to track COVID-19 in real time. *Lancet Infect. Dis.* **20**, 533–534 (2020).
14. Lucas, C. *et al.* Longitudinal analyses reveal immunological misfiring in severe COVID-19. *Nature* **584**, 463–469 (2020).
15. Lucas, C. *et al.* Delayed production of neutralizing antibodies correlates with fatal COVID-19. *Nat. Med.* **27**, 1178–1186 (2021).
16. Wang, E. Y. *et al.* Diverse functional autoantibodies in patients with COVID-19. *Nature* **595**, 283–288 (2021).
17. Mathew, D. *et al.* Deep immune profiling of COVID-19 patients reveals distinct immunotypes with therapeutic implications. *Science* **369**, eabc8511 (2020).
18. Su, Y. *et al.* Multi-Omics Resolves a Sharp Disease-State Shift between Mild and Moderate COVID-19. *Cell* **183**, 1479-1495.e20 (2020).
19. Gupta, A. *et al.* Extrapulmonary manifestations of COVID-19. *Nat. Med.* **26**, 1017–1032 (2020).
20. Daugherty, S. E. *et al.* Risk of clinical sequelae after the acute phase of SARS-CoV-2 infection: retrospective cohort study. *BMJ* **373**, n1098 (2021).
21. DeVries, A., Shambhu, S., Sloop, S. & Overhage, J. M. One-Year Adverse Outcomes Among US Adults With Post-COVID-19 Condition vs Those Without COVID-19 in a Large Commercial Insurance Database. *JAMA Health Forum* **4**, e230010 (2023).
22. Dennis, A. *et al.* Multi-organ impairment and long COVID: a 1-year prospective, longitudinal cohort study. *J. R. Soc. Med.* 1410768231154703 (2023) doi:10.1177/01410768231154703.
23. Al-Aly, Z., Xie, Y. & Bowe, B. High-dimensional characterization of post-acute sequelae of COVID-19. *Nature* **594**, 259–264 (2021).
24. Xie, Y., Xu, E., Bowe, B. & Al-Aly, Z. Long-term cardiovascular outcomes of COVID-19. *Nat. Med.* **28**, 583–590 (2022).
25. Xu, E., Xie, Y. & Al-Aly, Z. Long-term neurologic outcomes of COVID-19. *Nat. Med.* **28**, 2406–2415 (2022).
26. Tabacof, L. *et al.* Post-acute COVID-19 Syndrome Negatively Impacts Physical Function, Cognitive Function, Health-Related Quality of Life, and Participation. *Am. J. Phys. Med. Rehabil.* **101**, 48–52 (2022).
27. Chen, C. *et al.* Global Prevalence of Post-Coronavirus Disease 2019 (COVID-19) Condition or Long COVID: A Meta-Analysis and Systematic Review. *J. Infect. Dis.* **226**, 1593–1607 (2022).
28. Ballering, A. V., van Zon, S. K. R., Olde Hartman, T. C., Rosmalen, J. G. M., & Lifelines Corona Research Initiative. Persistence of somatic symptoms after COVID-19 in the Netherlands: an observational cohort study. *Lancet Lond. Engl.* **400**, 452–461 (2022).
29. Poh, C. M. *et al.* Two linear epitopes on the SARS-CoV-2 spike protein that elicit neutralising antibodies in COVID-19 patients. *Nat. Commun.* **11**, 2806 (2020).
30. Li, Y. *et al.* Linear epitopes of SARS-CoV-2 spike protein elicit neutralizing antibodies in COVID-19 patients. *Cell. Mol. Immunol.* **17**, 1095–1097 (2020).
31. Wallukat, G. *et al.* Functional autoantibodies against G-protein coupled receptors in patients with persistent Long-COVID-19 symptoms. *J. Transl. Autoimmun.* **4**, 100100 (2021).
32. Szewczykowski, C. *et al.* Long COVID: Association of Functional Autoantibodies against G-Protein-Coupled Receptors with an Impaired Retinal Microcirculation. *Int. J. Mol. Sci.* **23**, 7209 (2022).
33. Kamath, K. *et al.* Antibody epitope repertoire analysis enables rapid antigen discovery and multiplex serology. *Sci. Rep.* **10**, 5294 (2020).
34. Fafi-Kremer, S. *et al.* Long-Term Shedding of Infectious Epstein-Barr Virus after Infectious Mononucleosis. *J. Infect. Dis.* **191**, 985–989 (2005).

35. Gordon, C. L. *et al.* Tissue reservoirs of antiviral T cell immunity in persistent human CMV infection. *J. Exp. Med.* **214**, 651–667 (2017).
36. Woodruff, M. C. *et al.* Chronic inflammation, neutrophil activity, and autoreactivity splits long COVID. *Nat. Commun.* **14**, 4201 (2023).
37. Altmann, D. M., Whettlock, E. M., Liu, S., Arachchillage, D. J. & Boyton, R. J. The immunology of long COVID. *Nat. Rev. Immunol.* (2023) doi:10.1038/s41577-023-00904-7.
38. Peluso, M. J. *et al. Multimodal Molecular Imaging Reveals Tissue-Based T Cell Activation and Viral RNA Persistence for Up to 2 Years Following COVID-19*. http://medrxiv.org/lookup/doi/10.1101/2023.07.27.23293177 (2023) doi:10.1101/2023.07.27.23293177.
39. Narasimhan, P. B., Marcovecchio, P., Hamers, A. A. J. & Hedrick, C. C. Nonclassical Monocytes in Health and Disease. *Annu. Rev. Immunol.* **37**, 439–456 (2019).
40. Merad, M., Sathe, P., Helft, J., Miller, J. & Mortha, A. The Dendritic Cell Lineage: Ontogeny and Function of Dendritic Cells and Their Subsets in the Steady State and the Inflamed Setting. *Annu. Rev. Immunol.* **31**, 563–604 (2013).
41. Mina, Y. *et al.* Deep Phenotyping of Neurologic Postacute Sequelae of SARS-CoV-2 Infection. *Neurol. - Neuroimmunol. Neuroinflammation* **10**, e200097 (2023).
42. Ruiz-Pablos, M., Paiva, B., Montero-Mateo, R., Garcia, N. & Zabaleta, A. Epstein-Barr Virus and the Origin of Myalgic Encephalomyelitis or Chronic Fatigue Syndrome. *Front. Immunol.* **12**, 656797 (2021).
43. Swank, Z. *et al.* Persistent Circulating Severe Acute Respiratory Syndrome Coronavirus 2 Spike Is Associated With Post-acute Coronavirus Disease 2019 Sequelae. *Clin. Infect. Dis.* **76**, e487–e490 (2023).
44. Stein, S. R. *et al.* SARS-CoV-2 infection and persistence in the human body and brain at autopsy. *Nature* **612**, 758–763 (2022).
45. Cheung, C. C. L. *et al.* Residual SARS-CoV-2 viral antigens detected in GI and hepatic tissues from five recovered patients with COVID-19. *Gut* **71**, 226–229 (2022).
46. Leow, M. K.-S. *et al.* Hypocortisolism in survivors of severe acute respiratory syndrome (SARS). *Clin. Endocrinol. (Oxf.)* **63**, 197–202 (2005).
47. Su, Y. *et al.* Multiple early factors anticipate post-acute COVID-19 sequelae. *Cell* **185**, 881-895.e20 (2022).
48. Husebye, E. S., Pearce, S. H., Krone, N. P. & Kämpe, O. Adrenal insufficiency. *The Lancet* **397**, 613–629 (2021).
49. Peluso, M. J. *et al.* Chronic viral coinfections differentially affect the likelihood of developing long COVID. *J. Clin. Invest.* **133**, e163669 (2023).
50. Gold, J. E., Okyay, R. A., Licht, W. E. & Hurley, D. J. Investigation of Long COVID Prevalence and Its Relationship to Epstein-Barr Virus Reactivation. *Pathog. Basel Switz.* **10**, 763 (2021).

Main Figure Legends

Figure 1. Demographic and clinical stratification of participants with Long COVID. (A) Schematic of MY-LC study. Numbers indicate participants after exclusion (see *'Methods'*). **(B)** Select demographics for LC (top row, purple) and CC (bottom row, yellow) groups. Centre values in 'Age' column represent average group values (n = 40 CC, 99 LC). Statistical significance is reported for relevant post-hoc comparisons ('Age') or Chi-square tests ('Sex' and 'Acute Disease Severity'). Complete statistical results are detailed in **Extended Data Table 2**. **(C)** Box plots of days from acute symptom onset between LC and CC groups. Significance was assessed using a two-tailed Brown-Mood median test with an alpha of 0.05 (n = 39 CC, 99 LC). **(D)** Box plots of LCPS for each individual (n = 35 HC, 20 CC, 98 LC). Significance was assessed using Kruskal-Wallis tests corrected for multiple comparisons using Bonferroni's method. **(E)** Prevalence of top 30 self-reported binary symptoms ranked from most prevalent (right) to least prevalent (left).

Symptoms are coloured according to common physiological system: Constitutional (Const., light green); Neurological (Neuro., blue); Pulmonary (Pulm., gold); Musculoskeletal (MSK, red); Gastrointestinal (GI, purple); Cardiac (dark green); Endocrine (Endo., pink); Ear, Nose, Throat (ENT, grey); and Sexual Dysfunction (Sex Dys., teal). For all box plots **(C,D)**, central lines indicate group medians; top and bottom lines indicate 75th and 25th percentiles, respectively; whiskers represent 1.5× IQR; and individual data points mark outliers. *Abbreviations: IQR, interquartile range; Long COVID propensity scores, LCPS. For **(A)**, clockwise, from top left: HCW, historical, unvaccinated SARS-CoV-2 exposed controls; Ext. LC, external participants with Long COVID; CC, convalescent infected individuals without persistent symptoms; LC, convalescent infected individuals with persistent symptoms; HC, healthy controls with no prior exposure. For **(E)**, top to bottom: EMR, electronic medical record; n.s., not significant; Dif., difficulty; UI, urination; Subj., subjective; Alt., altered; Decr., decreased; Abd., abdominal; reg., regulating; temp, body temperature; Musc, muscle; Indig., indigestion.*

Figure 2. Exaggerated SARS-CoV-2 specific humoral responses and altered circulating immune mediators among Long COVID participants. **(A)** SARS-CoV-2 antibody responses-assessed by ELISA (n = 22 HC, 17 CC, 70 LC). Vaccination status for each cohort is indicated by "x2" indicating the number of SARS-CoV-2 vaccine doses at sample collection. Significance for difference in group medians was assessed using Kruskal-Wallis with FDR (Benjamini-Hochberg) for multiple comparison. Central lines indicate group median values; whiskers, 95% CI estimates. **(B)** Coefficients from linear models are reported for various outcomes. Model predictors are indicated on x-axis. Significant predictors ($p \leq 0.05$) are in purple. Detailed model results are reported in **Extended Data Table 5. (C)** PIWAS line profiles of IgG binding within participants with >1 vaccine dose plotted along SARS-CoV-2 Spike amino acid sequence. Various Spike protein domains are indicated by coloured boxes (top). 95th percentile values are arranged by group: LC (purple, n = 80), HC (orange, n = 39) and CC (yellow, n = 38) with peaks ≥2.5 PIWAS value annotated by their consensus linear motif sequence (bold) and surrounding residues. Significantly enriched peaks in LC group are marked (*), as calculated by Outlier Sum statistics. **(D)** Three-dimensional mapping of LC-enriched motif sequences onto trimeric Spike protein. (S1, light grey; NTD, light blue; RBD, red; and S2, dark grey, with various LC-enriched motifs annotated.) (**E**) Box plots of z-score enrichments for IgG binding to Spike sequence KFLPFQQ amongst participants who have received ≥1 vaccine doses. A z-score >3 indicates significant binding relative to control populations. Box plots of z-score transformed cortisol **(F)** ACTH **(G)**, and sample-collection times **(H)** by group. Participants with potentially confounding medical comorbidities (e.g., pre-existing pituitary adenoma, adrenal insufficiency, oral steroid use) were removed before analysis. **(I)** Coefficients from linear models of cortisol levels. Significant predictors ($p \leq 0.05$) are in purple. Detailed model results are reported in **Extended Data Table 6**. Box plots **(E–H)** are represented as in **Fig. 1**. Significance for difference in group medians was assessed using Kruskal-Wallis with Bonferroni's correction for multiple comparison. *Abbreviations: ACTH, adrenocorticotropic hormone; NTD, N terminal domain; O.S., Outlier Sum; PIWAS, Protein-based Immunome Wide Association Study; RBD, receptor-binding domain; SP, signal peptide; VAD, vaccines at sample draw.*

Figure 3. Long COVID participants showed limited but selective autoantibodies against the human exoproteome. (A) Heatmap depicting REAP reactivities across the MY-LC cohort (n = 25 HC, 13 CC, 98 LC). Each column is one participant, grouped by cohort (for HC and CC) or by LCPS (for LC). Column clustering within groups was performed by k-means clustering. Each row represents one protein. Proteins were grouped using Human Protein Atlas mRNA expression data for different tissues. Reactivities depicted have at least one participant with a REAP score ≥3. **(B)** The number of autoantibody reactivities per individual by group. Significance assessed by Kruskal-Wallis. Box plots are represented as in **Fig. 1**. **(C)** Correlation plot depicting the relationship between number of autoantibody reactivities per individual and LCPS. Correlation was assessed by Spearman. Black line depicts linear regression with 95% CI shaded. Colours depict LC LCPS group (cluster 1, red; cluster 2, green; cluster 3, blue). Each dot represents one

individual. **(D)** Violin plot depicting the number of GPCR autoantibodies per individual. Significance assessed by Kruskal-Wallis. Each dot represents one individual. **(E)** Assessment of the frequency of individual autoantibody reactivities in participants with LC and controls. Significance assessed by Fisher's exact test. Y-axis depicts the negative $\log_{10}$ of unadjusted p-value, with the Bonferroni adjusted significance threshold depicted by the black dashed line. X-axis depicts the difference in the proportion of autoantibody positive individuals in each group. Each dot represents one autoantibody reactivity. *Abbreviations: CNS, central nervous system; GPCR, G-protein coupled receptor; Pit., pituitary.*

Figure 4. Long COVID participants demonstrate elevated levels of antibody responses to herpesviruses. (A) Violin plots depicting the REAP score distributions for SARS-CoV2 S1 RBD between LC (n = 69) and CC participants (n = 10) with two doses of mRNA vaccine. Statistical significance assessed by Wilcoxon rank-sum adjusted for multiple comparisons by Benjamini-Hochberg method. **(B)** Violin plots depicting the REAP score distributions for a given viral antigen between LC (n = 25 HC, 13 CC, 98 LC). Statistical significance assessed by Wilcoxon rank-sum adjusted for multiple comparisons by Benjamini-Hochberg method. Only antigens with ≥2 LC and ≥2 control individuals with reactivity were included. **(C)** Seropositivity as assessed by SERA for EBV amongst LC (n = 99) and control participants (n = 78). Significance assessed by Fisher's exact test adjusted for multiple comparisons by Benjamini-Hochberg method. **(D,E)** REAP scores amongst EBV-seropositive individuals only for EBV p23 **(D)** and gp42 **(E)** by group (n = 25 HC, 13 CC, 98 LC). **(F)** SERA-derived z-scores for gp42 motif PVXF[ND]K amongst EBV-seropositive individuals only plotted by group. Dashed line represents z-score threshold for epitope positivity defined by SERA **(**n = 39 HC, 38 CC, and 80 LC). **(G)** Three-dimensional mapping of LC-enriched linear peptide sequence PVXF[ND]K (magenta) onto EBV gp42 (purple) in complex with gH (light grey) and gL (dark grey) (PDB: 5T1D). **(H)** Correlation plot depicting the relationship between EBV gp42 PVXF[ND]K z-score and percent IL-4/IL-6 $CD4^+$ T cells (of total $CD4^+$ T cells) for participants. Only EBV-seropositive individuals were included. Correlation assessed by Spearman. Black line depicts linear regression with 95% CI shaded. **(**n = 39 HC, 38 CC, and 80 LC). **(I)** Correlation plot depicting the relationship between EBV p23 REAP score and percent $CD4^+$ TEMRA (of total $CD3^+$ T cells). Only EBV-seropositive individuals were included. Correlation assessed by Spearman. Black line depicts linear regression with 95% CI shaded. Colours depict LCPS Clusters as in **Fig. 3**. Box plots are represented as in **Fig. 1**. Statistical significance of difference in medians determined by Kruskal-Wallis. Post-hoc tests performed using Dunn's test with Holm's method to adjust for multiple comparisons. *Abbreviation: EBV, Epstein-Barr virus; REAP, rapid extracellular antigen profiling; SERA, serum epitope repertoire analysis; TM, transmembrane domain.*

Figure 5. Biochemical factors differentiate participants with Long COVID from matched controls. All data shown represent a matched subset of participants (n = 41 HC, 40 CC, 81 LC) selected by a Gale-Shapley procedure on demographic factors (**Extended Data Fig. 9A**). **(A)** PCA projection of participant data comprising cytokine, flow cytometry, and various antibody responses (α-SARS-CoV-2, non-SARS-CoV-2 viral antibodies, and aAb). Marginal histograms display data density along each principal component dimension. **(B)** ROC curve analysis from unsupervised KNN classification. AUC and 95% CI intervals (DeLong's Method) are reported. **(C)** McFadden's pseudo R-squared are reported as bar plot for each data segment. An integrated, parsimonious McFadden's pseudo R-squared is reported for the final classification model ('All'). **(D)** LASSO regression identifies a minimal set of immunologic features differentiating participants with LC from others. Unlabeled dots are significant predictive features not included in the final LASSO regression model. Dots are coloured according to individual data segments: orange, Flow; blue, plasma cytokines; pink, viral epitopes; green, α-SARS-CoV-2; yellow, aAb. *Abbreviations: aAb, autoantibodies; α-SARS-CoV-2, anti-SARS-CoV-2 antibodies; AUC, area under the curve; CI, confidence interval; Flow, flow cytometry; FPR, false positive rate; KNN, k-nearest neighbours;*

LC, Long COVID; PCA, principal component analysis; ROC, receiver operating characteristics; TPR, true positive rate.

Methods

Ethics Statement

This study was approved by the Mount Sinai Program for the Protection of Human Subjects (IRB #20-01758) and Yale Institutional Review Board (IRB #2000029451 for MY-LC; IRB #2000028924 for enrollment of pre-vaccinated Healthy Controls; HIC #2000026109 for External Long COVID). Informed consent was obtained from all enrolled participants.

MY-LC Study Design, Enrollment Strategy, and Inclusion / Exclusion Criteria

MY-LC was a cross-sectional, multi-site study comprised of five different groups with differing SARS-COV-2 exposure histories and varied Long COVID status. Participants enrolled in the Long COVID group underwent complete medical evaluations by physicians to rule out alternative medical etiologies for their persistent symptoms before study enrollment.

Participants with persistent symptoms following acute COVID-19 were recruited from Long COVID clinics within the Mount Sinai Healthcare System and the Center for Post COVID Care at Mount Sinai Hospital. Participants enrolled in healthy and convalescent study arms were recruited via IRB-approved advertisements delivered through email lists, study flyers located in hospital public spaces, and on social media platforms. Informed consent was provided by all participants at the time of enrollment. All participants provided peripheral blood samples and completed symptom surveys the day of sample collection (described below). Self-reported medical histories for all MY-LC participants were also collected at study visits and further reviewed through examination of electronic medical records by collaborating clinicians.

Inclusion criteria for individuals in the Long COVID group ("LC") were age ≥ 18 years; previous confirmed or probable COVID-19 infection (according to World Health Organization guidelines[51]); and persistent symptoms > 6 weeks following initial COVID-19 infection. Inclusion criteria for enrollment of individuals in the healthy control group ("HC") were age ≥ 18 years, no prior COVID-19 infection, and completion of a brief, semi-structured verbal screening with research staff confirming no active symptomatology. Inclusion criteria for individuals in the convalescent control group ("CC") were age ≥ 18 years; previous confirmed or probable prior COVID-19 infection; and completion of a brief, semi-structured verbal screening with research staff confirming no active symptomatology.

Pre-specified exclusion criteria for this study were inability to provide informed consent; and any condition preventing a blood test from being performed. Additionally, all participants had electronic health records reviewed by study clinicians following enrollment and were subsequently excluded prior to analyses for the following reasons: (1) current pregnancy, (2) immunosuppression equivalent to or exceeding prednisone 5 mg daily, (3) active malignancy or chemotherapy, and (4) any monogenic disorders. For specific immunological analyses, pre-existing medical conditions were additionally excluded prior to analyses due to high potential for confounding (e.g., participants with hypothyroidism were excluded prior to analysis of circulating T3/T4 levels; participants with pituitary adenomas were excluded prior to analysis of cortisol levels). Specific exclusions are marked by "Δ" in figures and detailed in relevant legends.

The recruitment of individuals in healthcare worker group (HCW) is described at length elsewhere[52]. Individuals in the external Long COVID group (Ext. LC) were identified from The Winchester Center for Lung Disease's Post-COVID-19 Recovery Program at Yale New Haven Hospital by collaborating

clinicians. All participants underwent medical evaluation for persistent symptoms following COVID-19. Participants from this group were identified retrospectively for inclusion in the MY-LC study according to the established MY-LC protocol: age ≥ 18 years; previous confirmed or probable COVID-19 infection (according to World Health Organization guidelines[39]); and persistent symptoms > 6 weeks following initial COVID-19 infection.

Participant Surveys

A comprehensive suite of surveys was administered to MY-LC study participants, combining validated patient-reported outcomes (PROs) with custom, purpose-developed tools by the MY-LC study team. Baseline demographic data collected from surveys included gender, age, body mass index (BMI), race, and medical comorbidities. Additionally, participants in the Long COVID and convalescent groups were asked to provide COVID-19 clinical data including date of symptom onset and acute disease severity (non-hospitalized vs. hospitalized), any SARS-CoV-2 polymerase chain reaction (PCR) diagnostic testing results, and any SARS-CoV-2 antibody testing results. Finally, all participants were asked to report SARS-CoV-2 vaccination status including date of vaccinations and vaccine brand.
At the time of blood collection, all participants completed PROs for fatigue (Fatigue Severity Scale (FSS) [53], fatigue visual analogue scale [F-VAS]), post-exertional malaise (DePaul Symptom Questionnaire Post-Exertional Malaise Short Form [DSQ-PEM Short Form])[54], breathlessness (Medical Research Council [MRC] Breathlessness Scale[55]), cognitive function (Neuro-QOL v2.0 Cognitive Function Short Form[56]), health-related quality of life (HRQoL) (EuroQol EQ-5D-5L[57]), anxiety (GAD-7[58]), depression (PHQ-2[59]), pain (P-VAS), sleep (Single-Item Sleep Quality Scale[60]), as well as pre- and post-COVID-19 employment status (author-developed). Lastly, participants in the MY-LC study were asked to self-report any current persistent symptoms from a study-provided list.

All survey data were collected and securely stored using REDCap[61,62] (Research Electronic Data Capture) electronic data capture tools hosted within the Mount Sinai Health System.

Long COVID Propensity Score (LCPS)

Calculation of propensity scores for each participant was achieved through construction of a multivariable logistic regression model generated with Long COVID vs. "Others" (Healthy Controls + Convalescent controls) as the outcome. The model candidate variables included survey responses from the following instruments described previously: FSS, F-VAS, DSQ-PEM Short Form, MRC Breathlessness Scale, Neuro-QOL v2.0 Cognitive Function Short Form, EQ-5D-5L, GAD-7, PHQ-2, P-VAS, Single-Item Sleep Quality Scale. Model selection using Akaike's Information Criteria (AIC) was used to select the final, parsimonious model. Odds ratios from the final model were normalized by dividing them by their respective standard error (SE) and rounding off to the nearest integer. These integer values were considered the score items for these specific variables and a cumulative prediction score for each subject was calculated by summation (*Equation 1*, below). As the score did not significantly differ between healthy controls and convalescent controls, the two control groups were combined as a single group ("Others") for final analysis. A ROC curve analysis was performed to identify the optimal cutoff for the LCPS using the maximum value of Youden's index J for Long COVID vs Others. A 10-fold cross-validation was used for internal validation and to obtain 95% confidence interval (CI) for the area under the curve (AUC). Data were analyzed using Stata version 16 (StataCorp, College Station, Texas).

$$Equation\ 1: LCPS = 7 * \sum GAD + 1 * \sum MRC + 2 * \sum PHQ2 + 3 \sum EQ5 + 28 * \sum FSS$$

Blood Sample Processing

Whole blood was collected in sodium-heparin-coated vacutainers (BD 367874, BD Biosciences) from participants at Mount Sinai Hospital in New York City, New York. Following blood draw, all participant samples were assigned unique MY-LC study identifiers and de-identified by clinical staff. Samples were couriered directly to Yale University in New Haven, CT the same day as the sample collection. Blood samples were processed on the same day as collection. Plasma samples were collected after centrifugation of whole blood at 600×g for 10 minutes at room temperature (RT) without brake. Plasma was then transferred to 15-mL polypropylene conical tubes, aliquoted, and stored at –80 °C. The peripheral blood mononuclear cell (PBMC) layer was isolated according to the manufacturer's instructions using SepMate tubes (StemCell). Cells were washed twice with phosphate-buffered saline (PBS) before counting. Pelleted cells were briefly treated with ACK lysis buffer (ThermoFisher) for 2 minutes and then counted. Viability was estimated using standard Trypan blue staining and a Countess II automated cell counter (ThermoFisher). PBMCs were stored at –80 °C for cryopreservation or plated directly for flow cytometry studies. Plasma samples from the External Long COVID group were obtained using BD Vacutainer CPT tubes (#362753) according to manufacturer's instructions and stored in aliquots at –80 °C prior to analysis.

Flow cytometry

Freshly isolated PBMCs were plated at 1–2 × 10^6 cells per well in a 96-well U-bottom plate. Cells were resuspended in Live/Dead Fixable Aqua (ThermoFisher) for 20 min at 4 °C. Cells were washed with PBS and followed by Human TruStain FcX (BioLegend) incubation for 10 min at RT. Cocktails of staining antibodies were added directly to this mixture for 30 minutes at RT. Prior to analysis, cells were washed and resuspended in 100 µl 4% PFA for 30 min at 4 °C. For intracellular cytokine staining following stimulation, the surface marker-stained cells were resuspended in 200 µl cRPMI (RPMI-1640 supplemented with 10% FBS, 2 mM L-glutamine, 100 U/ml penicillin, and 100 mg/ml streptomycin, 1 mM sodium pyruvate) and stored at 4 °C overnight. Subsequently, these cells were washed and stimulated with 1× Cell Stimulation Cocktail (eBioscience) in 200 µl cRPMI for 1 h at 37 °C. 50 µl of 5× Stimulation Cocktail in cRPMI (plus protein transport 442 inhibitor, eBioscience) was added for an additional 4 hours of incubation at 37 °C. Following stimulation, cells were washed and resuspended in 100 µl 4% paraformaldehyde for 30 min at 4 °C. To quantify intracellular cytokines, cells were permeabilized with 1× permeabilization buffer from the FOXP3/Transcription Factor Staining Buffer Set (eBioscience) for 10 min at 4 °C. All subsequent staining cocktails were made in this buffer. Permeabilized cells were then washed and resuspended in a cocktail containing Human TruStain FcX (BioLegend) for 10 min at 4 °C. Finally, intracellular staining cocktails were added directly to each sample for 1 h at 4 °C. Following this incubation, cells were washed and prepared for analysis on an Attune NXT (ThermoFisher). Data were analyzed using FlowJo software version 10.8 software (BD). Antibody information can be seen in **Supplementary Table 1**.

A PERMANOVA test was used to assess the relationship between all circulating immune cell populations presented in **Extended Data Fig. 2** and participant age, sex, Long COVID status, as well as BMI. The PERMANOVA test was run using the "VEGAN" package in R[63].

SARS-CoV-2 antibody testing by ELISA

ELISAs were performed as previously described[15]. Briefly, Triton X-100 and RNase A were added to plasma samples at final concentrations of 0.5% and 0.5 mg/ml, respectively, and incubated at room temperature for 30 minutes prior to use to reduce risk from any potential virus in plasma. MaxiSorp plates (96 wells; 442404, Thermo Scientific) were coated with 50 µl per well of recombinant SARS-CoV-2 Total S (SPN-C52H9-100 µg, ACROBiosystems), RBD (SPD-C52H3-100 µg, ACROBiosystems) and the nucleocapsid protein (NUN-C5227-100 µg, ACROBiosystems) at a concentration of 2 µg/ml in PBS and were incubated overnight at 4 °C. The coating was removed, and plates were incubated for 1 hour at room temperature with 200 µl of blocking solution (PBS with 0.1% Tween-20 and 3% milk powder). Plasma

was diluted serially at 1:100, 1:200, 1:400 and 1:800 in dilution solution (PBS with 0.1% Tween-20 and 1% milk powder), and 100 µl of diluted serum was added for 2 hours at room temperature. Human anti-spike (SARS-CoV-2 human anti-spike [AM006415; 91351, Active Motif] and anti-nucleocapsid SARS-CoV-2 human anti-nucleocapsid (1A6; MA5-35941, Active Motif) were serially diluted to generate a standard curve. Plates were washed three times with PBS-Tween (PBS with 0.1% Tween-20) and 50 µl of HRP anti-human IgG antibody (1:5,000; A00166, GenScript) added to each well in dilution solution. After 1 hour of incubation at room temperature, plates were washed six times with PBS-Tween. Plates were developed with 100 µl of TMB Substrate Reagent Set (555214, BD Biosciences) and the reaction was stopped after 5 min by the addition of 2N sulfuric acid. Plates were then read at an excitation/emission wavelength of 450 nm and 570 nm.

Multiplex proteomic analysis

Participant plasma was isolated and stored at –80 °C as described above. Plasma was shipped to Eve Technologies (Calgary, Alberta, Canada) on dry ice and analytes were measured using the following panels: Human Cytokine/Chemokine 71-plex Discovery Assay (HD71), Steroid/Thyroid 6plex Discovery Assay (STTHD), TGF-Beta 3-plex Discovery Assay (TGFβ1-3), Human Myokine Assay (HMYOMAG-10), Human Neuropeptide Assay (HNPMAG-05), Human Pituitary Assay (HPTP1), Human Cytokine P3 Assay (HCYP3-07), Human Cytokine Panel 4 Assay (HCYP4-19), Human Adipokine Panel 2 Assay (HADK2-03), Human Cardiovascular Disease Panel Assay (HDCVD9), Human CVD2 Assay (HCVD2-8), Human Complement Panel Assay (HDCMP1), Human Adipokine Assay (HDADK5). Analysis of plasma proteomics was completed in two batches with internal controls in each shipment to assess for and correct any analyte batch effects (described below)

To integrate analytes across batches, two samples from the same representative individuals from each group (2 from LC, 2 from CC, and 2 from HC) were measured in each analysis batch. The median difference between all paired samples between the first and second batch was used as an additive corrective factor to integrate samples across batches. After batch integration, each feature was z-scored using all measurements across both batches. Following z-scoring, features that were found to have persistent batch effects, as defined by a Wilcoxon rank sum test $p < 0.05$ post-correction, were not considered for downstream analysis.

Real-time Taqman assay for detection of EBV DNA

Nucleic Acid Extraction

Nucleic acid was extracted from 200uL freeze-thawed serum using the MagMAX Viral/Pathogen Nucleic Acid Isolation Kit (ThermoFisher, #A42352), automated on the KingFisher Flex (Thermo Fisher Scientific, Waltham, MA, USA) per manufacturer's protocol. The manufacturer's protocol was additionally modified to reduce salt carry-over by adding a third wash step with 500 µL 80% ethanol and eluting in 50 µL nuclease-free water.

Real-time Taqman PCR

PCR primers for the TaqMan assay were previously validated[64]: EBV p143 forward (5′-GGA.ACC.TGG.TCA.TCC.TTG.C) and EBV p143 reverse (5′ ACG.TGC.ATG.GAC.CGG.TTA.AT) (Thermo Fisher Scientific, Waltham, MA, USA). A fluorogenic probe (5'-(FAM)-CGC AGG CAC TCG TAC TGC TCG CT-(MGB)-3') with a FAM reporter molecule attached to the 5′ end and an MGB quencher linked at the 3′ end was acquired in parallel (Thermo Fisher Scientific). The PCR amplification was performed in a 20-µl volume containing 10 µL 2× Luna Universal Probe One-Step RT-qPCR Kit (New England BioLabs, Ipswich, MA, US), 300 pmol of each primer per µl, 200 pmol of the TaqMan

probe, and 5 µl of isolated DNA. Amplification and detection were performed on a CFX96 Touch instrument (Bio-Rad, Hercules, CA, US). After a 1-minute hold step at 95 °C, the PCR cycling program consisted of 42 two-step cycles of 15 s at 95 °C and 30 s at 60 °C. Real-time measurements were taken, and a threshold cycle (C_t) value for each sample was calculated if fluorescence exceeded a threshold limit. Each specimen was run in duplicate and was considered positive only if both replications were above the threshold limit. Each run contained multiple H2O controls (no template), and a standard curve containing serial dilutions of quantitative synthetic DNA (described below, ATCC, VR-3247SD). An additional EBV Plasma Control was included as a positive control for each assay plate (Thermo Fisher Scientific, #961231).

Estimating Genome Copy Number Standards

For standardization of qPCR detection of EBV viral genomes from participant plasma, a commercially available standard containing 5.59×10^8 EBV genome copies per ml (ATCC, VR-3247SD) was used. Serial log dilutions of this standard, ranging from 10^6 to 10^0 copies per ml, were made to establish the sensitivity of the TaqMan RT-PCR and included on each assay plate. The standard curve was created in the usual way by plotting the C_t values against the standard of known concentration. *x*-*y* scatter diagrams were drawn, and the correlation coefficient (r^2) was determined. Linear regression analysis was done using GraphPad Prism.

Linear Peptide Profiling

SERA serum screening

A detailed description of the SERA assay has been published[65]. For this study, plasma was incubated with a fully random 12-mer bacterial display peptide library (1×10^{10} diversity, 10-fold oversampled) at a 1:25 dilution in a 96-well, deep well plate format. Antibody-bound bacterial clones were selected with 50 µL Protein A/G Sera-Mag SpeedBeads (GE Life Sciences, #17152104010350) (IgG). The selected bacterial pools were resuspended in growth media and incubated at 37 °C shaking overnight at 300 RPM to propagate the bacteria. Plasmid purification, PCR amplification of peptide-encoding DNA and barcoding with well-specific indices was performed as described. Samples were normalized to a final concentration of 4 nM for each pool and run on the Illumina NextSeq500. Every 96-well plate of samples processed for this study contained healthy control run standards to assess and evaluate assay reproducibility and possible batch effects.

For IgM isotype screening by SERA, the above IgG protocol was adjusted as follows: 1) after serum incubation with the library, *E. coli* cells were centrifuged, the supernatant removed, and the cells were resuspended in 500 µL 1× PBS containing a 1:100 dilution of biotin-SP (long-spacer) conjugated donkey anti-Human IgM secondary antibody (Jackson Immunoresearch, 709-066-073); 2) The plate was incubated for 1 hour at 4 °C with orbital shaking (800 rpm), the cells were again centrifuged, supernatant removed, and cells were resuspended in 700 µL of 1× PBS + 100 µL of Dynabeads MyOne streptavidin T1 coated magnetic beads (ThermoFisher Scientific, 65601); 3) The plate was incubated for 1 hour at 4 °C with orbital shaking (800 rpm), after which time the plate was magnetized and the beads-antibody complex along with their bound peptide-bearing cells were captured. All subsequent steps were identical for IgG and IgM screening as described. IgM antibody repertoires were evaluated for Epstein-Barr virus antibodies in two ways; 4) Samples were analyzed on an existing EBV IgM epitope panel that was developed and validated on clinically confirmed mononucleosis patients and EBV IgM negative controls.

PIWAS analysis

The published PIWAS method[66] was used to identify antigen and epitope signals against the Uniprot reference SARS-CoV-2 proteome (UP000464024). For each sample, approximately 1–3 million 12-mers were obtained from the SERA assay and these were decomposed into constituent 5- and 6-mers. An enrichment score for each k-mer was calculated by dividing the number of unique 12-mers containing the k-mer divided by the number of expected k-mer reads for the sample, based on amino acid proportions in the sample. A z-score per k-mer was then calculated by comparing the enrichment score with those from a large pre-pandemic cohort (n = 1,500) on a log10 scale. A PIWAS value at each amino acid position along a protein sequence represents an averaged score within a 5 amino acid frame using the tiling z-scores of 5-mers and 6-mers spanning the sequence. 95th quantile bands were calculated based on each population separately.

Protein-wide identification of epitopes (PIE)

PIE methodology for epitope identification was performed to locate regions on a protein sequence that had stronger outlier signals in the case samples relative to control samples from a large pre-pandemic cohort (n = 1,500). The distribution of case sample values relative to the control was analyzed at each amino acid position on the SARS-CoV-2 Spike protein sequence. Specifically, at each position, all case and control sample values were normalized using median absolute deviation based on the distribution of the control sample values. An outlier threshold was defined as $Q_{75} + 1.5*(Q_{75} - Q_{25})$, where Q_x is the x^{th} percentile of the control values at that specific position[67]. An outlier sum statistic was then calculated as the sum of signal values above the outlier threshold in the case samples[68]. A null distribution for the outlier sum value was calculated by permuting case/control labels and recalculating 1000 times. A p-value was calculated based on a z-score by comparing the observed outlier sum statistic to the null distribution. A significant p-value threshold was set to 0.001 after false discovery rate (FDR) adjustment by the Benjamini–Hochberg procedure and an outlier sum threshold was set to the 99.5^{th} percentile value of all positions with FDR adjusted p-value > 0.001. All sequence positions that exceeded both thresholds were identified, and adjacent positions were merged into regions representing epitopes on the protein.

IMUNE-based motif discovery

Peptide motifs representing epitopes or mimotopes of SARS CoV-2-specific antibodies were discovered using the IMUNE algorithm[69]. A total of 164 antibody repertoires from 98 hospitalized subjects from the Yale IMPACT study were used for motif discovery. The majority of subjects were confirmed SARS CoV-2 positive by NAT. IMUNE compared ~30 disease repertoires with ~30 pre-pandemic controls and identified peptide patterns that were statistically enriched (p-value ≤ 0.01) in ≥25% of disease and absent from 100% of controls. Multiple assessments were run with different subsets of cases and controls. Peptide patterns identified by IMUNE were clustered using a point accepted mutation 30 (PAM30) matrix and combined into motifs. The output of IMUNE included hundreds of candidate IgG and IgM motifs. A motif was classified as positive in a given sample if the enrichment was ≥3 times the standard deviation above the mean of the training control set. The candidate motifs were further refined based on at least 98% specificity. The final set of motifs was validated for sensitivity and specificity on an additional 1,500 pre-pandemic controls and 406 unique confirmed COVID-19 cases from four separate cohorts.

Motif grouping by similarity

For SARS-CoV-2, motifs were grouped if they shared at least 3 of 5 amino acid identities, resulting in 76 motifs being assigned into 24 groups. The motif within an epitope group with the greatest sensitivity and mean enrichment was included in the SARS-CoV-2 Infection IgG panel results. In some cases, two motifs were selected from the same group since their combination improved sensitivity. The remaining motifs that did not fall into a group were further down-selected based on a specificity of >99.5%, leaving 24 additional motifs.

Rapid Extracellular Antigen Profiling (REAP)

REAP Library Expansion

The initial yeast library (Exo201) was generated as previously described[16,70]. In Exo201, only extracellular domains >49 amino acids in length were included in the library. To generate the library used for this study, Exo201 was with all extracellular domains of multi-pass membrane proteins greater than 15 amino acids and 225 extracellular viral antigens. DNA for new antigens was synthesized as either a Gene Fragment (for antigens over 300 nucleotides) or as an Oligo pool by TWIST Bioscience, containing a 5' sequence (CTGTTATTGCTAGCGTTTTAGCA) and 3' sequence (GCGGCCGCTTCTGGTGGC) for PCR amplification. The oligo pool was PCR amplified and transformed into yeast with barcode fragments, followed by barcode-antigen pairing identification as previously described[1,2]. This new yeast library was then pooled with the initial library (Exo201) in the ratio of 1:1 to generate the new version of the library (Exo205) which contained 6,452 unique antigens.

REAP Protocol

Participant IgG isolation and REAP selections were performed as previously described[16,70]. Briefly, IgG was purified from participant plasma using protein G magnetic beads followed by adsorption to yeast transformed with the pDD003 empty vector to remove yeast-reactive IgG. The Exo205 yeast library was induced in SGO-Ura medium, and 10^8 induced yeast cells were washed with PBE and added to wells of a sterile 96-well plate. 10 µg of purified participant IgG was added to the yeast library in duplicate in 100 µL PBE and incubated for 1 hour at 4C. Yeast cells were washed with PBE and incubated with 1:100 biotin anti-human IgG Fc antibody (clone QA19A42, Biolegend) for 30 minutes. Yeast cells were washed with PBE and incubated with a 1:20 dilution of Streptavidin MicroBeads (Miltenyi Biotec) for 30 minutes. Yeast were resuspended in PBE and IgG-bound yeast were isolated by positive magnetic selection using the MultiMACS M96 Separator (Miltenyi Biotec) according to manufacturer instructions. Selected yeast were resuspended in 1 mL SDO -Ura and incubated at 30 ºC for 24 hours and then plasmid DNA was harvested for NGS analysis. Briefly, DNA was extracted from yeast libraries using Zymoprep-96 Yeast Plasmid Miniprep kits or Zymoprep Yeast Plasmid Miniprep II kits (Zymo Research) according to standard manufacturer protocols. A first round of PCR was used to amplify a DNA sequence containing the protein display barcode on the yeast plasmid. A second round of PCR was performed on 1 µL step 1 PCR product using Nextera i5 and i7 dual-index library primers (Illumina). PCR products were pooled, run on a 1% agarose gel, and DNA corresponding to the band at 257 base pairs was cut. DNA (NGS library) was extracted using a QIAquick Gel Extraction Kit (Qiagen) according to standard manufacturer protocols. NGS library was sequenced using an Illumina NextSeq550 and an NextSeq high output sequencing kit with 75 base pair single-end sequencing according to standard manufacturer protocols. Approximately 500,000 reads (on average) per sample was collected and the pre-selection library was sampled at ten times greater read depth than other samples. Samples with less than 50,000 reads were classified as a sequencing failure and removed from further analysis.

REAP data analysis

REAP scores were calculated as previously described[16,70]. Briefly, barcode counts were extracted from raw NGS data using custom codes and counts from technical replicates were summed. Next, aggregate and clonal enrichment was calculated using edgeR[71] and custom computer scripts. Aggregate enrichment is the $\log_2$ fold change of all barcodes associated with a particular protein summed in the post-library relative to the pre-library, with zeroes in the place of negative fold changes. Log_2 fold change values for clonal enrichment were calculated in an identical manner, but barcode counts across all unique barcodes

associated with a given protein were not summed. Clonal enrichment for a given reactivity was defined as the fraction of clones out of total clones that were enriched ($\log_2$ fold change ≥ 2). Aggregate (E_a) and clonal enrichment (E_c) for a given protein, a scaling factor (β_u) based on the number of unique yeast clones (yeast that have a unique DNA barcode) displaying a given protein, and a scaling factor (β_f) based on the overall frequency of yeast in the library displaying a given protein were used as inputs to calculate the REAP score, which is defined as follows:

$$\text{Equation 2: REAP score} = E_a \times (E_c)^2 \times \beta_u \times \beta_f$$

β_u and β_f are logarithmic scaling factors that progressively penalize the REAP score of proteins with low numbers of unique barcodes or low frequencies in the library, and are described in detail in previous publications[16,70].

Antigens with an average REAP score greater than 0.5 across all samples were defined as non-specific and excluded from further analysis. Autoantibody reactivities were defined as antigens with REAP score greater than or equal to 1.

REAP Antigen ELISA Validation

96-well MaxiSorp plates (Thermo Scientific #442404) were coated with 200 ng per well of recombinant EBV p23 protein (ProSpec #ebv-274) in PBS and incubated overnight at 4 °C. Plates were dumped out and incubated with 3% Omniblock non-fat dry milk (American Bioanalytical #AB10109-00100) in PBS for 2 hours at RT. Plates were washed 3× with 200 ul wash buffer (PBS 0.05% Tween). Samples were diluted in 1% Omniblock non-fat dry milk in PBS and added to the plate to incubate 2 hours at RT. Plates were washed 6× with wash buffer. Goat anti-human IgG Fc HRP (Sigma Aldrich, #AP112P) diluted 1:10000 in 1% Omniblock non-fat dry milk in PBS was added to the plates and incubated 1 hour at RT. Plates were washed 6×. Plates were developed with 100 µl of TMB Substrate Reagent Set (BD Biosciences #555214) and the reaction was stopped after 5 min by the addition of 2 N sulfuric acid. Plates were then read at a wavelength of 450 nm.

Machine Learning

Data Preprocessing.

All collected data for immune profiling were collated. Features containing redundant information were manually removed from the dataset (e.g., nested flow cytometry populations include only the extant population).

All features were linearly scaled to unit variance and zero-centered using the R programming language base libraries[72,73]. Median absolute deviation was calculated for each feature across all samples, with missing values removed. Features with a median absolute deviation equal to zero or features where data was not available in at least half the samples were not included in downstream analysis. Prior to visualization of the data using principal component analysis, features were additionally quantile-normalized using the "normalize.quantiles" function of the "preprocessCore" package in R[74].

Gale-Shapley matching of participants by demographics.

To ensure that immunologic features of participants in the LC cohort would be compared against the most similar set of controls in the CC and HC cohorts, a Gale-Shapley matching procedure was employed[75]. Participants in the LC cohort were first matched against participants in the CC cohort. Unmatched

participants in the LC cohort were subsequently matched against participants in the HC cohort. Preference lists required by the Gale-Shapley algorithm were determined using an affinity function calculated as the cosine similarity of participants in a unit scaled and zero centered demographics matrix containing age, sex, vaccination status, and days from the initial onset of acute COVID-19. The matching was performed by the "galeShapley.marriageMarket" function of the "matchingR" package in R[72]. To evaluate matching efficacy, differences between groups in age, sex, vaccination status, acute COVID-19 hospitalization status, and days from initial onset of acute COVID-19 were assessed using a Chi-square test. For age, participants were segmented into groups as either less than 32 years of age, between 33 and 51 years of age, or greater than 52 years of age. For days from symptom onset, participants were segmented into groups as either 1–2 months from acute infection, 2–5 months from acute infection, 6–8 months from acute infection, or ≥9 months from acute infection. An alpha of 0.05 was used throughout.

Unsupervised Analysis.

Principal component analysis was performed on the set of normalized features for all matched participants [76]. To assess how well participants were grouped by all features, a k-nearest neighbor classifier with k=10 was applied separating participants with Long COVID from those without (either convalescent participants or healthy controls). A k of 10 was chosen by heuristic as approximately equal to the square root of the number of samples included[77]. A range of values for k from 5-15 were tested and found to give similar results. Area under the receiver operating characteristic curve (AUC) and 95% confidence intervals were calculated using DeLong's method; p-values were calculated using the Mann-Whitney U statistic[78,79].

Supervised Analysis.

Principal components regression was applied to each of a predefined set of data segments: autoantibodies, SARS-CoV-2 antibodies, non-SARS-CoV-2 viral antibodies, plasma proteomics, and flow cytometry readouts. The precise definitions of these data segments are provided as metadata. The first *n* principal components based on explained variance (see below for selection method) were selected from the normalized feature set and used to fit a logistic regression model (implemented as a binomial generalized linear regression with a logit link) for classification of participants with Long COVID as compared to matched convalescent participants without long term symptoms and uninfected controls.

To determine the optimal value for *n* (number of principal components), values were scanned, and seven-fold cross validation was performed on the data set. The average mean squared error was calculated for each cross-validation iteration at a particular value of *n*. For the binomial regression run using a logit link function, McFadden's pseudo-R^2 was calculated and averaged across each of the cross-validation folds.

Plots of explained variance and mean squared error across all scanned values for *n* were generated and visually inspected to choose an optimal value for *n* that maximized explained variance while minimizing overfitting as identified by increasing average mean squared error. This procedure was performed on each of the segments, and an optimal *n* was chosen for each of the following: autoantibodies ($n = 5$), SARS-CoV-2 antibodies ($n = 3$), non-SARS-CoV-2 viral antibodies ($n = 33$), plasma proteomics ($n = 20$), and flow cytometry ($n = 21$).

A model fitted on the first *n* principal components (or any linear transformation) was related to each of the original features as follows. Each principal component may be considered as a weighted linear combination of the original features. The principal component loading vectors were used to project the fitted beta values from the logistic regression model using the linearity of expectation, $E(X + Y) = E(X) + E(Y)$, such that the estimated parameter for each variable was the weighted sum of the parameter

estimates for the principal components to which it contributed. The variance of fit for each of the original features was similarly projected from the fitted principal components as the variance of a sum of random variables Var(X + Y) = Var(X) + Var(Y) + 2Cov(X, Y). P-values were calculated for each variable in the original feature space using z-scores.

Following per-segment model construction and evaluation, features with a Bonferroni-corrected p-value of less than 0.05 were selected for inclusion in a final principal components regression. These selected features were considered as a separate integrated data segment and processed in the same way as each individual data segment with a selected ($n = 9$) number of included principal components. A least absolute shrinkage and selection operator (LASSO) regression was employed to select a subset of the features with p-values less than 0.05 as a minimal model, and McFadden's pseudo-R^2 was calculated.

An implementation has been made publicly accessible as an R library on GitHub at (*https://github.com/rahuldhodapkar/puddlr*).

Symptom Bi-clustering.

Participants with Long COVID were clustered based on binary self-reporting of Long COVID symptoms. Hamming distance was used with complete linkage clustering as an agglomeration method. Visualization of the bi-clustering was performed using the '*ComplexHeatmap*' package in R[80]. Cluster stability was assessed by bootstrapped resampling with 100 iterations using the '*fpc*' package in R[81].

General Statistical Analysis

Study sample sizes were not pre-determined through formal power analysis. Specific statistical methodology can be found in relevant figure legends and manuscript text. Generally, comparison of immunophenotypic features including systemic cytokine levels and antibody concentrations between study cohorts was performed using estimates of group medians, primarily with non-parametric Kruskal-Wallis tests. All statistical tests were two sided.

The difference in median between the days from the symptom onset (DFSO) of acute COVID-19 in the LC and CC groups was assessed using a two-tailed Brown-Mood median test with an alpha of 0.05. The test was performed using the '*coin*' package in R[82]. Flow cytometry populations were assessed using estimates of group means with permutational testing using PERMANOVA to control for within-group heterogeneity (described above).

In cases where Kruskal-Wallis testing indicated significant differences, post-hoc testing using Dunn's test was performed. Correction for multiple comparisons was performed using Bonferroni or Bonferroni-Holm method as indicated. All statistical tests were performed using R, PRISM, and MATLAB software.

Data availability

All of the raw fcs files for the flow cytometry analysis are available at the FlowRepository platform (http://flowrepository.org/) under Repository ID: FR-FCM-Z6KL. Protein structures were visualized using UniProt repository under the following accession numbers: trimeric Spike (PDB: 6VXX) and EBV gH/gL (PDB: 5T1D). Raw data are included in Supplementary Table 3.

Code availability

Computer codes are available as indicated (e.g., https://github.com/rahuldhodapkar/puddlr) or otherwise available upon request.

Additional References

51. World Health Organization. Public health surveillance for COVID-19: interim guidance. (2022).
52. Lucas, C. *et al.* Impact of circulating SARS-CoV-2 variants on mRNA vaccine-induced immunity. *Nature* **600**, 523–529 (2021).
53. Krupp, L. B., LaRocca, N. G., Muir-Nash, J. & Steinberg, A. D. The fatigue severity scale. Application to patients with multiple sclerosis and systemic lupus erythematosus. *Arch. Neurol.* **46**, 1121–1123 (1989).
54. Cotler, J., Holtzman, C., Dudun, C. & Jason, L. A. A Brief Questionnaire to Assess Post-Exertional Malaise. *Diagn. Basel Switz.* **8**, 66 (2018).
55. Stenton, C. The MRC breathlessness scale. *Occup. Med. Oxf. Engl.* **58**, 226–227 (2008).
56. Iverson, G. L., Connors, E. J., Marsh, J. & Terry, D. P. Examining Normative Reference Values and Item-Level Symptom Endorsement for the Quality of Life in Neurological Disorders (Neuro-QoL^{TM}) v2.0 Cognitive Function-Short Form. *Arch. Clin. Neuropsychol. Off. J. Natl. Acad. Neuropsychol.* **36**, 126–134 (2021).
57. Herdman, M. *et al.* Development and preliminary testing of the new five-level version of EQ-5D (EQ-5D-5L). *Qual. Life Res. Int. J. Qual. Life Asp. Treat. Care Rehabil.* **20**, 1727–1736 (2011).
58. Spitzer, R. L., Kroenke, K., Williams, J. B. W. & Löwe, B. A brief measure for assessing generalized anxiety disorder: the GAD-7. *Arch. Intern. Med.* **166**, 1092–1097 (2006).
59. Kroenke, K., Spitzer, R. L. & Williams, J. B. W. The Patient Health Questionnaire-2: validity of a two-item depression screener. *Med. Care* **41**, 1284–1292 (2003).
60. Snyder, E., Cai, B., DeMuro, C., Morrison, M. F. & Ball, W. A New Single-Item Sleep Quality Scale: Results of Psychometric Evaluation in Patients With Chronic Primary Insomnia and Depression. *J. Clin. Sleep Med. JCSM Off. Publ. Am. Acad. Sleep Med.* **14**, 1849–1857 (2018).
61. Harris, P. A. *et al.* The REDCap consortium: Building an international community of software platform partners. *J. Biomed. Inform.* **95**, 103208 (2019).
62. Harris, P. A. *et al.* Research electronic data capture (REDCap)--a metadata-driven methodology and workflow process for providing translational research informatics support. *J. Biomed. Inform.* **42**, 377–381 (2009).
63. Jari Oksanen [aut, cre], Gavin L. Simpson [aut], F. Guillaume Blanchet [aut], Roeland Kindt [aut], Pierre Legendre [aut], Peter R. Minchin [aut], R.B. O'Hara [aut], Peter Solymos [aut], M. Henry H. Stevens [aut], Eduard Szoecs [aut], Helene Wagner [aut], Matt Barbour [aut], Michael Bedward [aut], Ben Bolker [aut], Daniel Borcard [aut], Gustavo Carvalho [aut], Michael Chirico [aut], Miquel De Caceres [aut], Sebastien Durand [aut], Heloisa Beatriz Antoniazi Evangelista [aut], Rich FitzJohn [aut], Michael Friendly [aut], Brendan Furneaux [aut], Geoffrey Hannigan [aut], Mark O. Hill [aut], Leo Lahti [aut], Dan McGlinn [aut], Marie-Helene Ouellette [aut], Eduardo Ribeiro Cunha [aut], Tyler Smith [aut], Adrian Stier [aut], Cajo J.F. Ter Braak [aut], James Weedon [aut]. vegan: Community Ecology Package.
64. Niesters, H. G. *et al.* Development of a real-time quantitative assay for detection of Epstein-Barr virus. *J. Clin. Microbiol.* **38**, 712–715 (2000).
65. Kamath, K. *et al.* Antibody epitope repertoire analysis enables rapid antigen discovery and multiplex serology. *Sci. Rep.* **10**, 5294 (2020).
66. Haynes, W. A., Kamath, K., Waitz, R., Daugherty, P. S. & Shon, J. C. Protein-Based Immunome Wide Association Studies (PIWAS) for the Discovery of Significant Disease-Associated Antigens. *Front. Immunol.* **12**, 625311 (2021).
67. Tukey, J. W. *Exploratory data analysis*. (Addison-Wesley Pub. Co, 1977).
68. Tibshirani, R. & Hastie, T. Outlier sums for differential gene expression analysis. *Biostatistics* **8**, 2–8 (2007).

69. Pantazes, R. J. *et al.* Identification of disease-specific motifs in the antibody specificity repertoire via next-generation sequencing. *Sci. Rep.* **6**, 30312 (2016).
70. Wang, E. Y. *et al.* High-throughput identification of autoantibodies that target the human exoproteome. *Cell Rep. Methods* **2**, 100172 (2022).
71. Robinson, M. D., McCarthy, D. J. & Smyth, G. K. edgeR : a Bioconductor package for differential expression analysis of digital gene expression data. *Bioinformatics* **26**, 139–140 (2010).
72. R Core Team, R. R: A language and environment for statistical computing. (2013).
73. Wickham, H. *ggplot2: Elegant Graphics for Data Analysis*. (Springer New York, 2009). doi:10.1007/978-0-387-98141-3.
74. Bolstad, B. M., Irizarry, R. A., Åstrand, M. & Speed, T. P. A comparison of normalization methods for high densityoligonucleotide array data based on variance and bias. *Bioinformatics* **19**, 185–193 (2003).
75. Gale, D. & Shapley, L. S. College Admissions and the Stability of Marriage. *Am. Math. Mon.* **69**, 9–15 (1962).
76. Becht, E. *et al.* Dimensionality reduction for visualizing single-cell data using UMAP. *Nat. Biotechnol.* **37**, 38–44 (2019).
77. Zhang, Z. Introduction to machine learning: k-nearest neighbors. *Ann. Transl. Med.* **4**, 218–218 (2016).
78. Robin, X. *et al.* pROC: an open-source package for R and S+ to analyze and compare ROC curves. *BMC Bioinformatics* **12**, 77 (2011).
79. DeLong, E. R., DeLong, D. M. & Clarke-Pearson, D. L. Comparing the areas under two or more correlated receiver operating characteristic curves: a nonparametric approach. *Biometrics* **44**, 837–845 (1988).
80. Gu, Z., Eils, R. & Schlesner, M. Complex heatmaps reveal patterns and correlations in multidimensional genomic data. *Bioinforma. Oxf. Engl.* **32**, 2847–2849 (2016).
81. Christian Hennig. Flexible Procedures for Clustering.
82. Hothorn, T., Hornik, K., van de Wiel, M. A. & Zeileis, A. Implementing a Class of Permutation Tests: The coin Package. *J. Stat. Softw.* **28**, 1–23 (2008).

Acknowledgments

The authors would like to express their immense gratitude for the community of MY-LC study participants who volunteered both their time and effort in aiding the completion of this study, and who also helped inform and educate on the effective and equitable communication of the results from this study. Various graphical schematics were created with BioRender.com. The authors would also like to thank Sumit Borah for helpful commentary on this manuscript. This work was supported by grants from National Institute of Allergy and Infectious Diseases (R01AI157488 to A.I.), FDA Office of Women's Health Research Centers of Excellence in Regulatory Science and Innovation (CERSI) (to A.I.), Fast Grant from Emergent Ventures at the Mercatus Center (to A.I.), RTW Foundation (D.P.), the Howard Hughes Medical Institute Collaborative COVID-19 Initiative (to A.I. and R.M.), and the Howard Hughes Medical Institute (to A.I. and R.M.).

Author contributions

Experimental conceptualization, methodology, and data visualization were performed by J.K., J.W., J.J. P.L., R.D., J.G., A.T., A.A.M., K.K., K.G., V.M., M.P., S.O. E.S., A.C.G., M.M.; formal analysis conducted by J.K., J.J., P.L. R.D., A.T., A.D., L.G. and A.A.M.; resources provided by D.V.D., A.M.R., D.P., and A.I.; clinical review of electronic health records was performed by J.K., J.W., J.G. and L.T.; sample collection, processing, and biospecimen validation were performed by J.K.; J.W., J.J., P.L., J.G., A.T., L.T., V.M., M.P., T.M., B.B., T.K., C.L., J.S., D.M., E.B., J.T.M., K.A., T.J.Z., L.X., Y.D., E.P., K.A., I.O., G.V, D.L., J.P. C.S.D.; writing – original draft by J.K. and A.I.; writing – review & editing by

J.K., J.W., J.J. P.L., R.D., J.G., A.T., A.A.M., K.K., K.G., N.K., H.K., D.V.D., A.M.R., D.P., and A.I.; data curation by J.K., J.J., R.D.; supervised by D.V.D., A.M.R., D.P. and A.I.; funding acquisition by D.V.D., A.M.R., D.P. and A.I.

Declaration of Interests

In the past three years, H.K. received expenses and/or personal fees from UnitedHealth, Element Science, Eyedentifeye, and F-Prime. He is a co-founder of Refactor Health and HugoHealth, and is associated with contracts, through Yale New Haven Hospital, from the Centers for Medicare & Medicaid Services and through Yale University from the Food and Drug Administration, Johnson & Johnson, Google, and Pfizer. N.K. is a scientific founder at Thyron, served as a consultant to Boehringer Ingelheim, Pliant, Astra Zeneca, RohBar, Veracyte, Galapagos, Fibrogen, and Thyron over the last 3 years, reports equity in Pliant and Thyron, and acknowledges grants from Veracyte, Boehringer Ingelheim, BMS. A. I. co-founded and consults for RIGImmune, Xanadu Bio and PanV, consults for Paratus Sciences, InvisiShield Technologies, and is a member of the Board of Directors of Roche Holding Ltd. A.M.R. and Y.D. are inventors of a patent describing the REAP technology. A.M.R. is the founder and director of Seranova Bio; and A.M.R. and Y.D. hold equity in Seranova Bio. All other authors have no conflict of interest to declare.

Additional Information

Supplementary information is included within this manuscript as Supplementary Tables 1-3.

Correspondence and requests for materials should be addressed to: A.I., D.P., A.M.R., and D.V.D.

Extended Data Figure Legends

Extended Data Figure 1. Additional demographic and clinical analysis of Long COVID cohort. (A) Box plots of Min-Max normalized survey responses (n = 35 HC, 20 CC, 98 LC). Individual survey instruments are arranged in columns with corresponding health dimensions below. Surveys in red were aggregated to generate Long COVID Propensity Scores (LCPS). Significance was assessed using Kruskal-Wallis tests corrected for multiple comparisons using Bonferroni's method. **(B)** Receiver-Operator Curve (ROC) analysis of LCPS scores. Area under the curve (AUC) is reported with Bootstrap Bias-corrected 95% confidence intervals (CI) of AUC. **(C)** Ring plots of prevalence of Postural Orthostatic Tachycardia Syndrome (POTS) among Long COVID cohort. "No diagnosis" is represented by grey regions, "positive diagnosis" is represented by shaded purple regions. Purple regions are further stratified by diagnostic modality: clinical = diagnosed through clinical evaluation (light purple); Tilt-table = diagnosed by Tilt-table (middle purple); Stand / Lean = diagnosed by Stand / LEAN test (dark purple). **(D)** Ring plots of prevalence of self-reported negative impacts on employments status among individuals with Long COVID. Negative responses are represented by grey region, positive responses are indicated by purple region. **(E)** Heatmap of self-reported binary symptoms clustered by Hamming distances (rows and columns) and colored according to physiological system as previous. Columns are annotated by LCPS scores with bootstrapped cluster reproducibility scores reported in parentheses (bootstrapped Jaccard similarity) **(F)** Boxplots of Long Covid Propensity Score (LCPS) plotted by group (HC = healthy control; CC = convalescent control; LC = Long COVID) and cluster. Central lines represent group medians, bottom and top lines represent 25th and 75th percentiles, respectively. Whiskers represent 1.5× inter-quartile range (IQR). Significance for difference in median LCPS was assessed using Kruskal-Wallis with correction for multiple comparisons using Bonferroni-Holm.

Extended Data Figure 2. Immunological differences in myeloid and lymphocyte effectors among participants with Long COVID. (A-B) Violin plots of myeloid peripheral blood mononuclear populations (PBMCs) plotted by group as percentages of respective parent populations (gating schemes detailed in

Extended Data Fig. 10). **(B, right)** Coefficients from linear model are shown. Model predictors are indicated on x-axis. Significant predictors ($p \leq 0.05$) are plotted in purple. Detailed model results are reported in **Extended Data Table 4**. **(C)** Violin plots of B lymphocyte subsets from PBMCs plotted as percentages of respective parent populations (gating schemes detailed in **Extended Data Fig. 10**). **(D,E)** Violin plots of various CD4 (top row) and CD8 (bottom row) populations. (**F**) Violin plots of IL-4 and IL-6 double-positive $CD4^+$ (left) and $CD8^+$ (right) T cells plotted as percentages of total $CD4^+$ or $CD8^+$ T cells. **(G)** A PERMANOVA test of the association between all cell populations shown and participant age, sex, LC status, and body mass index (BMI). For all violin plots **(A–F)**, significance was assessed using Kruskal-Wallis corrected for multiple comparisons using Bonferroni-Holm. Each dot represents a single patient (n = 40 HC, 33 CC, 99 LC). Central bars indicate the median value of each group. Only significant differences between group medians are shown.

Extended Data Figure 3. Circulating myeloid, B cell, and cytokine producing immune cell populations among MY-LC participants. (A–I) Violin plots of various myeloid, B, and T cell PBMC populations stratified by healthy (HC), convalescent (CC), and Long COVID (LC) groups. Significance for differences in group medians was assessed using Kruskal-Wallis tests with correction for multiple comparisons using Bonferroni-Holm. Each dot represents a single patient (n = 40 HC, 33 CC, 99 LC) **(J–K)** Coefficients from linear models for various PBMC populations. Bars in purple indicate significant predictors of specific PBMC populations ($p \leq 0.05$).

Extended Data Figure 4. Absolute Counts of in myeloid and lymphocyte effectors among participants with Long COVID. (A-B) Violin plots of myeloid peripheral blood mononuclear populations (PBMCs) plotted by group (HC, healthy control; CC, convalescent control; LC, Long COVID) as absolute cell counts (gating schemes detailed in **Extended Data Figure 10A**). Significance for differences in group medians was assessed using Kruskal-Wallis tests with correction for multiple comparisons using Bonferroni-Holm. **(C)** Violin plots of B lymphocyte subsets from peripheral blood mononuclear populations (PBMCs) plotted as absolute cell counts (gating schemes detailed in **Extended Data Figure 10D**). Significance was assessed using Kruskal-Wallis with correction for multiple comparison using Bonferroni-Holm. **(D, E)** Violin plots of various CD4 (top row) and CD8 (bottom row) populations. Significance was assessed using Kruskal-Wallis with correction for multiple comparison using Bonferroni-Holm. (**F**) Violin plots of IL-4 and IL-6 double positive $CD4^+$ (left) and $CD8^+$ (right) T cells plotted as absolute cell counts. Significance was assessed using Kruskal-Wallis with correction for multiple comparison using Bonferroni-Holm. For all plots **(A–F)**, central bar in the violin plot indicated the median value of each group. Each dot represents a single patient (n = 37 HC, 28 CC, 94 LC)**.**

Extended Data Figure 5. Humoral Analysis of SARS-CoV-2 specific antibodies. (**A**) Dot plots of IgG concentrations from historical, unvaccinated SARS-CoV-2 exposed controls (HCW+) and unvaccinated Long COVID participants. Central lines indicate median group values with bars representing 95% CI estimates. Vaccination status for each cohort is indicated by the form "x0" where the digit indicates the number of SARS-CoV-2 vaccine doses. Significance for differences in group medians were assessed using Kruskal-Wallis with correction for multiple comparison using FDR (Benjamini-Hochberg). Each dot represents a single patient (n = 19 HCW, 19 LC). (**B**) Coefficients from linear models are reported for anti-RBD antibody responses. Model predictors are reported along the x-axis and included age, sex (categorical), Long COVID status (categorical), body mass index (BMI), and number of vaccinations at blood draw. Significant predictors ($p \leq 0.05$) are plotted in purple. Detailed model results are reported in **Extended Data Table 5**. (**C**) Boxplots of antibody binding to various SARS-CoV-2 linear peptide sequences plotted by group (HC = healthy control; CC = convalescent control; LC = Long COVID) amongst participants who have received 1 or more vaccine doses. Each dot represents one individual. Central bars represent groups medians, with bottom and top bars representing 25^{th} and 75^{th} percentiles, respectively. Dashed line

represents z-score threshold for epitope positivity defined by SERA. Statistical significance determined by Kruskal-Wallis with correction for multiple comparisons using Bonferroni-Holm. Each dot represents an individual patient: LC (purple, n = 80), HC (orange, n = 39) and CC (yellow, n = 38). **(D)** Proportion of each group amongst participants who have received 1 or more vaccine doses (LC: n = 80, control: n = 77) that is seropositive (z-score ≥ 3) for each of 7 linear Spike motifs mapping to outlier peaks. Motifs with significantly different seropositivity between groups are highlighted in red, as determined by Fisher's exact test corrected for multiple comparisons by FDR (Benjamini-Hochberg). **(E)** Coefficients from linear models are reported for anti-RBD antibody responses. Model predictors are reported along the x-axis and included age, sex (categorical), Long COVID status (categorical), body mass index (BMI), and number of vaccinations at blood draw. Significant predictors ($p \leq 0.05$) are plotted in purple. Detailed model results are reported in **Extended Data Table 5**. *Abbreviation: HCW+, previously SARS-CoV-2 infected healthcare worker.*

Extended Data Figure 6. Significantly different soluble plasma factors across MY-LC cohorts. (A–H) Violin plots of various z-score transformed circulating plasma factors across healthy (HC), convalescent (CC), and Long COVID (LC) cohorts. Significance of difference in group medians was assessed using Kruskal-Wallis corrected for multiple comparisons using Bonferroni's method. P-values from multiple Kruskal-Wallis testing were adjusted using the Benjamini-Hochberg procedure. **(I)** Negative Log_{10} transformed p-values from Kruskal-Wallis tests plotted against Spearman correlations with LCPS for various plasma factors. Reported p-values are adjusted for multiple comparisons using FDR (Benjamini-Hochberg). Horizontal line represents significance threshold for a difference in group medians. Vertical lines represent the minimum correlation values for plasma factors significantly correlating with LCPS scores. Red depicts factors with significant differences in group medians and significant correlations with LCPS.

Extended Data Figure 7. Analysis of private autoantibodies within the MY-LC cohort. (A–B) Correlation plots depicting relationships between number of autoantibody reactivities and %DN of B cells **(A)** or days from symptom onset (DFSO) and number of autoantibody reactivities **(B)**. For all panels, correlation was assessed using Spearman's method. Black line depicts linear regression with 95% CI shaded. Colors depict Long COVID cluster (cluster 3, blue; cluster 2, green; cluster 1, red). Each dot represents one individual. **(C)** Grouped box plot depicting reactivity magnitude per individual in the listed GO Process domain. Reactivity magnitude is calculated as the sum of REAP scores for all reactivities per individual in a given GO Process domain. Statistical significance assessed by Kruskal-Wallis and adjusted for multiple comparisons using FDR (Benjamini-Hochberg) correction. Boxplot colored box depicts 25th to 75th percentile of the data, with the middle line representing the median, and outliers depicted as points. **(D)** Heatmap depicting autoantibody reactivity for GPCRs included in the REAP library. Each column is one participant, grouped by control or LCPS cluster. HC = healthy control, CC = convalescent control, LC = Long COVID. *Abbreviations: GPCR = G-protein coupled receptor.*

Extended Data Figure 8. Non-SARS-CoV-2 humoral responses among participants with Long COVID. (A) Heatmap depicting REAP reactivities to viral antigens across the MY-LC cohort. Each column is one participant, grouped by control or LCPS cluster. Column clustering within groups performed by K-means clustering. Each row is one viral protein. Reactivities depicted have at least one participant with a REAP score >= 2. **(B)** REAP scores for VZV gE by group (HC = healthy control; CC = convalescent control; LC = Long COVID). Statistical significance determined by Kruskal Wallis with correction for multiple comparison using Bonferroni-Holm. Each dot represents one individual (n = 25 HC, 13 CC, 98 LC). Bottom and top lines depict 25th to 75th percentile of the data, with the middle line representing the median. Whiskers represent 1.5x the inter-quartile range (IQR). **(C)** Proportion of each group (LC: n = 99, control: n = 78) seropositive for each of 30 common pathogen panels as determined by SERA, grouped by pathogen-type (LC = Long COVID). Statistical significance determined by Fisher's exact test corrected

with FDR (Benjamini Hochberg). **(D)** Sum of SERA-derived z-scores for IgM reactivity to EBV antigens plotted by group. Statistical significance determined by Kruskal-Wallis with correction for multiple comparison using Bonferroni-Holm. Each dot represents one individual (n = 22 Mono-control, 40 HC, 38 CC, 98 LC). Boxplot colored box depicts 25th to 75th percentile of the data, with the middle line representing the median. Whiskers represent 1.5× the inter-quartile range (IQR). **(E)** Standard curve for Taqman PCR of EBV *BNRF1*. Serial dilutions of EBV standard ranging from 1 to 10^6 copies per 200 uL input material were made. C_t values are plotted against standard copy number, demonstrating ability to detect 1 genome copy. **(F)** Copies of EBV genome detected in participant serum by Taqman PCR for EBV *BNRF1* plotted by group. All samples were below the limit of detection. **(G)** Correlation plot depicting the relationship between EBV p23 REAP score and EBV p23 ELISA O.D. 450 nm. Correlation assessed by Spearman. Black line depicts linear regression with 95% CI shaded. Colors depict group (purple, LC; yellow, CC; orange, HC). Each dot represents one individual. **(H,I)** REAP scores for HSV1 gD1 (H) and HSV1 gL (I) amongst HSV1 seropositive individuals only, separated by group (HC = healthy control; CC = convalescent control; LC = Long COVID). Statistical significance determined by Kruskal Wallis with correction for multiple comparison using Bonferroni-Holm. Each dot represents one individual. Boxplot colored box depicts 25th to 75th percentile of the data, with the middle line representing the median. Whiskers represent 1.5× the inter-quartile range (IQR). Each dot represents one individual. **(J,K)** Correlation plot depicting the relationship between Long COVID Propensity Score (LCPS) and EBV gp42 PVXF[ND]K (J) or EBV p23 REAP score (K). Correlation assessed by Spearman. Each dot represents one individual. Colors depict Long COVID cluster (cluster 1, blue; cluster 2, green; cluster 3, red). Black line depicts the linear regression, with the 95% CI shaded. (**L-O**) Linear regressions of various SARS-CoV-2 antigens and IL-4/IL-6 double positive CD4 T cells. Spearman's correlation were calculated for each pair of variables, with corresponding p-values reported. Black lines depict linear regressions with the shaded area representing 95% confidence boundaries.

Extended Data Figure 9. Gale-Shapley matching of Long COVID group and controls harmonizes samples by disease and demographics characteristics. (A) Features used in the preference list construction for Gale-Shapley matching are shown. Individual paired samples are shown for participant age and days from initial acute COVID-19 infection (dfso). Paired plots for sex and vaccination status are shown. **(B)** Additionally, differences between populations in the severity of initial acute COVID-19 infection are shown. No differences between groups are significant by a Chi-square test. **(C,D)** Box plots of selected features assessed in the Ext. LC group. Center lines represent median values with error bars representing 1.5 standard deviation. **(E)** Distribution of respiratory symptoms ("dyspnea" or "shortness of breath") between individuals with Long COVID in the MY-LC study and the Ext. LC group. Significance was assessed using Fisher's exact test. **(F–H)** ROC curve analysis using cortisol, cDC1, and galectin-1 levels as an individual classifier of Long COVID status. AUC and 95% CI intervals (DeLong's Method) for each feature are displayed (top). Kernel-density smoothed histograms for HC, CC and LC cohorts for selected model predictors. Vertical lines depict threshold values for each feature with maximal discriminatory accuracy (bottom).

Extended Data Figure 10. Flow Cytometry gating schematics. (A–D). Various gating strategies for granulocyte and myeloid populations **(A)**, T lymphocytes **(B)**, intracellular cytokine staining **(C),** and B lymphocytes **(D)**.

Extended Data Table Legends

Extended Data Table 1. Clinical Demographics of MY-LC Cohort. Summary demographic and clinical characteristics for the MY-LC Study. Participants were stratified into three study arms at enrollment: (1) Long COVID (prior SARS-CoV-2 infection with persistent, unexplained symptoms); (2) healthy study site cohort (no prior SARS-CoV-2 infection); or (3) convalescent COVID-19 cohort (prior SARS-CoV-2

infection without persistent symptoms). Various demographic features and clinical characteristics are reported by row for each cohort (row measurement units are specified in parentheses). Within each cell, counts or clinical feature averages are reported, with sample standard deviations, relative cohort percentages, and participant numbers reported where pertinent. Results from statistical tests are reported as p-values and accompanying test statistics: † Chi-square test p-value (Chi-square test statistic, degrees of freedom (df)); †† Kruskal-Wallis ANOVA p-value; ††† Fisher's exact test p-value (Odd's Ratio: [95% Confidence Interval (Baptista-Pike)]); ‡ Mann-Whitney U test p-value. Post-hoc comparisons were conducted using Dunn's test with Tukey's correction for multiple comparison (column comparison order left-right: 1-2, 1-3, 2-3). Participant medical histories were collected and collated from binary self-reports of prior medical history and review of electronic medical records by study staff (positive responses in either participant self-report or EMR review were considered an overall binary positive response). Abbreviations: *n, number; M, male; F, female; BMI, body mass index; +PCR, positive result from SARS-CoV-2 nucleic acid test; +Ab, positive result from SARS-CoV-2 antibody test; Y, Yes; N, No.*

Extended Data Table 2. Normalized survey responses across MY-LC cohorts. Survey responses for participants are organized by individual instruments (columns) and MY-LC cohorts (rows). Participant responses for each survey instrument were summed and normalized using standard min-max normalization procedures such that a value of 1 equals the maximum possible aggregate score and 0 equals the minimum possible aggregate score. Additionally, individual survey elements were oriented through inversion such that higher normalized scores on each instrument indicate a higher intensity or degree of agreement with survey prompts. For each cohort, median values are displayed.

Extended Data Table 3. Determinations of optimal LCPS threshold. Classification metrics across different LCPS thresholds ('Cut-offs') (*Upper table*). Summary area-under the curve (AUC) statistics and bootstrap confidence intervals for Receiver-Operator curve analysis (ROC) (*lower table*)

Extended Data Table 4. Modeling of select flow cytometry populations. (A–L) Detailed linear modeling results are reported for various cytokine producing T cell populations analyzed by flow cytometry.

Extended Data Table 5. Modeling of anti-SARS-CoV-2 antibody and linear motif responses. (A–E) Detailed linear modeling results are reported for SARS-CoV-2 specific antibody responses and peptide motifs with corresponding model formulations.

Extended Data Table 6. Modeling of cortisol levels. Detailed linear modeling results are reported for cortisol levels across groups with corresponding model formulation.

Extended Data Table 7. Inter-model Long COVID classification comparison. Cohen's Kappa analysis of agreement between LCPS and Integrated immunological classification of Long COVID status.

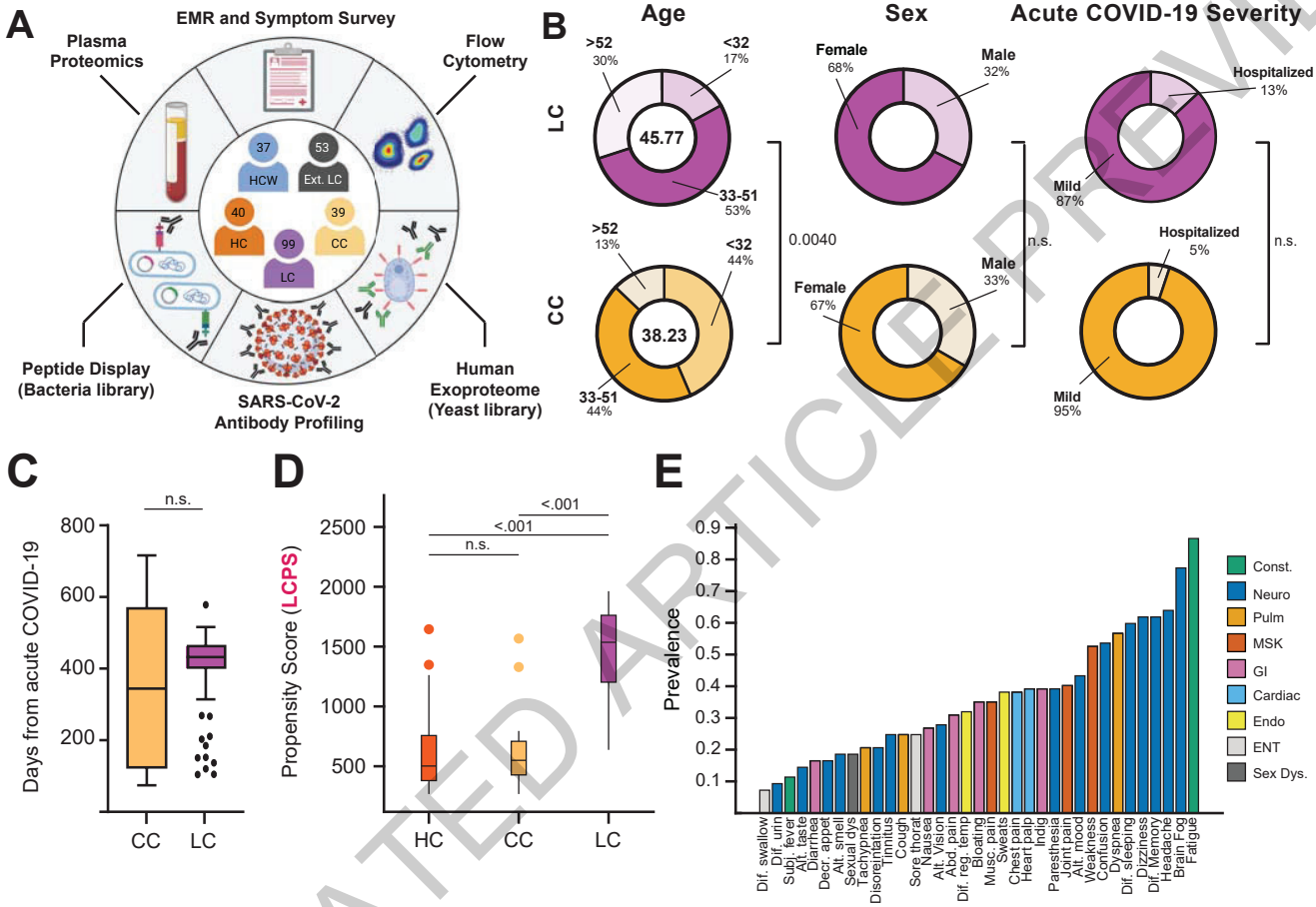

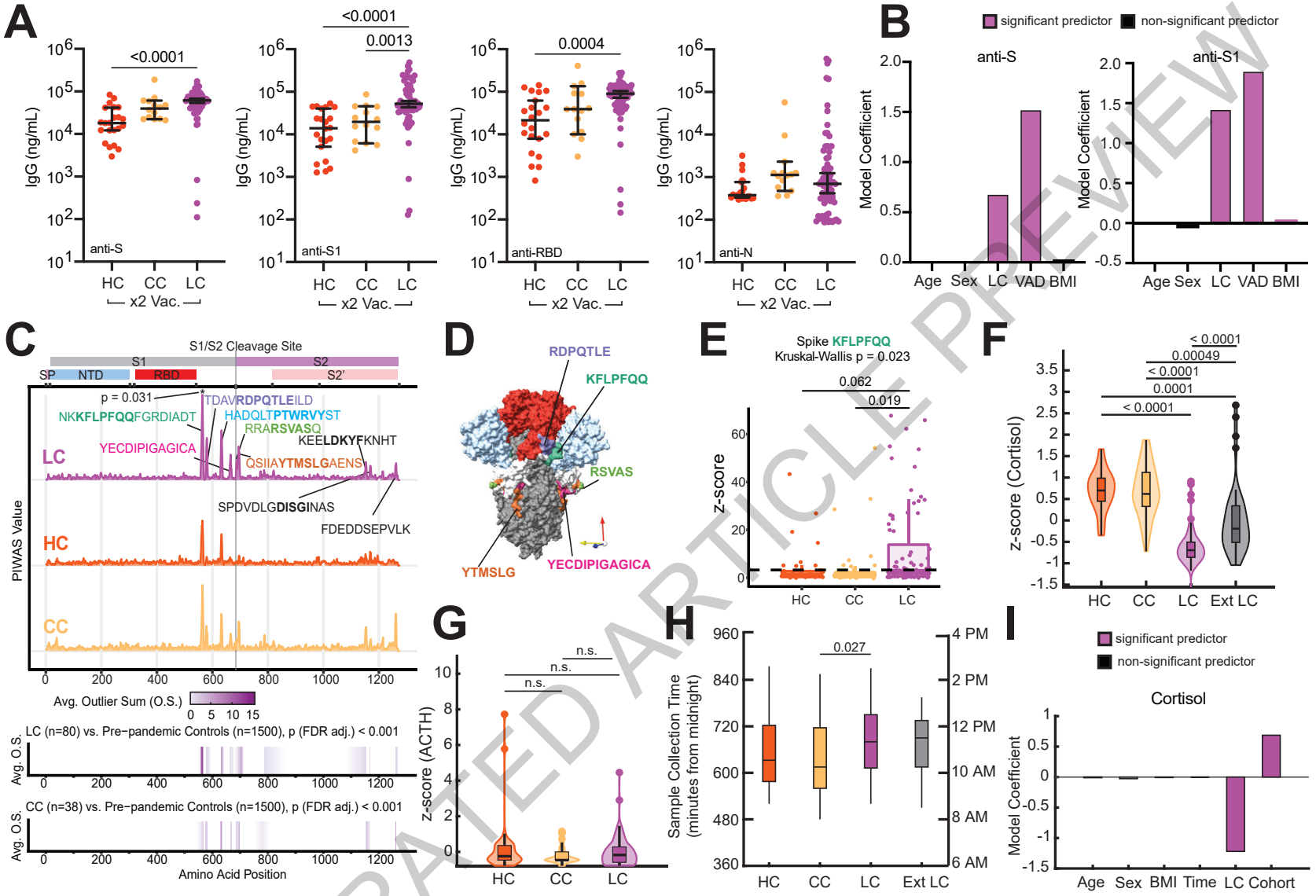

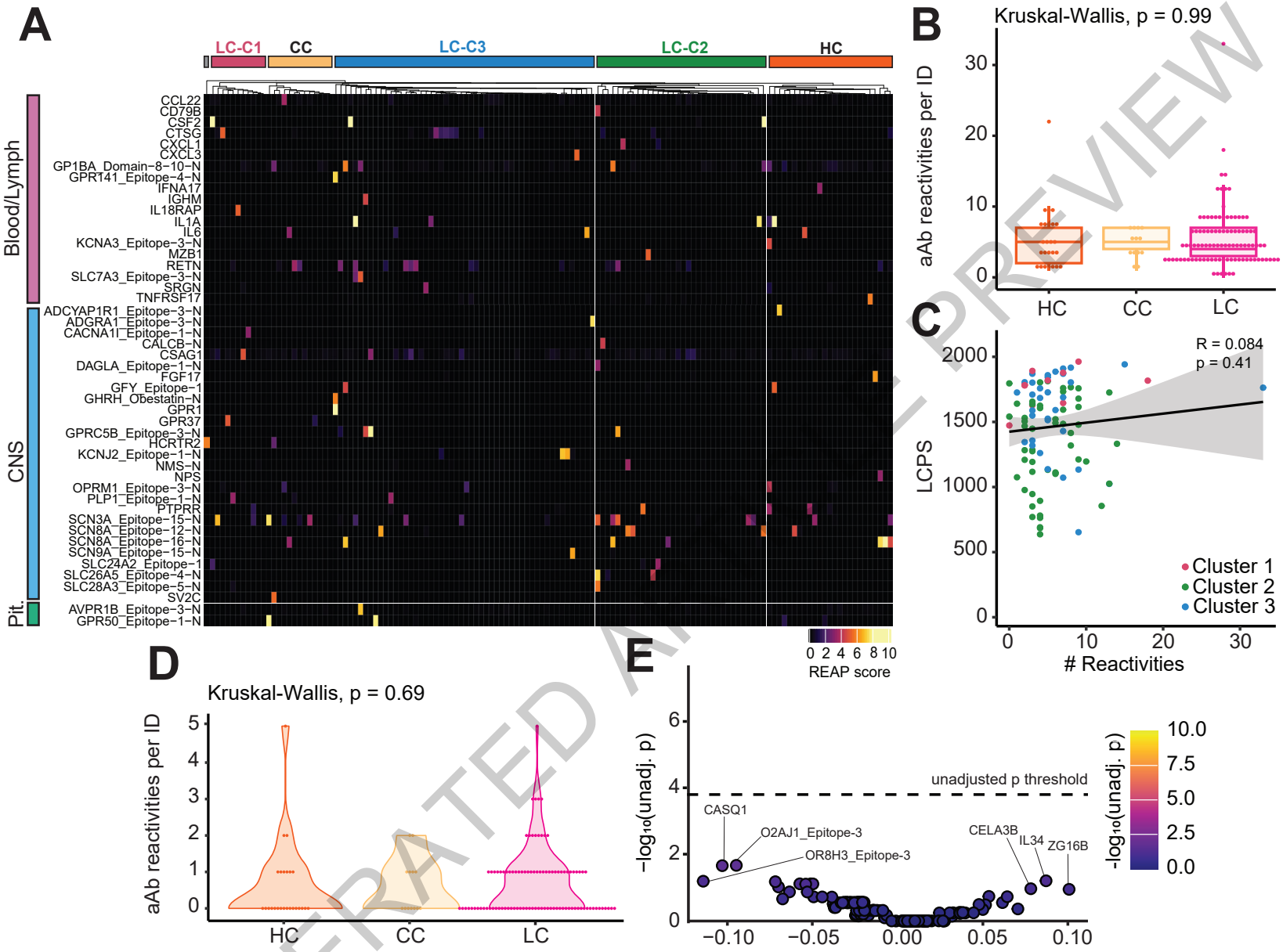

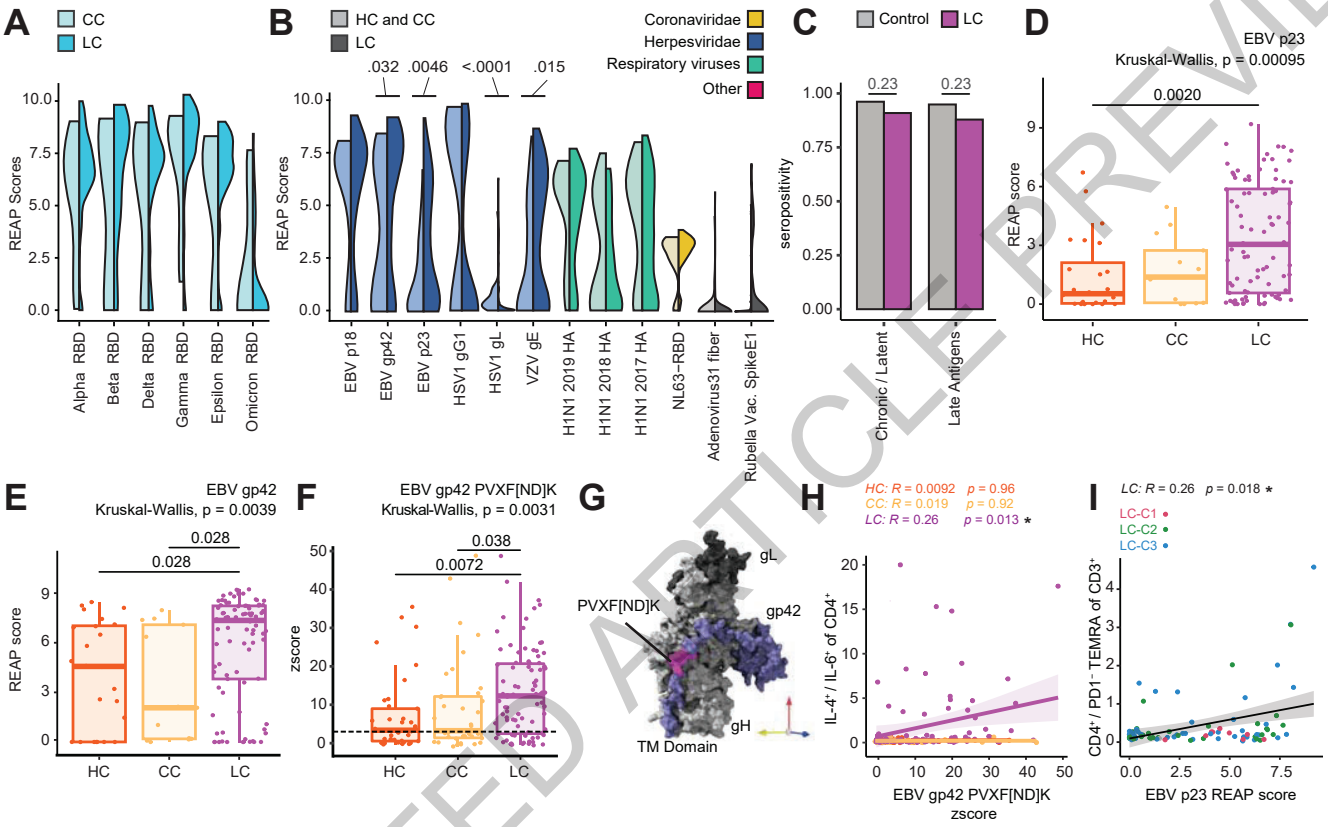

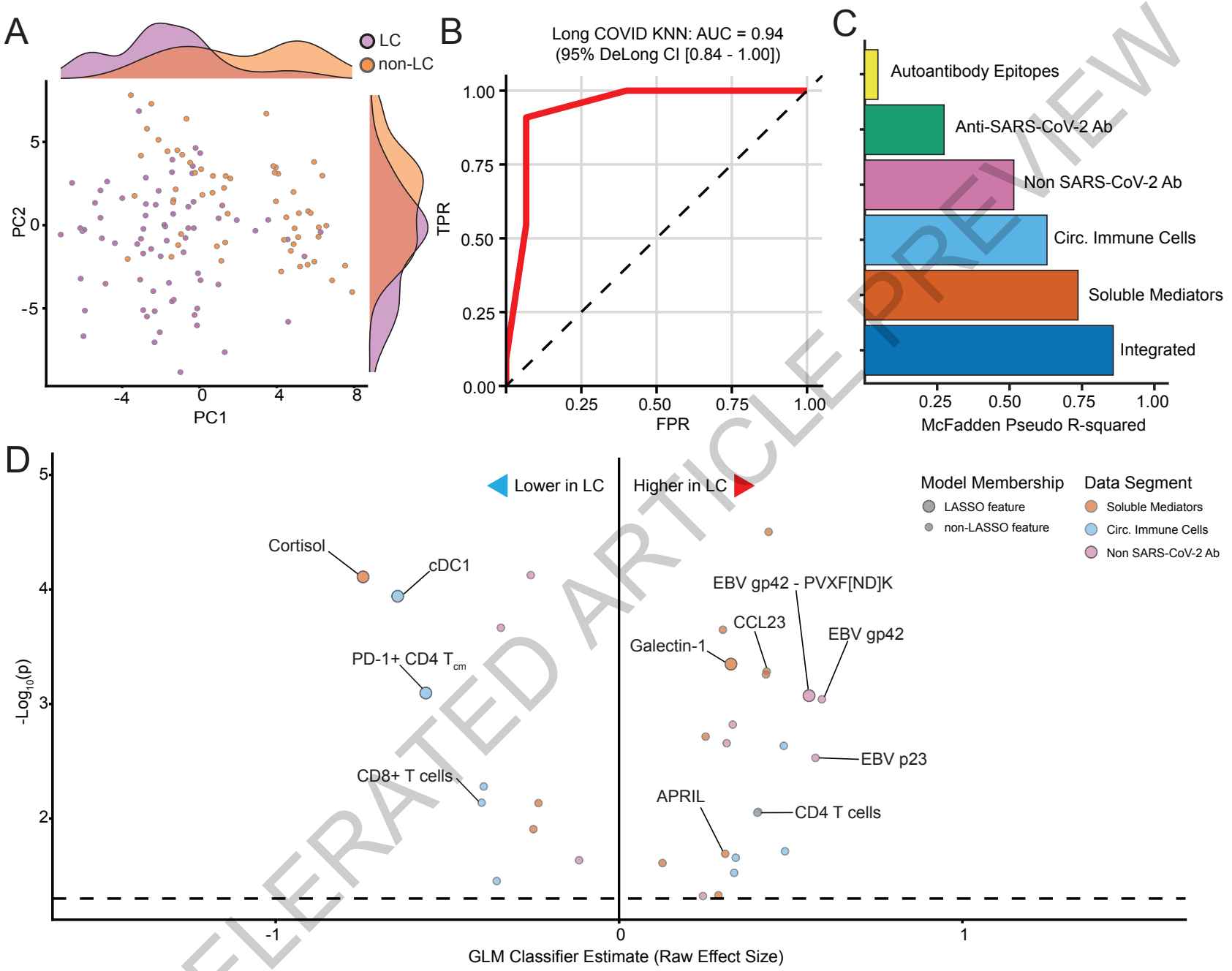

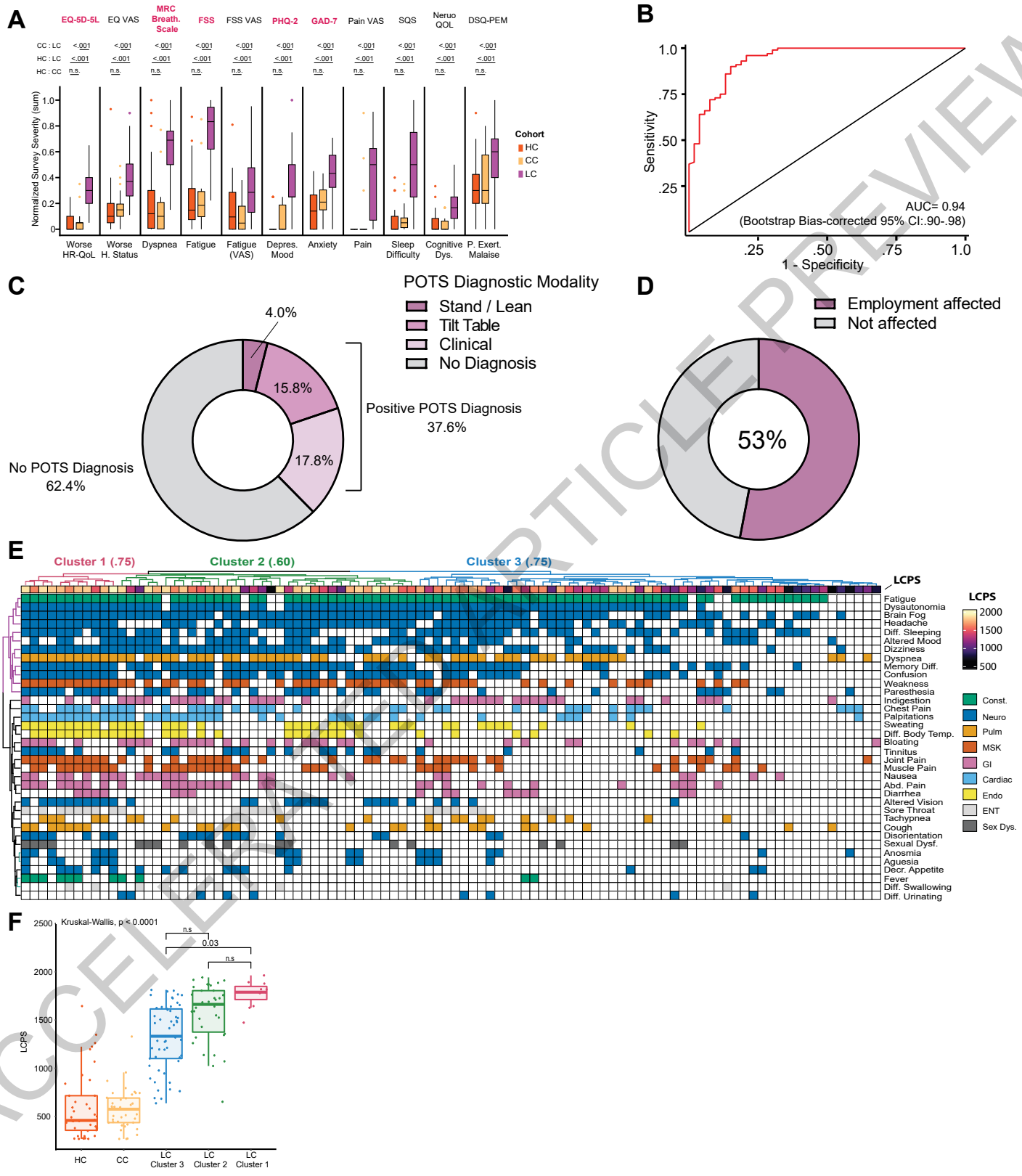

Extended Data Fig. 1

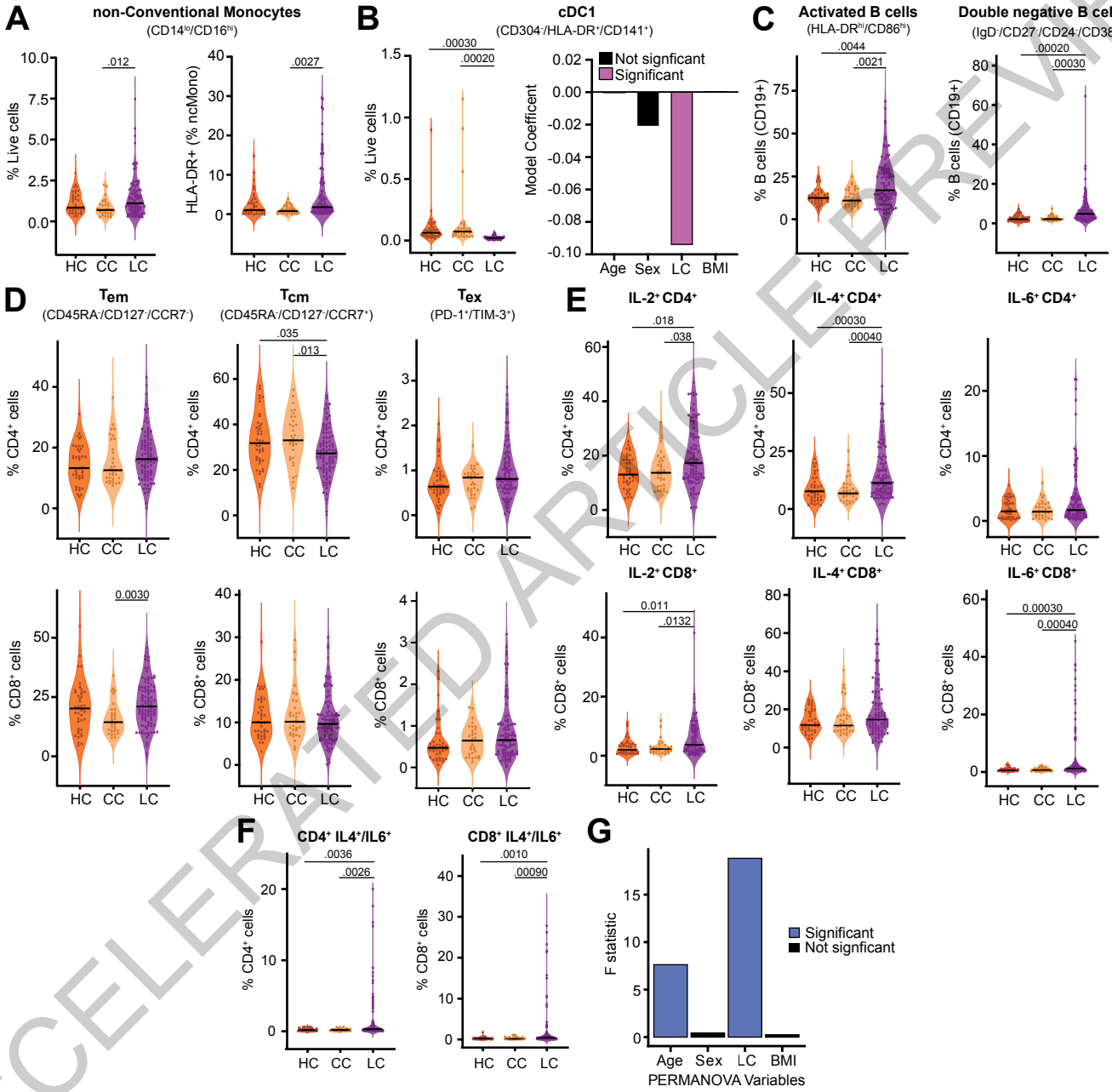

Extended Data Fig. 2

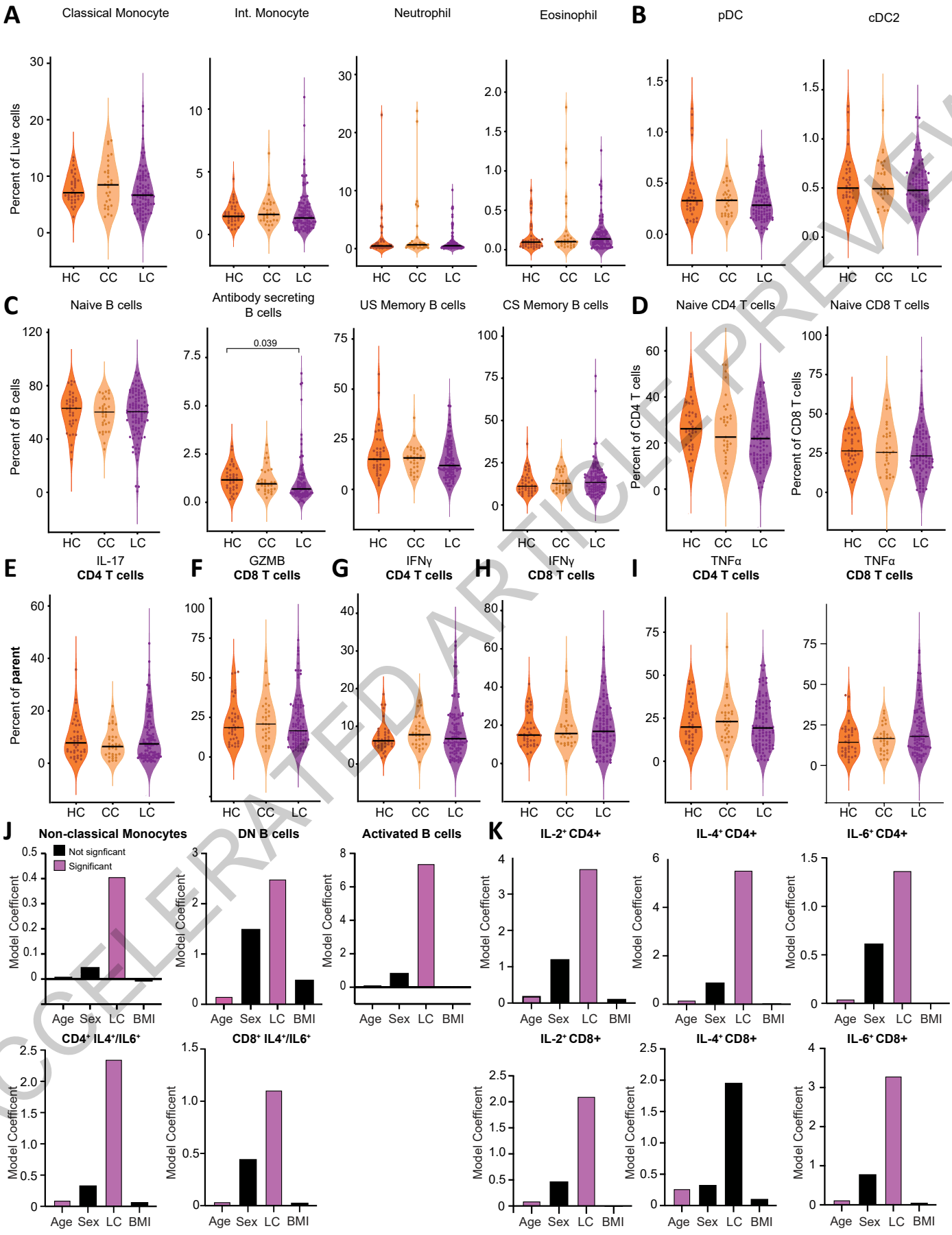

Extended Data Fig. 3

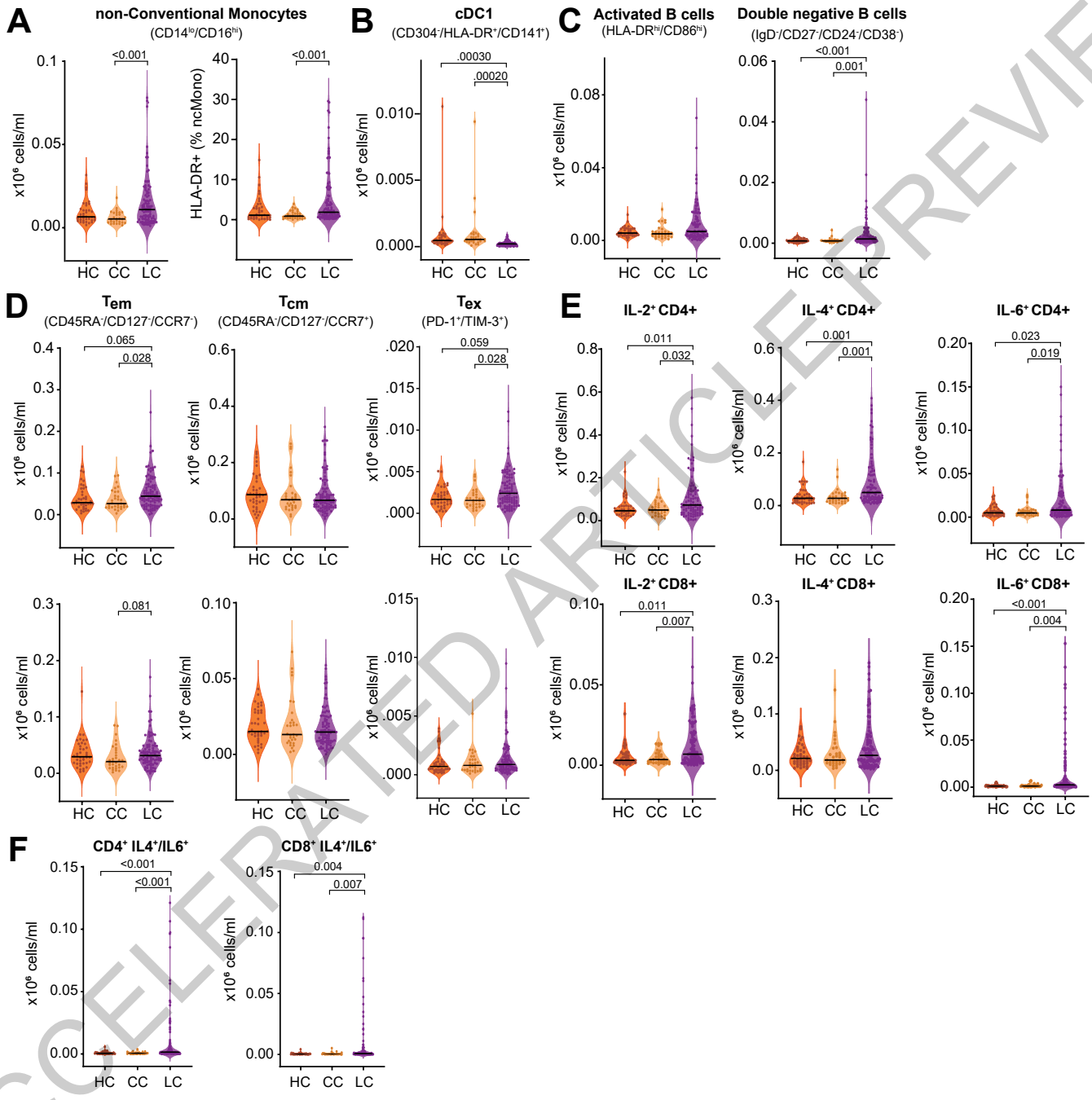

Extended Data Fig. 4

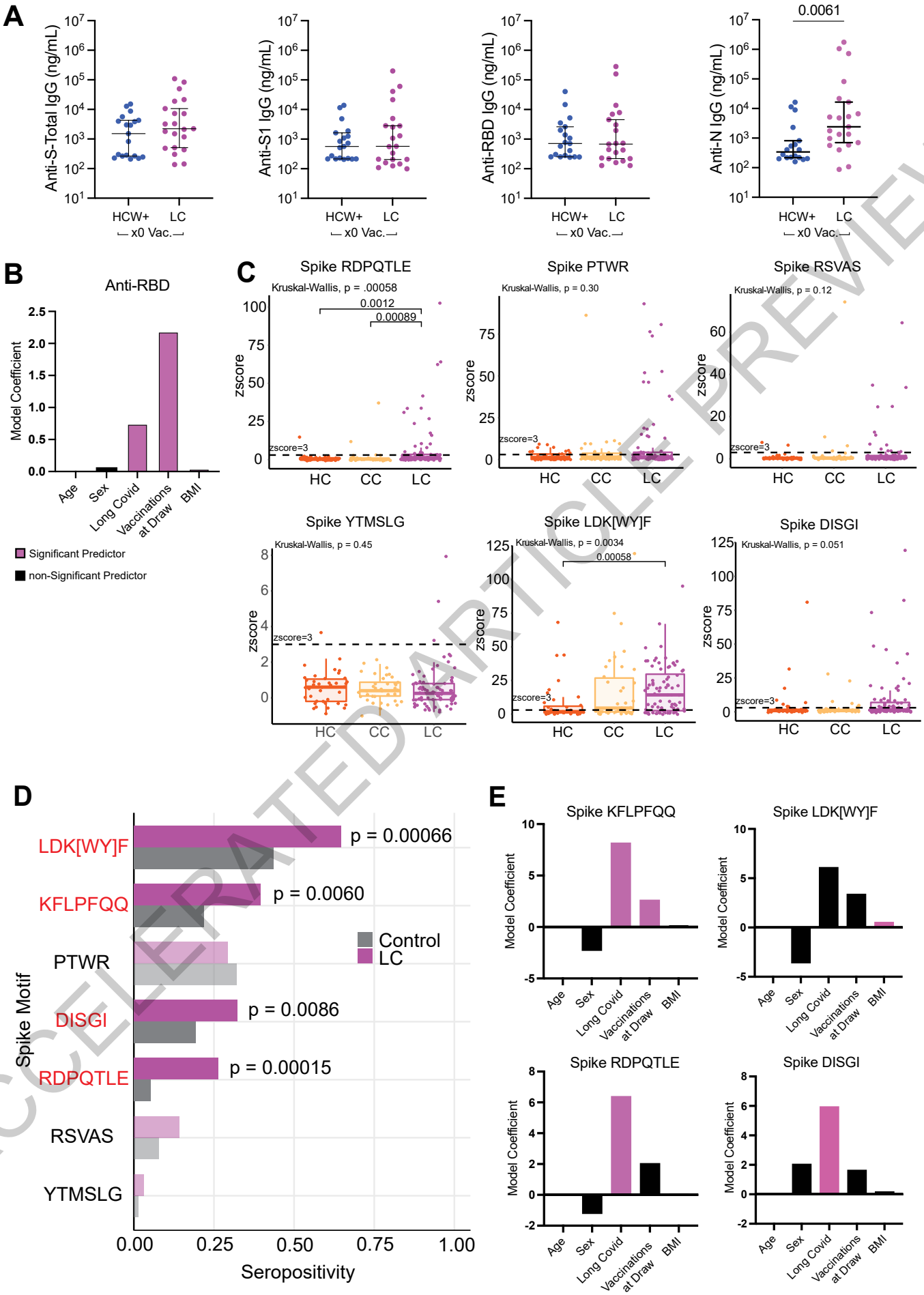

Extended Data Fig. 5

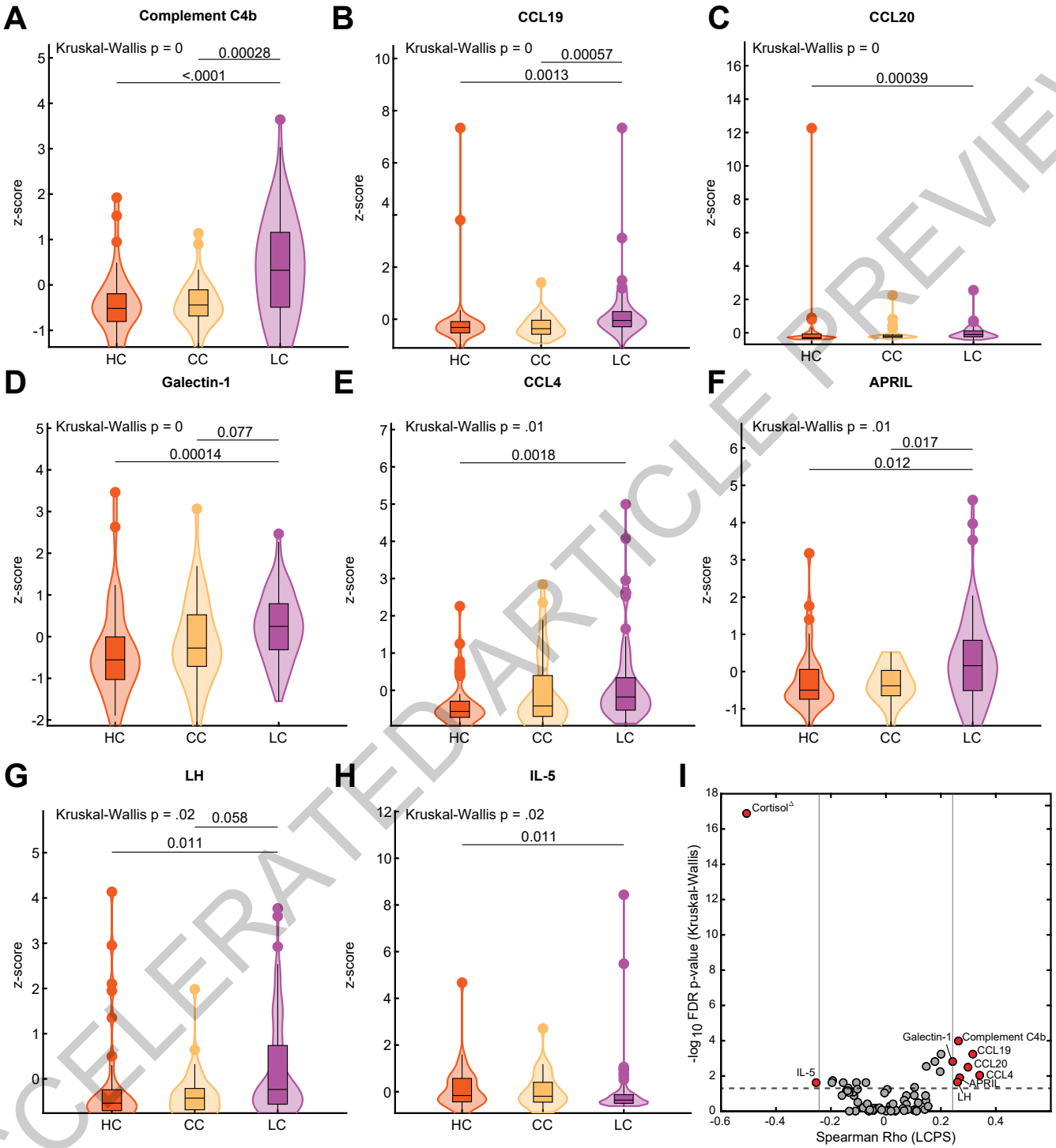

Extended Data Fig.6

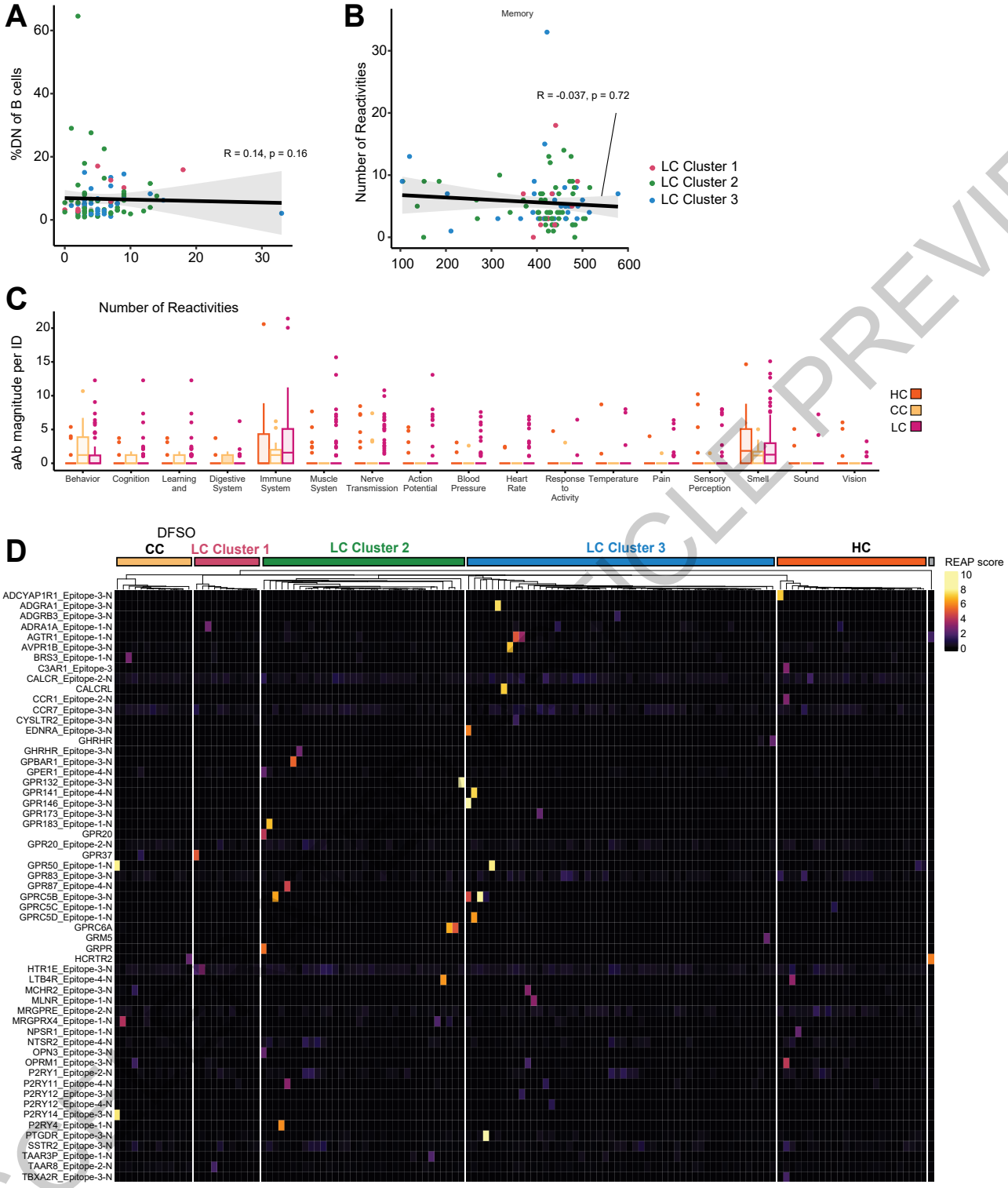

Extended Data Fig. 7

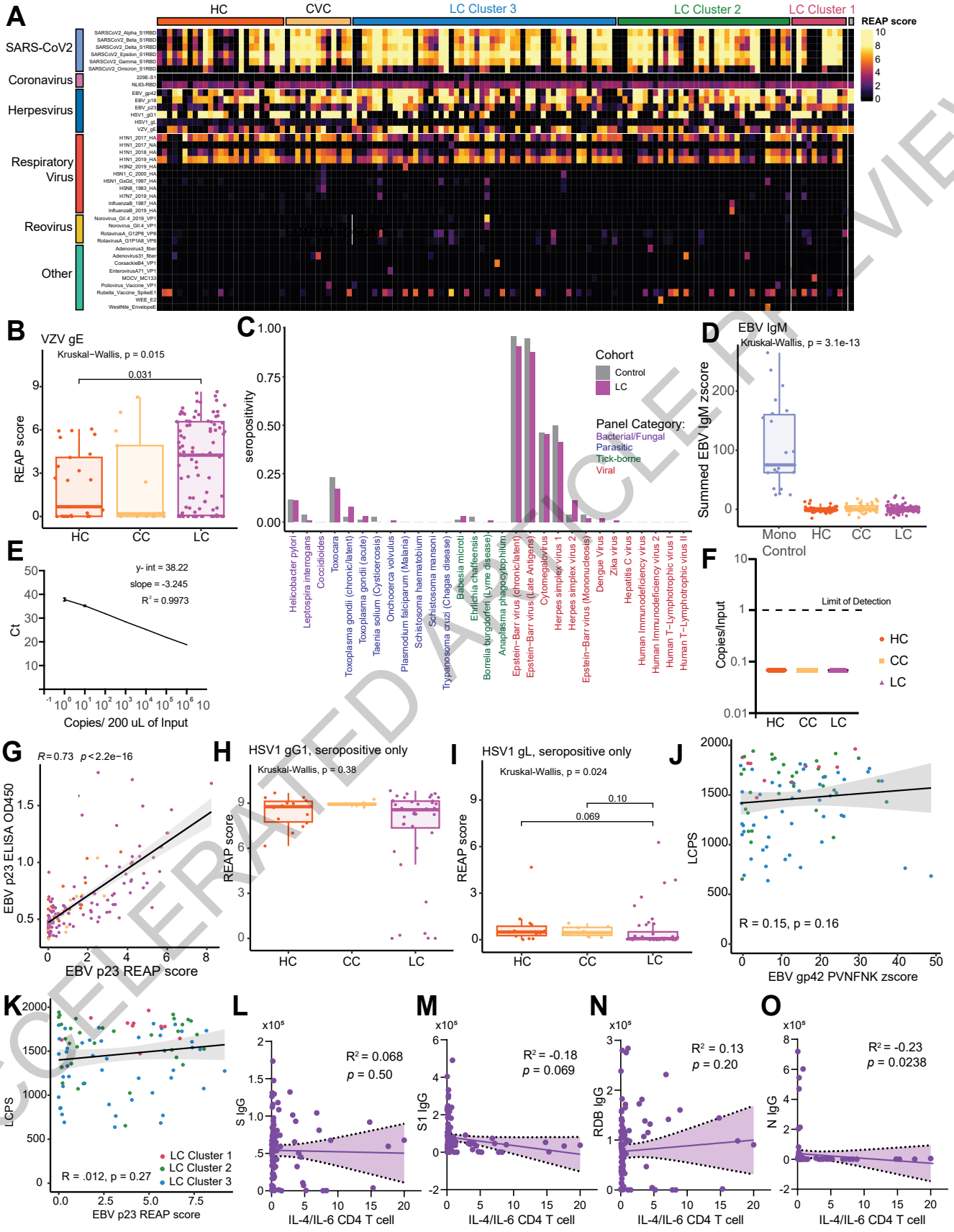

Extended Data Fig. 8

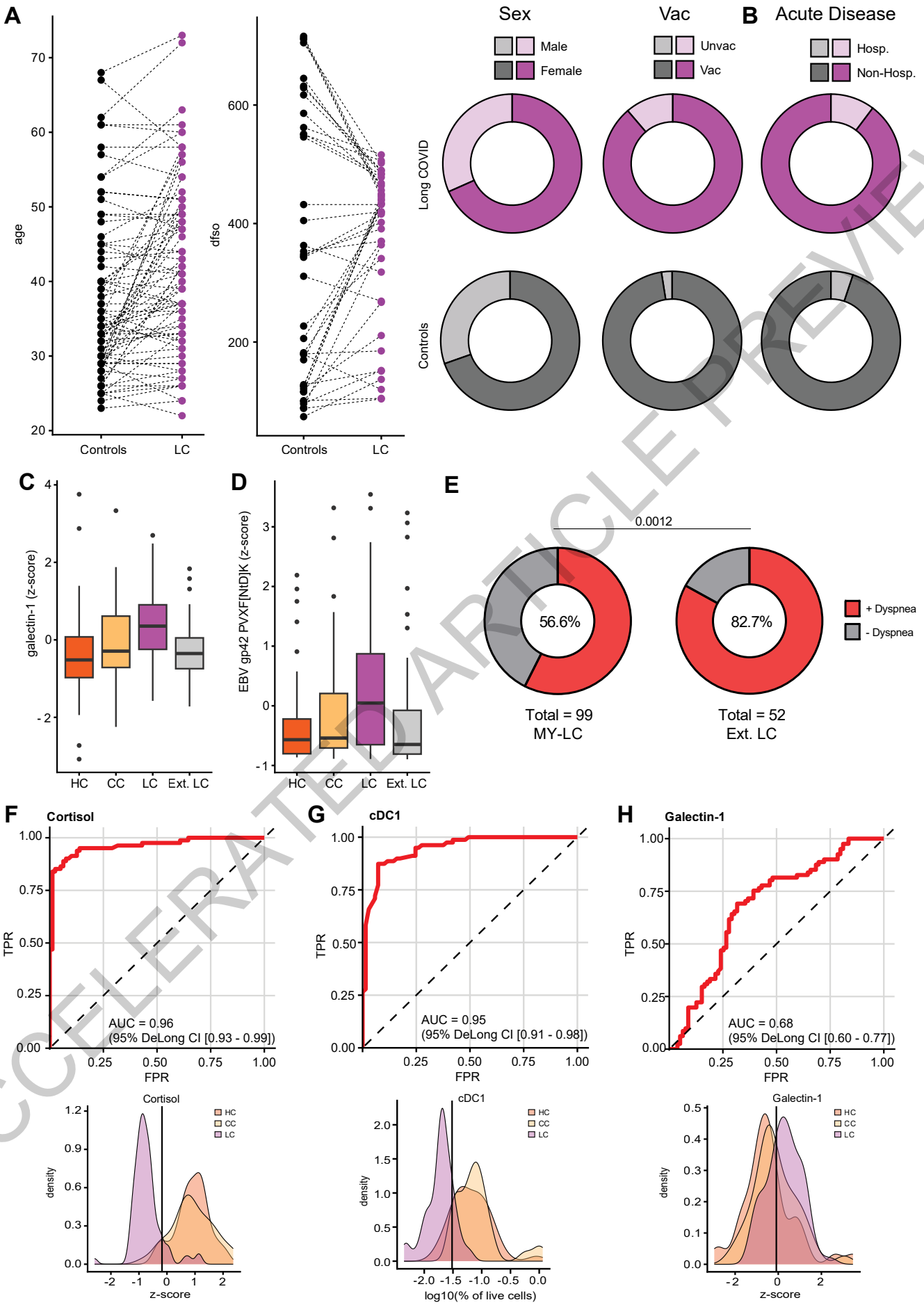

Extended Data Fig. 9

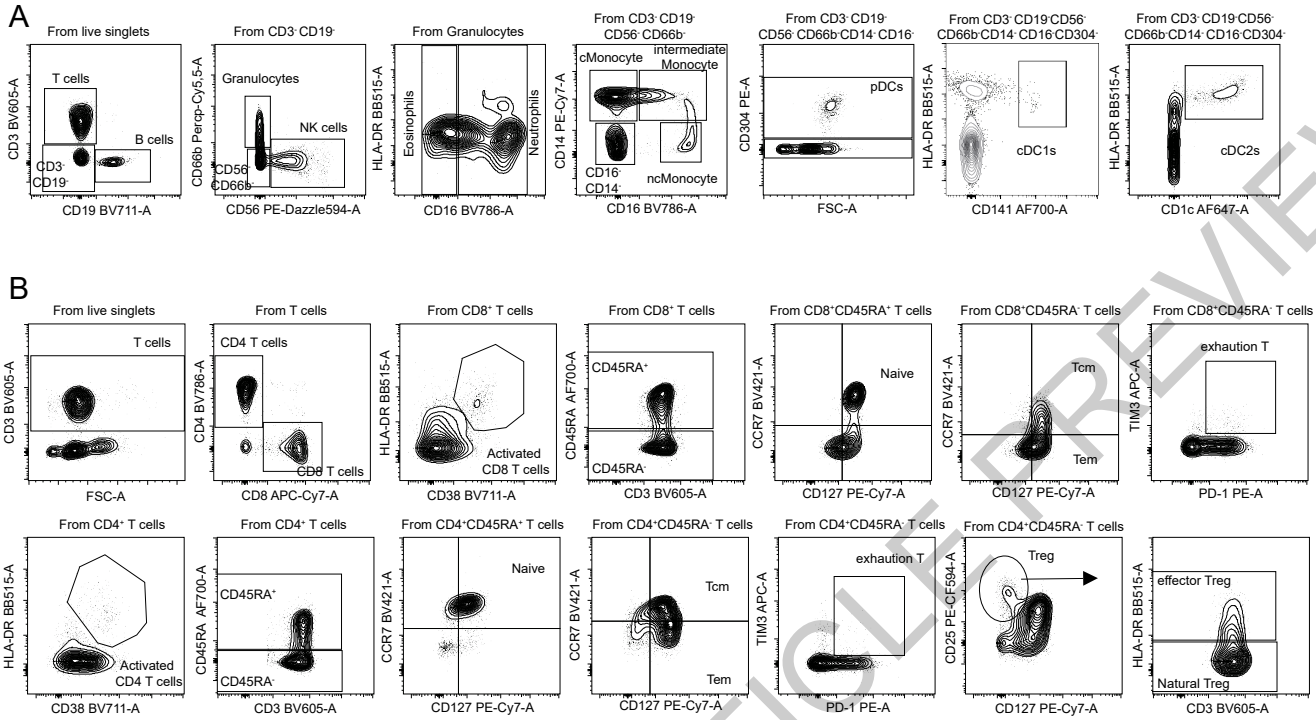

Extended Data Fig. 10

Demographics	Long COVID	Healthy Site Controls	Convalescent COVID-19 Controls	p-value (test statistics)	post-hoc (1-2, 1-3, 2-3)	Total
Enrolled Participants (n)	101	42	42	*Long COVID vs Not Long COVID*	-	185
Excluded Participants (n)	2 (1.98%)	2 (4.76%)	3 (7.14%)	p = 0.41 (**OR:** 0.4040 [0.07569-1.779]) †	-	-
Cohort Size (n)	99.00	40.00	39.00	-	-	178
age (years)	45.77 ± 13.18 (n = 99)	36.73 ± 10.17 (n = 40)	38.23 ± 11.67 (n = 39)	p < 0.0001 ††	0.0006, 0.0040, >0.9999	42.08 ± 12.87 (n = 178)
sex (M | F)	32 | 67 (32.32% | 67.68%) (n = 99)	12 | 28 (30% | 70%) (n = 40)	13 | 26 (33.33% | 66.67%) (n = 39)	p = 0.9465 (.1101, 2) †††		57 | 121 (32.02% | 67.98%) (n = 178)
BMI	26.04 ± 7.02 (n = 99)	24.86 ± 6.78 (n = 39)	24.56 ± 3.41 (n = 38)	p = 0.32 ††		25.46 ± 6.36 (n = 176)
Race						
Asian	5 (5.05%)	4 (10%)	3 (7.69%)	-	-	12 (6.74%)
Black	7 (7.07%)	1 (2.5%)	2 (5.13%)	-	-	10 (5.62%)
American Indian / Alaskan Native	0 (0%)	1 (2.5%)	0 (0%)	-	-	1 (0.56%)
Native Hawaiian and Other Pacific Islander	1 (1.01%)	0 (0%)	0 (0%)	-	-	1 (0.56%)
White	74 (74.75%)	27 (67.5%)	27 (69.23%)	-	-	128 (71.91%)
Other	5 (5.05%)	7 (17.5%)	6 (15.38%)	-	-	18 (10.11%)
Unknown	7 (7.07%)	0 (0%)	0 (0%)	-	-	7 (3.93%)
Ethnicity						
Hispanic	8 (8.08%)	13 (32.5%)	9 (23.08%)		-	30 (16.85%)
COVID-19 Clinical Testing				*Positive test vs. No Positive Test*		
Clinically Confirmed COVID-19 (+PCR | +Ab)	70 (70.71%)	-	33 (84.62%)			103 (69.13%)
Probable COVID-19 (Negative Diagnostic)	26 (26.26%)	-	1 (2.56%)	p = .1276 (**OR:** .4389 [.1707 - 1.115]) †	-	27 (18.12%)
Probable COVID-19 (No Diagnostic)	3 (3.03%)	-	5 (12.82%)		-	8 (6.56%)
SARS-CoV-2 Exposure						
Acute COVID-19 Hospitalized (Y | N)	13 (13.13%)	-	2 (5.13%)	p = .2324 (**OR:** 2.797 [.6551 - 12.90]) †	-	15 (9.55%)
Vaccination Status						
Unvaccinated	19 (19.19%)	1 (2.5%)	0 (0%)	-	-	-
1 vaccine dose (Y | N)	11 (11.11%)	0 (0%)	0 (0%)	-	-	-
2 vaccine doses (Y | N)	69 (69.7%)	22 (78.57%)	15 (83.33%)	-	-	-
3 vaccine doses (Y | N)	0 (0%)	17 (42.5%)	24 (61.54%)	-	-	-
Past Medical History						
Most recent Thyroid Stimulating Hormone (TSH)	1.82 (0.378-6.54) (n = 57)	-	-	-	-	-
Most recent Hemoglobin (Hb)	13.9 (10.2-17.7) (n = 86)	-	-	-	-	-
Self-Reported and EMR Aggregated Diagnoses				**Long COVID vs. Other**		
Hypertension	16 (15.84%)	6 (14.29%)	1 (2.38%)	p = 0.1805 (**OR:** 1.983 [.7725 - 5.040]) †	-	23 (12.71%)
Diabetes Mellitus Type I and II	4 (3.96%)	1 (2.38%)	0 (0%)	p = 0.3839 (**OR:** 3.284 [.5247 - 40.64]) †	-	5 (2.76%)
Kidney Dysfunction (e.g. Chronic)	4 (3.96%)	0 (0%)	0 (0%)	p = 0.1303 (**OR:** n.c.) †	-	4 (2.21%)
Liver Dysfunction (e.g. Fatty)	2 (1.98%)	1 (2.38%)	0 (0%)	p = >0.9999 (**OR:** 1.608 [.1839 - 23.57]) †	-	3 (1.66%)
Asthma	26 (25.74%)	2 (4.76%)	4 (9.52%)	p = 0.0014 (**OR:** 4.333 [1.671 - 10.67]) †	-	32 (17.68%)
COPD	2 (1.98%)	0 (0%)	0 (0%)	p = 0.5035 (**OR:** n.c.) †	-	2 (1.1%)
Other Lung Dysfunction (e.g. Chronic)	1 (0.99%)	0 (0%)	0 (0%)	p = >0.9999 (**OR:** n.c.) †	-	1 (0.55%)
Stroke	1 (0.99%)	0 (0%)	0 (0%)	p = >0.9999 (**OR:** n.c.) †	-	1 (0.55%)
Spinal Cord Injury	1 (0.99%)	1 (2.38%)	0 (0%)	p = >0.9999 (**OR:** 0.7959 [.04151 - 15.30]) †	-	2 (1.1%)
Neurological Dysfunction (e.g. Parkinson's, Epilepsy, Dementia)	1 (0.99%)	0 (0%)	1 (2.38%)	p = >0.9999 (**OR:** 0.7959 [.04151 - 15.30]) †	-	2 (1.1%)
Obesity	8 (7.92%)	6 (14.29%)	0 (0%)	p = >0.9999 (**OR:** 1.070 [.3422 - 3.283]) †	-	14 (7.73%)
Immunological Dysfunction (e.g. Autoimmune)	3 (2.97%)	1 (2.38%)	3 (7.14%)	p = 0.7014 (**OR:** 0.5859 [0.1446 - 2.244]) †	-	7 (3.87%)
Cancer	6 (5.94%)	0 (0%)	1 (2.38%)	p = 0.1342 (**OR:** 5.032 [0.7916 - 58.44]) †	-	7 (3.87%)
Anxiety	25 (24.75%)	7 (16.67%)	10 (23.81%)	p = 0.5978 (**OR:** 1.232 [0.6171 - 2.425]) †	-	42 (23.2%)
Depression	16 (15.84%)	2 (4.76%)	9 (21.43%)	p = 0.8339 (**OR:** 1.192 [0.5394 - 2.607]) †	-	27 (14.92%)
Other Psychological Diagnoses	2 (1.98%)	0 (0%)	1 (2.38%)	p = >0.9999 (**OR:** 1.608 [0.1839 - 23.57]) †	-	3 (1.66%)
Eating Disorder	2 (1.98%)	0 (0%)	2 (4.76%)	p = >0.9999 (**OR:** 0.7938 [0.1223 - 5.164]) †	-	4 (2.21%)
Irritable bowel syndrome	15 (14.85%)	0 (0%)	3 (7.14%)	p = 0.0129 (**OR:** 4.524 [1.295 - 15.09]) †	-	18 (9.94%)
Other	0 (0%)	0 (0%)	0 (0%)	-	-	0 (0%)
None	22 (21.78%)	29 (69.05%)	28 (66.67%)	p = <0.0001 (**OR:** 0.1103 [0.05787 - 0.2181]) †	-	79 (43.65%)
Prior Autoimmune Diagnoses (Yes | No)	18 | 81 (18.18% | 81.82%) (n = 99)	2 | 38 (5% | 95%) (n = 40)	3 | 32 (8.57% | 91.43%) (n = 35)	p = .0765 (5.140, 2) †††	-	23 | 151 (13.22% | 86.78%) (n = 174)
Hypothyroidism	9 (9.09%)	0 (0%)	1 (5.56%)	-	-	10 (6.67%)
Crohn's Disease	1 (1.01%)	0 (0%)	0 (0%)	-	-	1 (0.67%)
Hyperthyroidism	1 (1.01%)	0 (0%)	1 (5.56%)	-	-	2 (1.33%)
Inclusion Body Myositis	1 (1.01%)	0 (0%)	0 (0%)	-	-	1 (0.67%)
Microscopic colitis	1 (1.01%)	0 (0%)	0 (0%)	-	-	1 (0.67%)
Pernicious Anemia	1 (1.01%)	0 (0%)	0 (0%)	-	-	1 (0.67%)
Polymyositis	1 (1.01%)	0 (0%)	0 (0%)	-	-	1 (0.67%)
Polyarthralgia	1 (1.01%)	0 (0%)	0 (0%)	-	-	1 (0.67%)
Primary Biliary Cholangitis	1 (1.01%)	0 (0%)	0 (0%)	-	-	1 (0.67%)
Rheumatoid Arthritis	1 (1.01%)	1 (3.03%)	0 (0%)	-	-	2 (1.33%)
Sicca	1 (1.01%)	0 (0%)	0 (0%)	-	-	1 (0.67%)
Systemic Lupus Erythematosus	1 (1.01%)	1 (3.03%)	0 (0%)	-	-	2 (1.33%)
Ulcerative Colitis	1 (1.01%)	0 (0%)	0 (0%)	-	-	1 (0.67%)
Multiple Sclerosis (remission)	0 (0%)	0 (0%)	1 (5.56%)	-	-	1 (0.67%)

Extended Data Table 1

Cohort	eq5	eq5vas	mrc	fss_tot	fatigue_vas	phq2total	gadtotal	pain_vas	prom_sleep	neuroqol_t	pem
HC	0	0.1	0	0.148148148	0.12	0	0.095238095	0	0.3	0.140569395	0
CC	0.1	0.13	0	0.166666667	0.1	0	0.071428571	0	0.3	0.209964413	0.1
LC	0.3	0.35	0.3	0.833333333	0.69	0.166667	0.285714286	0.5	0.5	0.432384342	0.5

Extended Data Table 2

Detailed report of sensitivity and specificity

Cutpoint	Sensitivity	Specificity	Correctly Classified	LR+	LR-
(>=268)	100.00%	0.00%	55.25%	1.0000	
(>=271)	100.00%	4.94%	57.46%	1.0519	0.0000
(>=275)	100.00%	8.64%	59.12%	1.0946	0.0000
(>=296)	100.00%	11.11%	60.22%	1.1250	0.0000
(>=299)	100.00%	13.58%	61.33%	1.1571	0.0000
(>=310)	100.00%	16.05%	62.43%	1.1912	0.0000
(>=352)	100.00%	17.28%	62.98%	1.2090	0.0000
(>=358)	100.00%	18.52%	63.54%	1.2273	0.0000
(>=359)	100.00%	19.75%	64.09%	1.2462	0.0000
(>=369)	100.00%	20.99%	64.64%	1.2656	0.0000
(>=380)	100.00%	22.22%	65.19%	1.2857	0.0000
(>=397)	100.00%	25.93%	66.85%	1.3500	0.0000
(>=408)	100.00%	28.40%	67.96%	1.3966	0.0000
(>=414)	100.00%	29.63%	68.51%	1.4211	0.0000
(>=418)	100.00%	30.86%	69.06%	1.4464	0.0000
(>=436)	100.00%	32.10%	69.61%	1.4727	0.0000
(>=437)	100.00%	33.33%	70.17%	1.5000	0.0000
(>=443)	100.00%	35.80%	71.27%	1.5577	0.0000
(>=446)	100.00%	37.04%	71.82%	1.5882	0.0000
(>=452)	100.00%	38.27%	72.38%	1.6200	0.0000
(>=453)	100.00%	39.51%	72.93%	1.6531	0.0000
(>=454)	100.00%	40.74%	73.48%	1.6875	0.0000
(>=465)	100.00%	41.98%	74.03%	1.7234	0.0000
(>=467)	100.00%	43.21%	74.59%	1.7609	0.0000
(>=478)	100.00%	44.44%	75.14%	1.8000	0.0000
(>=492)	100.00%	45.68%	75.69%	1.8409	0.0000
(>=502)	100.00%	48.15%	76.80%	1.9286	0.0000
(>=506)	100.00%	49.38%	77.35%	1.9756	0.0000
(>=514)	100.00%	50.62%	77.90%	2.0250	0.0000
(>=520)	100.00%	51.85%	78.45%	2.0769	0.0000
(>=523)	100.00%	53.09%	79.01%	2.1316	0.0000
(>=554)	100.00%	54.32%	79.56%	2.1892	0.0000
(>=576)	100.00%	55.56%	80.11%	2.2500	0.0000
(>=583)	100.00%	56.79%	80.66%	2.3143	0.0000
(>=587)	100.00%	58.02%	81.22%	2.3824	0.0000
(>=594)	100.00%	59.26%	81.77%	2.4545	0.0000
(>=596)	100.00%	60.49%	82.32%	2.5313	0.0000
(>=600)	100.00%	61.73%	82.87%	2.6129	0.0000
(>=604)	100.00%	62.96%	83.43%	2.7000	0.0000
(>=620)	100.00%	64.20%	83.98%	2.7931	0.0000
(>=627)	100.00%	65.43%	84.53%	2.8929	0.0000
(>=635)	100.00%	66.67%	85.08%	3.0000	0.0000
(>=637)	100.00%	67.90%	85.64%	3.1154	0.0000
(>=651)	99.00%	69.14%	85.64%	3.2076	0.0145
(>=653)	99.00%	70.37%	86.19%	3.3412	0.0142
(>=674)	98.00%	70.37%	85.64%	3.3075	0.0284
(>=684)	98.00%	71.60%	86.19%	3.4513	0.0279
(>=689)	97.00%	71.60%	85.64%	3.4161	0.0419
(>=691)	97.00%	72.84%	86.19%	3.5714	0.0412
(>=694)	96.00%	72.84%	85.64%	3.5345	0.0549
(>=716)	96.00%	74.07%	86.19%	3.7029	0.0540
(>=728)	96.00%	76.54%	87.29%	4.0926	0.0523
(>=744)	96.00%	77.78%	87.85%	4.3200	0.0514
(>=755)	96.00%	81.48%	89.50%	5.1840	0.0491
(>=763)	96.00%	82.72%	90.06%	5.5543	0.0484
(>=770)	95.00%	82.72%	89.50%	5.4964	0.0604
(>=781)	94.00%	82.72%	88.95%	5.4386	0.0725
(>=795)	93.00%	82.72%	88.40%	5.3807	0.0846
(>=840)	93.00%	83.95%	88.95%	5.7946	0.0834
(>=851)	93.00%	85.19%	89.50%	6.2775	0.0822
(>=855)	92.00%	85.19%	88.95%	6.2100	0.0939
(>=869)	91.00%	85.19%	88.40%	6.1425	0.1057
(>=879)	91.00%	86.42%	88.95%	6.7009	0.1041
(>=894)	91.00%	87.65%	89.50%	7.3710	0.1027
(>=930)	90.00%	87.65%	88.95%	7.2900	0.1141
(>=946)	90.00%	88.89%	89.50%	8.1000	0.1125
(>=957)	89.00%	88.89%	88.95%	8.0100	0.1237
(>=977)	89.00%	90.12%	89.50%	9.0113	0.1221
(>=1024)	88.00%	90.12%	88.95%	8.9100	0.1332
(>=1026)	87.00%	90.12%	88.40%	8.8088	0.1442
(>=1069)	86.00%	90.12%	87.85%	8.7075	0.1553
(>=1072)	86.00%	91.36%	88.40%	9.9514	0.1532
(>=1075)	85.00%	91.36%	87.85%	9.8357	0.1642
(>=1101)	84.00%	91.36%	87.29%	9.7200	0.1751
(>=1112)	83.00%	91.36%	86.74%	9.6043	0.1861
(>=1117)	82.00%	91.36%	86.19%	9.4886	0.1970
(>=1132)	81.00%	91.36%	85.64%	9.3729	0.2080
(>=1134)	80.00%	91.36%	85.08%	9.2571	0.2189
(>=1137)	79.00%	91.36%	84.53%	9.1414	0.2299
(>=1146)	78.00%	91.36%	83.98%	9.0257	0.2408
(>=1193)	77.00%	91.36%	83.43%	8.9100	0.2518
(>=1196)	76.00%	91.36%	82.87%	8.7943	0.2627
(>=1197)	75.00%	91.36%	82.32%	8.6786	0.2736
(>=1209)	75.00%	92.59%	82.87%	10.1250	0.2700
(>=1212)	74.00%	92.59%	82.32%	9.9900	0.2808
(>=1224)	73.00%	92.59%	81.77%	9.8550	0.2916
(>=1261)	73.00%	93.83%	82.32%	11.8260	0.2878
(>=1262)	72.00%	93.83%	81.77%	11.6640	0.2984
(>=1275)	72.00%	95.06%	82.32%	14.5800	0.2945
(>=1283)	71.00%	95.06%	81.77%	14.3775	0.3051
(>=1285)	70.00%	95.06%	81.22%	14.1750	0.3156
(>=1295)	69.00%	95.06%	80.66%	13.9725	0.3261
(>=1319)	68.00%	95.06%	80.11%	13.7700	0.3366
(>=1329)	66.00%	95.06%	79.01%	13.3650	0.3577
(>=1332)	66.00%	96.30%	79.56%	17.8200	0.3531
(>=1345)	65.00%	96.30%	79.01%	17.5500	0.3635
(>=1348)	64.00%	96.30%	78.45%	17.2800	0.3738
(>=1357)	64.00%	97.53%	79.01%	25.9200	0.3691
(>=1415)	63.00%	97.53%	78.45%	25.5150	0.3794
(>=1430)	62.00%	97.53%	77.90%	25.1100	0.3896
(>=1448)	61.00%	97.53%	77.35%	24.7050	0.3999
(>=1468)	60.00%	97.53%	76.80%	24.3000	0.4101
(>=1473)	59.00%	97.53%	76.24%	23.8950	0.4204
(>=1479)	58.00%	97.53%	75.69%	23.4900	0.4306
(>=1485)	57.00%	97.53%	75.14%	23.0850	0.4409
(>=1492)	56.00%	97.53%	74.59%	22.6800	0.4511
(>=1505)	55.00%	97.53%	74.03%	22.2750	0.4614
(>=1514)	54.00%	97.53%	73.48%	21.8700	0.4716
(>=1521)	53.00%	97.53%	72.93%	21.4650	0.4819
(>=1525)	52.00%	97.53%	72.38%	21.0600	0.4922
(>=1531)	51.00%	97.53%	71.82%	20.6550	0.5024
(>=1541)	50.00%	97.53%	71.27%	20.2500	0.5127
(>=1549)	49.00%	97.53%	70.72%	19.8450	0.5229
(>=1567)	48.00%	97.53%	70.17%	19.4400	0.5332
(>=1588)	48.00%	98.77%	70.72%	38.8801	0.5265
(>=1591)	47.00%	98.77%	70.17%	38.0701	0.5366
(>=1594)	46.00%	98.77%	69.61%	37.2601	0.5467
(>=1606)	45.00%	98.77%	69.06%	36.4501	0.5569
(>=1615)	44.00%	98.77%	68.51%	35.6401	0.5670
(>=1625)	43.00%	98.77%	67.96%	34.8301	0.5771
(>=1628)	42.00%	98.77%	67.40%	34.0201	0.5872
(>=1635)	40.00%	98.77%	66.30%	32.4001	0.6075
(>=1640)	39.00%	98.77%	65.75%	31.5901	0.6176
(>=1641)	38.00%	98.77%	65.19%	30.7801	0.6277
(>=1645)	37.00%	98.77%	64.64%	29.9701	0.6379
(>=1656)	36.00%	100.00%	64.64%		0.6400
(>=1679)	35.00%	100.00%	64.09%		0.6500
(>=1684)	34.00%	100.00%	63.54%		0.6600
(>=1689)	33.00%	100.00%	62.98%		0.6700
(>=1710)	32.00%	100.00%	62.43%		0.6800
(>=1726)	31.00%	100.00%	61.88%		0.6900
(>=1727)	29.00%	100.00%	60.77%		0.7100
(>=1733)	28.00%	100.00%	60.22%		0.7200
(>=1758)	27.00%	100.00%	59.67%		0.7300
(>=1760)	25.00%	100.00%	58.56%		0.7500
(>=1763)	24.00%	100.00%	58.01%		0.7600
(>=1781)	23.00%	100.00%	57.46%		0.7700
(>=1766)	22.00%	100.00%	56.91%		0.7800
(>=1780)	21.00%	100.00%	56.35%		0.7900
(>=1782)	20.00%	100.00%	55.80%		0.8000
(>=1789)	19.00%	100.00%	55.25%		0.8100
(>=1796)	18.00%	100.00%	54.70%		0.8200
(>=1804)	17.00%	100.00%	54.14%		0.8300
(>=1805)	15.00%	100.00%	53.04%		0.8500
(>=1813)	14.00%	100.00%	52.49%		0.8600
(>=1817)	13.00%	100.00%	51.93%		0.8700
(>=1819)	12.00%	100.00%	51.38%		0.8800
(>=1843)	11.00%	100.00%	50.83%		0.8900
(>=1859)	10.00%	100.00%	50.28%		0.9000
(>=1870)	9.00%	100.00%	49.72%		0.9100
(>=1878)	7.00%	100.00%	48.62%		0.9300
(>=1886)	6.00%	100.00%	48.07%		0.9400
(>=1892)	5.00%	100.00%	47.51%		0.9500
(>=1910)	4.00%	100.00%	46.96%		0.9600
(>=1917)	3.00%	100.00%	46.41%		0.9700
(>=1942)	2.00%	100.00%	45.86%		0.9800
(>=1963)	1.00%	100.00%	45.30%		0.9900
(>1963)	0.00%	100.00%	44.75%		1.0000

Obs	ROC Area	-- Binomial Exact -- Std. Err.	[95% Conf.	Interval]
181	0.9542	0.0144	0.91477	0.98073

Extended Data Table 3

Non-Conve Monocytes

Deviance Residuals:

Min	1Q	Median	3Q	Max
-1.2431	-0.6313	-0.2381	0.3645	6.0574

Coefficients:

	Estimate	Std.	Error	tvalue	Pr(>|t|)
(Intercept)	0.877026	0.522789	1.678	0.0954	.
age	0.007451	0.006464	1.153	0.2507	
sex	0.046887	0.172084	0.272	0.7856	
LC_Status	0.408835	0.170405	2.399	0.0176	*
BMI	-0.00853	0.012437	-0.686	0.4938	

Non-Conve Monocytes HLA+

Deviance Residuals:

Min	1Q	Median	3Q	Max
-7.3616	-2.9382	-1.1851	0.9063	22.1521

Coefficients:

	Estimate	Std.	Error	tvalue	Pr(>|t|)
(Intercept)	-6.94943	2.73395	-2.542	0.011963	*
age	0.12776	0.03381	3.779	0.000221	***
sex	1.24725	0.89992	1.386	0.167665	
LC_Status	1.74339	0.89114	1.956	0.052142	.
BMI	0.08711	0.06504	1.339	0.182306	

Type 1 Convention Dendritic Cells

Deviance Residuals:

Min	1Q	Median	3Q	Max
-0.12165	-0.03953	-0.00801	0.00742	1.02724

Coefficients:

	Estimate	Std.	Error	tvalue	Pr(>|t|)
(Intercept)	0.162193	0.066561	2.437	0.0159	*
age	-0.00056	0.000823	-0.682	0.4959	
sex	-0.02122	0.02191	-0.969	0.3342	
LC_Status	-0.09443	0.021696	-4.353	2.38E-05	***
BMI	0.000622	0.001583	0.393	0.6948	

Activated B Cells

Residuals:

Min	1Q	Median	3Q	Max
-23.986	-6.091	-1.049	5.539	48.744

Coefficients:

	Estimate	Std.	Error	tvalue	Pr(>|t|)
(Intercept)	9.08034	5.57115	1.63	0.105	
age	0.09363	0.06919	1.353	0.178	
sex	0.84387	1.81763	0.464	0.643	
LC_Status	7.40264	1.81261	4.084	6.84E-05	***
BMI	-0.04619	0.13354	-0.346	0.73	

Double Negative B cells

Residuals:

Min	1Q	Median	3Q	Max
-7.576	-2.815	-0.658	1.157	52.161

Coefficients:

	Estimate	Std.	Error	tvalue	Pr(>|t|)
(Intercept)	-7.02352	2.91532	-2.409	0.01707	*
age	0.16038	0.03621	4.429	1.70E-05	***
sex	1.49259	0.95115	1.569	0.11847	
LC_Status	2.49518	0.94852	2.631	0.00932	**
BMI	0.04894	0.06988	0.7	0.4847	

Tem CD4 T Cells

Residuals:

Min	1Q	Median	3Q	Max
-1.7596	-0.6807	-0.3485	0.083	11.0757

Coefficients:

	Estimate	Std.	Error	tvalue	Pr(>|t|)
(Intercept)	-0.82009	0.803513	-1.021	0.309	
age	0.041576	0.010019	4.15	5.29E-05	***
sex	0.047212	0.261053	0.181	0.857	
LC_Status	-0.1996	0.256744	-0.777	0.438	
BMI	0.000742	0.018825	0.039	0.969	

Tcm CD4 T Cells

Residuals:

Min	1Q	Median	3Q	Max
-27.0735	-6.8841	-0.4319	7.1405	24.5309

Coefficients:

	Estimate	Std.	Error	tvalue	Pr(>|t|)
(Intercept)	29.40406	5.56566	5.283	3.92E-07	***
age	0.06115	0.0694	0.881	0.379558	
sex	-2.63517	1.80822	-1.457	0.146904	
LC_Status	-6.72872	1.77838	-3.784	0.000215	***
BMI	0.25222	0.13039	1.934	0.054762	.

Tex CD4 T Cells

Residuals:

Min	1Q	Median	3Q	Max
-0.89527	-0.35143	-0.09898	0.22272	1.91422

Coefficients:

	Estimate	Std.	Error	tvalue	Pr(>|t|)
(Intercept)	0.944372	0.267372	3.532	0.000533	***
age	-0.00619	0.003334	-1.857	0.065096	.
sex	0.076792	0.086866	0.884	0.377954	
LC_Status	0.268035	0.085433	3.137	0.002015	**
BMI	-0.0036	0.006264	-0.574	0.566536	

Tem CD8 T Cells

Residuals:

Min	1Q	Median	3Q	Max
-15.484	-6.836	-3.3	3.963	46.984

Coefficients:

	Estimate	Std.	Error	tvalue	Pr(>|t|)
(Intercept)	7.00271	5.51446	1.27	0.2059	
age	0.27509	0.06876	4.001	9.48E-05	***
sex	-1.34373	1.79159	-0.75	0.4543	
LC_Status	-3.99334	1.76202	-2.266	0.0247	*
BMI	-0.07715	0.12919	-0.597	0.5512	

Tcm CD8 T cells

Residuals:

Min	1Q	Median	3Q	Max
-12.243	-3.696	-1.506	2.224	17.986

Coefficients:

	Estimate	Std.	Error	tvalue	Pr(>|t|)
(Intercept)	5.44165	2.96292	1.837	0.068	.
age	0.06882	0.03695	1.863	0.0643	.
sex	0.14359	0.96262	0.149	0.8816	
LC_Status	-1.36665	0.94673	-1.444	0.1507	
BMI	0.12639	0.06941	1.821	0.0704	.

Tex CD8 T Cells

Residuals:

Min	1Q	Median	3Q	Max
-0.908	-0.3701	-0.1266	0.1828	2.4065

Coefficients:

	Estimate	Std.	Error	tvalue	Pr(>|t|)
(Intercept)	0.393476	0.306707	1.283	0.2013	
age	0.004086	0.003824	1.068	0.2869	
sex	-0.13021	0.099646	-1.307	0.1931	
LC_Status	0.145062	0.098001	1.48	0.1407	
BMI	0.01257	0.007185	1.749	0.0821	.

IL2CD4 T cells

Deviance Residuals:

Min	1Q	Median	3Q	Max
-19.034	-6.11	-1.206	5.001	22.748

Coefficients:

	Estimate	Std.	Error	tvalue	Pr(>|t|)
(Intercept)	1.5244	4.4706	0.341	0.733534	
age	0.2026	0.0556	3.645	0.000356	***
sex	1.2102	1.4618	0.828	0.408917	
LC_Status	3.7042	1.4512	2.553	0.011574	*
BMI	0.1181	0.1068	1.106	0.270366	

IL4CD4 T Cells

Deviance Residuals:

Min	1Q	Median	3Q	Max
-13.617	-5.901	-1.888	3.944	36.775

Coefficients:

	Estimate	Std.	Error	tvalue	Pr(>|t|)
(Intercept)	-0.51717	4.50706	-0.115	0.90878	
age	0.1791	0.05606	3.195	0.00167	**
sex	0.90329	1.47376	0.613	0.54075	
LC_Status	5.54373	1.46302	3.789	0.00021	***
BMI	0.02842	0.10765	0.264	0.79208	

IL6CD4 T cells

Deviance Residuals:

Min	1Q	Median	3Q	Max
-4.4009	-2.0594	-0.9374	1.1185	18.0007

Coefficients:

	Estimate	Std.	Error	tvalue	Pr(>|t|)
(Intercept)	-1.03E+00	1.81E+00	-0.572	0.5681	
age	4.64E-02	2.25E-02	2.063	0.0406	*
sex	6.18E-01	5.91E-01	1.046	0.2969	
LC_Status	1.37E+00	5.86E-01	2.338	0.0205	*
BMI	1.23E-05	4.32E-02	0	0.9998	

IL2CD8 T cells

Deviance Residuals:

Min	1Q	Median	3Q	Max
-6.804	-2.664	-1.233	1.852	34.907

Coefficients:

	Estimate	Std.	Error	tvalue	Pr(>|t|)
(Intercept)	-1.44863	2.372544	-0.611	0.542292	
age	0.100886	0.029508	3.419	0.000787	***
sex	0.47749	0.775795	0.615	0.539058	
LC_Status	2.108289	0.770145	2.738	0.006849	**
BMI	-0.00797	0.05667	-0.141	0.888272	

IL4CD8 T cells

Deviance Residuals:

Min	1Q	Median	3Q	Max
-16.612	-6.679	-2.26	3.9	40.765

Coefficients:

	Estimate	Std.	Error	tvalue	Pr(>|t|)
(Intercept)	0.78374	5.25246	0.149	0.882	
age	0.27454	0.06533	4.202	4.26E-05	***
sex	0.33304	1.7175	0.194	0.846	
LC_Status	1.96201	1.70499	1.151	0.251	
BMI	0.10858	0.12546	0.865	0.388	

IL6CD8 T cells

Deviance Residuals:

Min	1Q	Median	3Q	Max
-16.612	-6.679	-2.26	3.9	40.765

Coefficients:

	Estimate	Std.	Error	tvalue	Pr(>|t|)
(Intercept)	0.78374	5.25246	0.149	0.882	
age	0.27454	0.06533	4.202	4.26E-05	***
sex	0.33304	1.7175	0.194	0.846	
LC_Status	1.96201	1.70499	1.151	0.251	
BMI	0.10858	0.12546	0.865	0.388	

IL4IL6CD4 T cells

Deviance Residuals:

Min	1Q	Median	3Q	Max
-2.4764	-1.2321	-0.4384	0.2597	17.6501

Coefficients:

	Estimate	Std.	Error	tvalue	Pr(>|t|)
(Intercept)	-2.82468	1.39552	-2.024	0.0445	*
age	0.0412	0.01736	2.374	0.0187	*
sex	0.44764	0.45632	0.981	0.328	
LC_Status	1.10899	0.453	2.448	0.0154	*
BMI	0.03089	0.03333	0.927	0.3554	

IL4IL6CD8 T cells

Deviance Residuals:

Min	1Q	Median	3Q	Max
-6.3758	-2.7386	-1.1987	0.4918	30.1593

Coefficients:

	Estimate	Std.	Error	tvalue	Pr(>|t|)
(Intercept)	-5.83849	3.10489	-1.88	0.06176	.
age	0.10267	0.03862	2.659	0.00859	**
sex	0.33757	1.01526	0.332	0.73993	
LC_Status	2.35824	1.00787	2.34	0.02045	*
BMI	0.07273	0.07416	0.981	0.32817	

Extended Data Table 4

Anti-S

Deviance Residuals:

Min	1Q	Median	3Q	Max
-6.0875	-0.359	0.1374	0.5489	3.6782

Coefficients:

	Estimate	Std. Error	t	value	Pr(>|t|)
(Intercept)	6.355241	0.712105	8.925	6.33E-16	***
age	0.003949	0.007573	0.521	0.60272	
sex	0.003601	0.198135	0.018	0.98552	
LC_Status	0.681862	0.230898	2.953	0.00358	**
VAD	1.525492	0.128148	11.904	< 2.00E-16	***
BMI	0.025414	0.014638	1.736	0.08433	.

Anti-S1

Deviance Residuals:

Min	1Q	Median	3Q	Max
-6.1029	-0.6179	0.0336	0.794	3.7732

Coefficients:

	Estimate	Std. Error	t	value	Pr(>|t|)
(Intercept)	4.754091	0.808882	5.877	2.09E-08	***
age	0.000207	0.008602	0.024	0.9808	
sex	-0.05942	0.225062	-0.264	0.7921	
LC_Status	1.425864	0.262278	5.436	1.83E-07	***
VAD	1.903577	0.145563	13.077	< 2.00E-16	***
BMI	0.040236	0.016628	2.42	0.0166	*

Anti-RBD

Residuals:

Min	1Q	Median	3Q	Max
-6.0942	-0.6904	0.133	0.82	5.5916

Coefficients:

	Estimate	Std. Error	t	value	Pr(>|t|)
(Intercept)	4.702146	0.897883	5.237	4.70E-07	***
age	0.007358	0.009549	0.771	0.442	
sex	0.059682	0.249826	0.239	0.8115	
LC_Status	0.742004	0.291136	2.549	0.0117	*
VAD	2.182805	0.161579	13.509	< 2.00E-16	***
BMI	0.039673	0.018457	2.149	0.033	*

Seropositiv Spike Motif KFLPFQQ

Residuals:

Min	1Q	Median	3Q	Max
-14.263	-6.93	-3.938	-0.66	55.635

Coefficients:

	Estimate	Std. Error	t	value	Pr(>|t|)
(Intercept)	0.37259	7.96592	0.047	0.96275	
age	-0.07079	0.08471	-0.836	0.40452	
sex	-2.26258	2.21642	-1.021	0.30876	
LC_Status	8.16153	2.58293	3.16	0.00186	**
VAD	2.61206	1.43352	1.822	0.07016	.
BMI	0.15053	0.16375	0.919	0.35924	

Seropositiv Spike Motif LDKWYF

Residuals:

Min	1Q	Median	3Q	Max
-24.663	-12.466	-6.899	5.72	101.332

Coefficients:

	Estimate	Std. Error	t	value	Pr(>|t|)
(Intercept)	-0.54018	11.641	-0.046	0.963	
age	-0.04612	0.1238	-0.373	0.7099	
sex	-3.58417	3.23897	-1.107	0.27	
LC_Status	6.0783	3.77456	1.61	0.1091	
VAD	3.36872	2.09487	1.608	0.1096	
BMI	0.52293	0.2393	2.185	0.0302	*

Seropositiv Spike Motif RDPQTLE

Residuals:

Min	1Q	Median	3Q	Max
-8.71	-4.904	-2.189	-0.169	94.84

Coefficients:

	Estimate	Std. Error	t	value	Pr(>|t|)
(Intercept)	-3.84559	6.872183	-0.56	0.57648	
age	0.008607	0.073083	0.118	0.90639	
sex	-1.20714	1.912105	-0.631	0.52867	
LC_Status	6.383147	2.228285	2.865	0.00469	**
VAD	2.028998	1.236691	1.641	0.10268	
BMI	0.073859	0.141268	0.523	0.60176	

Seropositiv Spike Motif DISGI

Residuals:

Min	1Q	Median	3Q	Max
-12.264	-6.206	-4.179	-1.252	110.718

Coefficients:

	Estimate	Std. Error	t	value	Pr(>|t|)
(Intercept)	-7.55943	9.121243	-0.829	0.4084	
age	-0.00614	0.097001	-0.063	0.9496	
sex	2.036719	2.53788	0.803	0.4233	
LC_Status	5.940301	2.957536	2.009	0.0461	*
VAD	1.630025	1.641423	0.993	0.3221	
BMI	0.160742	0.187501	0.857	0.3925	

Extended Data Table 5

Generalized linear regression model

zscore_Cortisol ~ 1 + x0_Demographics_Age + x0_Demographics_Sex + x0_Demographics_BMI + x0_Sample_Time_Min + x0_LC_Status + x0_Study_Cohort

Distribution = Normal

Estimated Coefficients:

	Estimate	SE	tStat	pValue
(Intercept)	1.6342	0.32856	4.9737	1.33E-06
x0_Demographics_Age	-0.00847	0.002902	-2.9186	0.003882
x0_Demographics_Sex_2	-0.02619	0.081514	-0.32131	0.74828
x0_Demographics_BMI	-0.00774	0.005611	-1.3798	0.16905
x0_Sample_Time_Min	-0.00065	0.000431	-1.5003	0.13498
x0_LC_Status_1	-1.2198	0.089809	-13.582	6.92E-31
x0_Study_Cohort_2	0.68657	0.1	6.8658	6.73E-11

226 observations, 219 error degrees of freedom

Estimated Dispersion: 0.304

F-statistic vs. constant model: 44.1, p-value = 4.04E-35

Extended Data Table 6

kappa	kappa_lower_ci	kappa_upper_ci
0.786407767	0.645964174	0.92685136

Extended Data Table 7

nature portfolio

Corresponding author(s): Akiko Iwasaki, David Putrino, Aaron Ring, David van Dijk

Last updated by author(s): 06/12/2023

Reporting Summary

Nature Portfolio wishes to improve the reproducibility of the work that we publish. This form provides structure for consistency and transparency in reporting. For further information on Nature Portfolio policies, see our Editorial Policies and the Editorial Policy Checklist.

Statistics

For all statistical analyses, confirm that the following items are present in the figure legend, table legend, main text, or Methods section.

n/a	Confirmed	
☐	☒	The exact sample size (*n*) for each experimental group/condition, given as a discrete number and unit of measurement
☐	☒	A statement on whether measurements were taken from distinct samples or whether the same sample was measured repeatedly
☐	☒	The statistical test(s) used AND whether they are one- or two-sided *Only common tests should be described solely by name; describe more complex techniques in the Methods section.*
☐	☒	A description of all covariates tested
☐	☒	A description of any assumptions or corrections, such as tests of normality and adjustment for multiple comparisons
☐	☒	A full description of the statistical parameters including central tendency (e.g. means) or other basic estimates (e.g. regression coefficient) AND variation (e.g. standard deviation) or associated estimates of uncertainty (e.g. confidence intervals)
☐	☒	For null hypothesis testing, the test statistic (e.g. *F*, *t*, *r*) with confidence intervals, effect sizes, degrees of freedom and *P* value noted *Give P values as exact values whenever suitable.*
☒	☐	For Bayesian analysis, information on the choice of priors and Markov chain Monte Carlo settings
☒	☐	For hierarchical and complex designs, identification of the appropriate level for tests and full reporting of outcomes
☐	☒	Estimates of effect sizes (e.g. Cohen's *d*, Pearson's *r*), indicating how they were calculated

Our web collection on statistics for biologists contains articles on many of the points above.

Software and code

Policy information about availability of computer code

Data collection	All participant survey data were collected and securely stored using REDCap 13.4 (Research Electronic Data Capture) electronic data capture tools hosted within the Mount Sinai Health System. All other de-identified research data were stored securely in password protected internal electronic repositories. All Flow Cytometry data was collected and analyzed using FlowJo software version 10.8 software (BD).
Data analysis	All data analysis was performed using MATLAB (2023b), R, and GraphPad Prism (9.8.1). A repository of computer code used for analysis can be found at: https://github.com/rahuldhodapkar/puddlr

For manuscripts utilizing custom algorithms or software that are central to the research but not yet described in published literature, software must be made available to editors and reviewers. We strongly encourage code deposition in a community repository (e.g. GitHub). See the Nature Portfolio guidelines for submitting code & software for further information.

Data

Policy information about availability of data

All manuscripts must include a data availability statement. This statement should provide the following information, where applicable:

- Accession codes, unique identifiers, or web links for publicly available datasets
- A description of any restrictions on data availability
- For clinical datasets or third party data, please ensure that the statement adheres to our policy

All research data for study participants used in this manuscript are included in Supplementary Table 3. All of the raw fcs files for the flow cytometry analysis are

available at the FlowRepository platform (http://flowrepository.org/) under Repository ID: FR-FCM-Z6KL. Accession numbers for protein structure are used UniProt and are as follows: trimeric Spike (PDB: 6VXX) and EBV gH/gL (PDB: 5T1D).

Human research participants

Policy information about studies involving human research participants and Sex and Gender in Research.

Reporting on sex and gender	Sex was determined through self-report and review of electronic medical records. No sex disaggregated analysis was performed. Study demographics, including proportion sex by individual study group, are included in Extended Table 1.
Population characteristics	All relevant population demographics are described in Extended Table 1.
Recruitment	Participants with persistent symptoms following acute COVID-19 were recruited from Long COVID clinics within the Mount Sinai Healthcare System and the Center for Post COVID Care at Mount Sinai Hospital. Participants enrolled in healthy and convalescent study arms were recruited via IRB-approved advertisements delivered through email lists, study flyers located in hospital public spaces, and on social media platforms. Informed consent was provided by all participants at the time of enrollment. Individuals in the external Long COVID group ("Ext. LC") were identified from The Winchester Center for Lung Disease's Post-COVID-19 Recovery Program at Yale New Haven Hospital by collaborating clinicians. Recruitment from treatment clinics predisposes this study to a degree of self-selection bias among participants, which was accounted for through demographic matching procedures.
Ethics oversight	This study was approved by the Mount Sinai Program for the Protection of Human Subjects (IRB #20-01758) and Yale Institutional Review Board (IRB #2000029451 for MY-LC; IRB #2000028924 for enrollment of pre-vaccinated Healthy Controls; HIC #2000026109 for External Long COVID). Informed consent was obtained from all enrolled participants.

Note that full information on the approval of the study protocol must also be provided in the manuscript.

Field-specific reporting

Please select the one below that is the best fit for your research. If you are not sure, read the appropriate sections before making your selection.

☒ Life sciences ☐ Behavioural & social sciences ☐ Ecological, evolutionary & environmental sciences

For a reference copy of the document with all sections, see nature.com/documents/nr-reporting-summary-flat.pdf

Life sciences study design

All studies must disclose on these points even when the disclosure is negative.

Sample size	Sample size was not predetermined prior to enrollment of study participants. Samples sizes were chosen based on prior experience with multiplexed immune phenotyping assays and available study resources.
Data exclusions	Data exclusions are stated explicitly in Methods under the heading "MY-LC Study Design, Enrollment Strategy, and Inclusion / Exclusion Criteria " and are reproduced here for convenience: "Inclusion criteria for individuals in the Long COVID group ("LC") were age ≥ 18 years; previous confirmed or probable COVID-19 infection (according to World Health Organization guidelines1); and persistent symptoms > 6 weeks following initial COVID-19 infection. Inclusion criteria for enrollment of individuals in the healthy control group ("HC") were age ≥ 18 years, no prior COVID-19 infection, and completion of a brief, semi-structured verbal screening with research staff confirming no active symptomatology. Inclusion criteria for individuals in the convalescent control group ("CC") were age ≥ 18 years; previous confirmed or probable prior COVID-19 infection; and completion of a brief, semi-structured verbal screening with research staff confirming no active symptomatology. Pre-specified exclusion criteria for this study were inability to provide informed consent; and any condition preventing a blood test from being performed. Additionally, all participants had electronic health records reviewed by study clinicians following enrollment and were subsequently excluded prior to analyses for the following reasons: (1) current pregnancy, (2) immunosuppression equivalent to or exceeding prednisone 5 mg daily, (3) active malignancy or chemotherapy, and (4) any monogenic disorders. For specific immunological analyses, pre-existing medical conditions were additionally excluded prior to analyses due to high potential for confounding (e.g., participants with hypothyroidism were excluded prior to analysis of circulating T3/T4 levels; participants with pituitary adenomas were excluded prior to analysis of cortisol levels). Specific exclusions are marked by "Δ" in figures and detailed in relevant legends." "
Replication	Each participant plasma and PBMC sample was partitioned into aliquots for use in various assays. Technical replicates were performed on patient samples where sample volume limitations permitted. When performed (e.g. ELISA, qPCR), technical replicates were successful.
Randomization	Randomization was not applicable to this study as it is a cross-sectional, observational human research study of a pre-existing medical condition.
Blinding	Blinding of study investigators was not performed due to pre-existing intrinsic knowledge of clinical condition / study groups by both participants and investigators, as well as necessary logistical accommodations for scheduling of sample draws by study participants.

Behavioural & social sciences study design

All studies must disclose on these points even when the disclosure is negative.

Study description	*Briefly describe the study type including whether data are quantitative, qualitative, or mixed-methods (e.g. qualitative cross-sectional, quantitative experimental, mixed-methods case study).*
Research sample	*State the research sample (e.g. Harvard university undergraduates, villagers in rural India) and provide relevant demographic information (e.g. age, sex) and indicate whether the sample is representative. Provide a rationale for the study sample chosen. For studies involving existing datasets, please describe the dataset and source.*
Sampling strategy	*Describe the sampling procedure (e.g. random, snowball, stratified, convenience). Describe the statistical methods that were used to predetermine sample size OR if no sample-size calculation was performed, describe how sample sizes were chosen and provide a rationale for why these sample sizes are sufficient. For qualitative data, please indicate whether data saturation was considered, and what criteria were used to decide that no further sampling was needed.*
Data collection	*Provide details about the data collection procedure, including the instruments or devices used to record the data (e.g. pen and paper, computer, eye tracker, video or audio equipment) whether anyone was present besides the participant(s) and the researcher, and whether the researcher was blind to experimental condition and/or the study hypothesis during data collection.*
Timing	*Indicate the start and stop dates of data collection. If there is a gap between collection periods, state the dates for each sample cohort.*
Data exclusions	*If no data were excluded from the analyses, state so OR if data were excluded, provide the exact number of exclusions and the rationale behind them, indicating whether exclusion criteria were pre-established.*
Non-participation	*State how many participants dropped out/declined participation and the reason(s) given OR provide response rate OR state that no participants dropped out/declined participation.*
Randomization	*If participants were not allocated into experimental groups, state so OR describe how participants were allocated to groups, and if allocation was not random, describe how covariates were controlled.*

Ecological, evolutionary & environmental sciences study design

All studies must disclose on these points even when the disclosure is negative.

Study description	*Briefly describe the study. For quantitative data include treatment factors and interactions, design structure (e.g. factorial, nested, hierarchical), nature and number of experimental units and replicates.*
Research sample	*Describe the research sample (e.g. a group of tagged Passer domesticus, all Stenocereus thurberi within Organ Pipe Cactus National Monument), and provide a rationale for the sample choice. When relevant, describe the organism taxa, source, sex, age range and any manipulations. State what population the sample is meant to represent when applicable. For studies involving existing datasets, describe the data and its source.*
Sampling strategy	*Note the sampling procedure. Describe the statistical methods that were used to predetermine sample size OR if no sample-size calculation was performed, describe how sample sizes were chosen and provide a rationale for why these sample sizes are sufficient.*
Data collection	*Describe the data collection procedure, including who recorded the data and how.*
Timing and spatial scale	*Indicate the start and stop dates of data collection, noting the frequency and periodicity of sampling and providing a rationale for these choices. If there is a gap between collection periods, state the dates for each sample cohort. Specify the spatial scale from which the data are taken*
Data exclusions	*If no data were excluded from the analyses, state so OR if data were excluded, describe the exclusions and the rationale behind them, indicating whether exclusion criteria were pre-established.*
Reproducibility	*Describe the measures taken to verify the reproducibility of experimental findings. For each experiment, note whether any attempts to repeat the experiment failed OR state that all attempts to repeat the experiment were successful.*
Randomization	*Describe how samples/organisms/participants were allocated into groups. If allocation was not random, describe how covariates were controlled. If this is not relevant to your study, explain why.*
Blinding	*Describe the extent of blinding used during data acquisition and analysis. If blinding was not possible, describe why OR explain why blinding was not relevant to your study.*

Did the study involve field work? ☐ Yes ☐ No

Field work, collection and transport

Field conditions	*Describe the study conditions for field work, providing relevant parameters (e.g. temperature, rainfall).*
Location	*State the location of the sampling or experiment, providing relevant parameters (e.g. latitude and longitude, elevation, water depth).*
Access & import/export	*Describe the efforts you have made to access habitats and to collect and import/export your samples in a responsible manner and in compliance with local, national and international laws, noting any permits that were obtained (give the name of the issuing authority, the date of issue, and any identifying information).*
Disturbance	*Describe any disturbance caused by the study and how it was minimized.*

Reporting for specific materials, systems and methods

We require information from authors about some types of materials, experimental systems and methods used in many studies. Here, indicate whether each material, system or method listed is relevant to your study. If you are not sure if a list item applies to your research, read the appropriate section before selecting a response.

Materials & experimental systems

n/a	Involved in the study
☐	☒ Antibodies
☒	☐ Eukaryotic cell lines
☒	☐ Palaeontology and archaeology
☒	☐ Animals and other organisms
☒	☐ Clinical data
☒	☐ Dual use research of concern

Methods

n/a	Involved in the study
☒	☐ ChIP-seq
☐	☒ Flow cytometry
☒	☐ MRI-based neuroimaging

Antibodies

Antibodies used	All antibodies, dilutions, and catalog numbers are used in this manuscript are detailed in Supplementary Table 1.
Validation	All antibodies used in this study are commercially available, and all have been validated by the manufacturers and used by other publications. Likewise, we titrated these antibodies according to our own our staining conditions. The following were validated in the following species: BB515 anti-hHLA-DR (G46-6) (BD Biosciences) (Human, Rhesus, Cynomolgus, Baboon), BV785 anti-hCD16 (3G8) (BioLegend) (Human, African Green, Baboon, Capuchin Monkey, Chimpanzee, Cynomolgus, Marmoset, Pigtailed Macaque, Rhesus, Sooty Mangabey, Squirrel Monkey), PE-Cy7 anti-hCD14 (HCD14) (BioLegend) (Human), BV605 anti-hCD3 (UCHT1) (BioLegend) (Human, Chimpanzee), BV711 anti-hCD19 (SJ25C1) (BD Biosciences) (Human), AlexaFluor647 anti-hCD1c (L161) (BioLegend) (Human, African Green, Baboon, Cynomolgus, Rhesus), Biotin anti-hCD141 (M80) (BioLegend) (Human, African Green, Baboon), PE-Dazzle594 anti-hCD56 (HCD56) (BioLegend) (Human, African Green, Baboon, Cynomolgus, Rhesus), PE anti-hCD304 (12C2) (BioLegend) (Human), APCFire750 anti-hCD11b (ICRF44) (BioLegend) (Human, African Green, Baboon, Chimpanzee, Common Marmoset, Cynomolgus, Rhesus, Swine), PerCP/Cy5.5 anti-hCD66b (G10F5) (BD Biosciences) (Human), BV421 anti-CD15 (W6D3) (BioLegend) (Human), BV785 anti-hCD4 (SK3) (BioLegend) (Human), APCFire750 or BV711 anti-hCD8 (SK1) (BioLegend) (Human, Cross-Reactivity: African Green, Chimpanzee, Cynomolgus, Pigtailed Macaque, Rhesus, Sooty Mangabey), BV421 anti-hCCR7 (G043H7) (BioLegend) (Human, African Green, Baboon, Cynomolgus, Rhesus), AlexaFluor 700 anti-hCD45RA (HI100) (BD Biosciences) (Human), PE anti-hPD1 (EH12.2H7) (BioLegend) (Human, African Green, Baboon, Chimpanzee, Common Marmoset, Cynomolgus, Rhesus, Squirrel Monkey), APC antihTIM3 (F38-2E2) (BioLegend) (Human), BV711 anti-hCD38 (HIT2) (BioLegend) (Human, Chimpanzee, Horse), BB700 anti-hCXCR5 (RF8B2) (BD Biosciences) (Human), PE-Cy7 anti-hCD127 (HIL-7R-M21) (BioLegend) (Human), PE-CF594 anti-hCD25 (BC96) (BD Biosciences) (Human, Rhesus, Cynomolgus, Baboon), BV421 anti-hIL-17a (N49-653) (BD Biosciences) (Human), AlexaFluor 700 anti-hTNFa (MAb11) (BioLegend) (Human, Cat, Cross-Reactivity: Chimpanzee, Baboon, Cynomolgus, Rhesus, Pigtailed Macaque, Sooty Mangabey, Swine), APC/Fire750 anti-hIFNy (4S.B3) (BioLegend) (Human, Cross-Reactivity: Chimpanzee, Baboon, Cynomolgus, Rhesus), FITC anti-hGranzymeB (GB11) (BioLegend) (Human, Mouse, Cross-Reactivity: Rat), AlexaFluor 647 anti-hIL-4 (8D4-8) (BioLegend) (Human, Cross-Reactivity: Chimpanzee, Baboon, Cynomolgus, Rhesus), BB700 anti-hCD183/CXCR3 (1C6/CXCR3) (BD Biosciences) (Human, Rhesus, Cynomolgus, Baboon), PE-Cy7 anti-IL-6 (MQ2-13A5) (BioLegend) (Human), PE anti-hIL-2 (5344.111) (BD Biosciences) (Human), BV785 anti-hCD19 (SJ25C1) (BioLegend) (Human), BV421 anti-hCD138 (MI15) (BioLegend) (Human), AlexaFluor700 anti-hCD20 (2H7) (BioLegend) (Human, Baboon, Capuchin Monkey, Chimpanzee, Cynomolgus, Pigtailed Macaque, Rhesus, Squirrel Monkey), AlexaFluor 647 anti-hCD27 (M-T271) (BioLegend) (Human, Cross-Reacitivity: Baboon, Cynomolgus, Rhesus), PE/Dazzle594 anti-hIgD (IA6-2) (BioLegend) (Human), PE-Cy7 anti-hCD86 (IT2.2) (BioLegend) (Human, African Green, Baboon, Capuchin Monkey, Common Marmoset, Cotton-topped Tamarin, Chimpanzee, Cynomolgus, Rhesus), APC/Fire750 anti-hIgM (MHM-88) (BioLegend) (Human, African Green, Baboon, Cynomolgus, Rhesus), BV605 anti-hCD24 (ML5) (BioLegend) (Human, Cross-Reactivity: Chimpanzee), AlexaFluor 700 Streptavidin (1:300) (ThermoFisher).

Eukaryotic cell lines

Policy information about cell lines and Sex and Gender in Research

Cell line source(s)	*State the source of each cell line used and the sex of all primary cell lines and cells derived from human participants or vertebrate models.*
Authentication	*Describe the authentication procedures for each cell line used OR declare that none of the cell lines used were authenticated.*
Mycoplasma contamination	*Confirm that all cell lines tested negative for mycoplasma contamination OR describe the results of the testing for mycoplasma contamination OR declare that the cell lines were not tested for mycoplasma contamination.*
Commonly misidentified lines (See ICLAC register)	*Name any commonly misidentified cell lines used in the study and provide a rationale for their use.*

Palaeontology and Archaeology

Specimen provenance	*Provide provenance information for specimens and describe permits that were obtained for the work (including the name of the issuing authority, the date of issue, and any identifying information). Permits should encompass collection and, where applicable, export.*
Specimen deposition	*Indicate where the specimens have been deposited to permit free access by other researchers.*
Dating methods	*If new dates are provided, describe how they were obtained (e.g. collection, storage, sample pretreatment and measurement), where they were obtained (i.e. lab name), the calibration program and the protocol for quality assurance OR state that no new dates are provided.*

☐ Tick this box to confirm that the raw and calibrated dates are available in the paper or in Supplementary Information.

Ethics oversight	*Identify the organization(s) that approved or provided guidance on the study protocol, OR state that no ethical approval or guidance was required and explain why not.*

Note that full information on the approval of the study protocol must also be provided in the manuscript.

Animals and other research organisms

Policy information about studies involving animals; ARRIVE guidelines recommended for reporting animal research, and Sex and Gender in Research

Laboratory animals	*For laboratory animals, report species, strain and age OR state that the study did not involve laboratory animals.*
Wild animals	*Provide details on animals observed in or captured in the field; report species and age where possible. Describe how animals were caught and transported and what happened to captive animals after the study (if killed, explain why and describe method; if released, say where and when) OR state that the study did not involve wild animals.*
Reporting on sex	*Indicate if findings apply to only one sex; describe whether sex was considered in study design, methods used for assigning sex. Provide data disaggregated for sex where this information has been collected in the source data as appropriate; provide overall numbers in this Reporting Summary. Please state if this information has not been collected. Report sex-based analyses where performed, justify reasons for lack of sex-based analysis.*
Field-collected samples	*For laboratory work with field-collected samples, describe all relevant parameters such as housing, maintenance, temperature, photoperiod and end-of-experiment protocol OR state that the study did not involve samples collected from the field.*
Ethics oversight	*Identify the organization(s) that approved or provided guidance on the study protocol, OR state that no ethical approval or guidance was required and explain why not.*

Note that full information on the approval of the study protocol must also be provided in the manuscript.

Clinical data

Policy information about clinical studies

All manuscripts should comply with the ICMJE guidelines for publication of clinical research and a completed CONSORT checklist must be included with all submissions.

Clinical trial registration	*Provide the trial registration number from ClinicalTrials.gov or an equivalent agency.*
Study protocol	*Note where the full trial protocol can be accessed OR if not available, explain why.*
Data collection	*Describe the settings and locales of data collection, noting the time periods of recruitment and data collection.*

Outcomes | *Describe how you pre-defined primary and secondary outcome measures and how you assessed these measures.*

Dual use research of concern

Policy information about dual use research of concern

Hazards

Could the accidental, deliberate or reckless misuse of agents or technologies generated in the work, or the application of information presented in the manuscript, pose a threat to:

No	Yes	
☒	☐	Public health
☒	☐	National security
☒	☐	Crops and/or livestock
☒	☐	Ecosystems
☒	☐	Any other significant area

Experiments of concern

Does the work involve any of these experiments of concern:

No	Yes	
☒	☐	Demonstrate how to render a vaccine ineffective
☒	☐	Confer resistance to therapeutically useful antibiotics or antiviral agents
☒	☐	Enhance the virulence of a pathogen or render a nonpathogen virulent
☒	☐	Increase transmissibility of a pathogen
☒	☐	Alter the host range of a pathogen
☒	☐	Enable evasion of diagnostic/detection modalities
☒	☐	Enable the weaponization of a biological agent or toxin
☒	☐	Any other potentially harmful combination of experiments and agents

ChIP-seq

Data deposition

☐ Confirm that both raw and final processed data have been deposited in a public database such as GEO.

☐ Confirm that you have deposited or provided access to graph files (e.g. BED files) for the called peaks.

Data access links *May remain private before publication.*	*For "Initial submission" or "Revised version" documents, provide reviewer access links. For your "Final submission" document, provide a link to the deposited data.*
Files in database submission	*Provide a list of all files available in the database submission.*
Genome browser session (e.g. UCSC)	*Provide a link to an anonymized genome browser session for "Initial submission" and "Revised version" documents only, to enable peer review. Write "no longer applicable" for "Final submission" documents.*

Methodology

Replicates	*Describe the experimental replicates, specifying number, type and replicate agreement.*
Sequencing depth	*Describe the sequencing depth for each experiment, providing the total number of reads, uniquely mapped reads, length of reads and whether they were paired- or single-end.*
Antibodies	*Describe the antibodies used for the ChIP-seq experiments; as applicable, provide supplier name, catalog number, clone name, and lot number.*
Peak calling parameters	*Specify the command line program and parameters used for read mapping and peak calling, including the ChIP, control and index files used.*
Data quality	*Describe the methods used to ensure data quality in full detail, including how many peaks are at FDR 5% and above 5-fold enrichment.*
Software	*Describe the software used to collect and analyze the ChIP-seq data. For custom code that has been deposited into a community repository, provide accession details.*

Flow Cytometry

Plots

Confirm that:

☒ The axis labels state the marker and fluorochrome used (e.g. CD4-FITC).

☒ The axis scales are clearly visible. Include numbers along axes only for bottom left plot of group (a 'group' is an analysis of identical markers).

☒ All plots are contour plots with outliers or pseudocolor plots.

☒ A numerical value for number of cells or percentage (with statistics) is provided.

Methodology

Sample preparation	Freshly isolated PBMCs were plated at 1–2 × 106 cells per well in a 96-well U-bottom plate. Cells were resuspended in Live/Dead Fixable Aqua (ThermoFisher) for 20 min at 4°C. Cells were washed with PBS and followed by Human TruStain FcX (BioLegend) incubation for 10 min at RT. Cocktails of staining antibodies were added directly to this mixture for 30 minutes at RT. Prior to analysis, cells were washed and resuspended in 100 µl 4% PFA for 30 min at 4°C. For intracellular cytokine staining following stimulation, the surface marker-stained cells were resuspended in 200 µl cRPMI (RPMI-1640 supplemented with 10% FBS, 2 mM L-glutamine, 100 U/ml penicillin, and 100 mg/ml streptomycin, 1 mM sodium pyruvate) and stored at 4°C overnight. Subsequently, these cells were washed and stimulated with 1× Cell Stimulation Cocktail (eBioscience) in 200 µl cRPMI for 1 h at 37°C. Fifty µl of 5× Stimulation Cocktail in cRPMI (plus protein transport 442 inhibitor, eBioscience) was added for an additional 4 hours of incubation at 37°C. Following stimulation, cells were washed and resuspended in 100 µl 4% paraformaldehyde for 30 min at 4°C. To quantify intracellular cytokines, cells were permeabilized with 1× permeabilization buffer from the FOXP3/Transcription Factor Staining Buffer Set (eBioscience) for 10 min at 4°C. All subsequent staining cocktails were made in this buffer. Permeabilized cells were then washed and resuspended in a cocktail containing Human TruStain FcX (BioLegend) for 10 min at 4°C. Finally, intracellular staining cocktails were added directly to each sample for 1 h at 4°C. Following this incubation, cells were washed and prepared for analysis on an Attune NXT (ThermoFisher).
Instrument	Attune NXT (ThermoFisher)
Software	Data were analyzed using FlowJo software version 10.8 software (BD).
Cell population abundance	No sorting of PBMC fractions was performed in this study.
Gating strategy	Gating Strategy is described in Extended Figure S10

☒ Tick this box to confirm that a figure exemplifying the gating strategy is provided in the Supplementary Information.

Magnetic resonance imaging

Experimental design

Design type	*Indicate task or resting state; event-related or block design.*
Design specifications	*Specify the number of blocks, trials or experimental units per session and/or subject, and specify the length of each trial or block (if trials are blocked) and interval between trials.*
Behavioral performance measures	*State number and/or type of variables recorded (e.g. correct button press, response time) and what statistics were used to establish that the subjects were performing the task as expected (e.g. mean, range, and/or standard deviation across subjects).*

Acquisition

Imaging type(s)	*Specify: functional, structural, diffusion, perfusion.*
Field strength	*Specify in Tesla*
Sequence & imaging parameters	*Specify the pulse sequence type (gradient echo, spin echo, etc.), imaging type (EPI, spiral, etc.), field of view, matrix size, slice thickness, orientation and TE/TR/flip angle.*
Area of acquisition	*State whether a whole brain scan was used OR define the area of acquisition, describing how the region was determined.*

Diffusion MRI ☐ Used ☐ Not used

Preprocessing

Preprocessing software	*Provide detail on software version and revision number and on specific parameters (model/functions, brain extraction,*

Preprocessing software — *segmentation, smoothing kernel size, etc.).*

Normalization — *If data were normalized/standardized, describe the approach(es): specify linear or non-linear and define image types used for transformation OR indicate that data were not normalized and explain rationale for lack of normalization.*

Normalization template — *Describe the template used for normalization/transformation, specifying subject space or group standardized space (e.g. original Talairach, MNI305, ICBM152) OR indicate that the data were not normalized.*

Noise and artifact removal — *Describe your procedure(s) for artifact and structured noise removal, specifying motion parameters, tissue signals and physiological signals (heart rate, respiration).*

Volume censoring — *Define your software and/or method and criteria for volume censoring, and state the extent of such censoring.*

Statistical modeling & inference

Model type and settings — *Specify type (mass univariate, multivariate, RSA, predictive, etc.) and describe essential details of the model at the first and second levels (e.g. fixed, random or mixed effects; drift or auto-correlation).*

Effect(s) tested — *Define precise effect in terms of the task or stimulus conditions instead of psychological concepts and indicate whether ANOVA or factorial designs were used.*

Specify type of analysis: ☐ Whole brain ☐ ROI-based ☐ Both

Statistic type for inference (See Eklund et al. 2016) — *Specify voxel-wise or cluster-wise and report all relevant parameters for cluster-wise methods.*

Correction — *Describe the type of correction and how it is obtained for multiple comparisons (e.g. FWE, FDR, permutation or Monte Carlo).*

Models & analysis

n/a	Involved in the study
☐	☐ Functional and/or effective connectivity
☐	☐ Graph analysis
☐	☐ Multivariate modeling or predictive analysis

Functional and/or effective connectivity — *Report the measures of dependence used and the model details (e.g. Pearson correlation, partial correlation, mutual information).*

Graph analysis — *Report the dependent variable and connectivity measure, specifying weighted graph or binarized graph, subject- or group-level, and the global and/or node summaries used (e.g. clustering coefficient, efficiency, etc.).*

Multivariate modeling and predictive analysis — *Specify independent variables, features extraction and dimension reduction, model, training and evaluation metrics.*